Title
Interfacial Assembly of Soft Polymeric Janus Nanoparticles Towards Structuring Liquids

Author
Jiang, Yufeng

Publication Date
2021

Peer reviewed|Thesis/dissertation

Interfacial Assembly of Soft Polymeric Janus Nanoparticles Towards Structuring Liquids

By

Yufeng Jiang

A dissertation submitted in partial satisfaction of the

requirements for the degree of

Doctor of Philosophy

in

Engineering – Applied Science and Technology

in the

Graduate Division

of the

University of California, Berkeley

Committee in charge:

Professor Ting Xu, Chair

Professor Jie Yao

Professor Ahmad K. Omar

Fall 2021

Interfacial Assembly of Soft Polymeric Janus Nanoparticles Towards Structuring Liquids

Yufeng Jiang

Abstract

Interfacial Assembly of Soft Polymeric Janus Nanoparticles Towards Structuring Liquids

By

Yufeng Jiang

Doctor of Philosophy in Applied Science and Technology

University of California, Berkeley

Professor Ting Xu, Chair

The focus of this dissertation is to understand the basic principles that govern interfacial assembly towards structuring liquids via the jamming of interfacially active soft polymeric Janus nanoparticles(sJNPs) and develop such structured liquids to be adaptive. Liquid interfaces have desirable characteristics as a platform for materials, ion and charge transport, and material synthesis. There have been numerous studies on the use of surfactants and compatibilizers to create large interfacial areas by stabilizing one liquid in another but structuring the liquids into shapes other than spherical has been difficult to achieve. Colloidal particles are interfacially active (a 0.5mm particle can reduce the interfacial energy by 10^4 k_BT) and form a monolayer at the interface between two liquids to reduce interfacial energy. The size dispersity of the particles plays a large role in determining what type of monolayer is obtained. If the size dispersity is unity, a 2D crystallization occurs at high areal densities, whereas for polydisperse particle size distributions, the 2D assemblies will remain disordered and vitrify. Such behavior is well-documented for colloidal systems but changing the shape of the liquid supporting the assemblies leads to a fracturing of the assemblies, due to the longer time scale of the segregation of the particles to the interface relative to the deformation being applied. Compare to colloidal particles, the time scale of nanoparticle assembly is reduced by factor of ~10^4, based on the diffusion coefficient of the particles in solution. Due to their size, uniformly functionalized nanoparticles have an interfacial binding energy that is $10k_BT$ or less and, as such, the particles are weakly bound to the interface, and exchange with particles in the bulk dispersions. Consequently, any compressive forces applied to the nanoparticles, as for example when the shape of the liquid domains change and the system reduces the interfacial area to minimize

energy, will cause the nanoparticles to be ejected from the interface, and the liquid will assume an equilibrium spherical shape. One strategy to increase the binding energy is to have a heterogenous surface functionality, where one functional group prefers one liquid, and the second functional group preferentially interacts with the second liquid. If the different functionalities are sequestered to different hemispheres of the particle surface, one part of the particle interacts with one liquid and the second part with the other liquid i.e. the particle is Janus. The binding energy of Janus-type nanoparticles, like their surfactant counterparts, is markedly increased, allowing assemblies of the particles to withstand an in-plane (interfacial) compressive force, enabling the liquid domains on which the Janus nanoparticles are assembled, to be shaped. For hard Janus nanoparticle, the point at which the particles jam at the interfacial area is decreased defines the point at which further changes in the interfacial area are arrested. In this thesis we address the influence of the hardness or softness of the nanoparticles on the manner in which the assemblies are jammed and what role if any, does the softness or deformability of the nanoparticles have on the relaxation of the assemblies upon jamming. In particular, the Janus nanoparticles used in this thesis are formed from multiple polymer chains emanating from the nanoparticle core, where two distinct immiscible polymers are used. We address issues associate with the molecular weight of the polymer chains comprising this "fuzzy" nanoparticle, the length of the polymer chains relative to the core volume, and changes in the configuration of the polymer chains when they are assembled at the interface and relaxations of the polymer chains after the compressive force is applied. By the dissolution of salts in the aqueous phase (one of the two immiscible liquids) the binding energy was changed and the influence of this change on the interface activity was examined. The advantages and disadvantages on the "softness" of the particles is discussed relative to specific applications.

Dedication

This dissertation is a tribute and dedicated to my mom, Guiqin Yu, who has given me endless love, unconditional support, encouragement, and implementation of the idea to be compassionate and heartful.

May she rest in peace.

Interfacial Assembly of Soft Polymeric Janus Nanoparticles Towards Structuring Liquids

Table of Contents

Reference

Acknowledgements

The work in this dissertation was made possible by guidance from Professor Thomas P. Russell at the University of Massachusetts Amherst and Professor Ting Xu from the University of California at Berkeley. I appreciate the time and effort they invested in training me to become a scientist and an independent researcher. Their immense knowledge, dedication to science, creative approach, and management style have taught me what a true scientist looks like and has shaped me into a better researcher and human being. I also thank their finical support through the past years, especially during the pandemic. I am privileged and fortunate to have been given such a unique opportunity to work under their guidance, access to the world leading facilities in Lawrence Berkeley National Laboratory and collaborate with many experts in different fields. They have taught me that a PhD degree is not about the number of papers published, but rather a way of thinking. I express my gratitude for Prof. David Attwood and Prof. Ronald Gronski, who always offered help when needed through the preliminary and qualify exams. I also thank Prof. Jie Yao and Prof. Ahmad K. Omar to be my committee members.

I thank all my collaborators whose expertise was well-beyond my own knowledge that added significant value to this work. I express my gratitude to Dr. Brett Helms and Dr. Paul Ashby in Molecular Foundry for in-depth discussions and providing necessary instrumentation. I owe Prof. Axel H. E. Müller, Prof. André H. Gröschel, and Dr. Tina Löbling a special note of thanks, they generously synthesized and characterized Janus nanoparticles and provided the materials in a timely manner.

I appreciate all the members in Russell's group and Xu's group, who I received help and companionship throughout. I thank all of them for their help in my work, as well as the opportunity to work with them in many different subject areas. In particular, I would like to acknowledge Prof. Caili Huang who was my mentor when I first join Russell group and taught me how to use pendent drop analysis instrument, Prof. Feng Liu who guided me into the X-ray scattering world and involved me in many astonishing projects on polymer and photovoltaic thin film structure-performance relationship, Dr. Yu Chai who always brought positive energy, valued experience and characterization expertise to me.

Finally, I would like to thank my family for unconditional belief in me and support, without these I would not have been able to finish this degree. Sadly, my grandparents and my mom cannot witness my accomplishment. Over the years, all I

wanted was to make them proud of me. Their faith in me helped me overcome difficulties. I hope this dissertation serves as a testament towards the realization of a significant goal. I miss you and promise I will always make you proud.

Chapter 1

Introduction: Liquid Interfaces and Interfacially Active Materials

1.1 Liquid-Liquid System and Interfaces

Water and oil are immiscible and, hence, at equilibrium, they form a bilayer with the less dense oil phase on top of the dense water phase, forming a planar interface between the two liquids to minimize the interfacial area or the free energy. When the bilayer is vigorously shaken, droplets of oil in water or water in oil, depending on the volume fractions, form. When allowed to rest, the droplets coalesce to minimize interfacial area and eventually reforming the bilayer system, minimizing interfacial area. [1] Many applications, ranging from chemical reactions to paints to shampoos and other cosmetic products to foods like mayonnaise and milk, to encapsulation for drug delivery rely on the ability to stabilize one fluid phase in another, arresting coalescence and stabilizer droplets on one specific size. [2-4] Yet, the shape of the dispersed liquid phase is always spherical, since a sphere minimizes interfacial area for a given volume. Consequently, the liquid-liquid interface plays a central role, since the interface is where the dominant contribution to the free energy, specifically the enthalpy, arises due to the non-favorable interactions between the components at the interface.

Liquid–liquid interfaces play a key role in many physical, chemical, and biological processes.[5, 6] Interfaces constitute a platform for the assembly of mesoscopic and nanoscopic particles, where the replacement of non-favorable interactions between the liquids is replaced with the interactions between the two liquids and the particles. Consequently, a monolayer of particles assemble at the interface to reduce the interfacial energy, as seen with colloidosomes, that can densely pack at the interface, enabling the generation 2D or 3D structures with precise control over size, permeability and mechanical strength of the assemblies.[7, 8] Hierarchical structures can be fabricated by assembling particles at curved and planar interfaces, that lead to collective properties that can be manipulated by external stimuli or by controlling the interparticle interactions, that are governed by van der Waals, capillary, osmotic, electrostatic and dipolar forces.[9] While particulate assemblies rely on the 2D crystallization of the assemblies or the jamming of the assemblies in the plane of the interface to stabilize the structures, one can also use interfacial polymerization to stabilize one liquid phase in second.[10] A classic example of this is the interfacial polymerization of nylon, though countless other interfacial polymerizations have been reported. Using interfacial polymerization, highly non-equilibrium shapes of one liquid in another can be generated that have been used extensively, for example, in sensors and cargo loading.[11-14]

1.2 Structuring Liquids

Liquids have desirable properties for many energy-related technologies: high transport rates for ions, electrons or particulates, low friction, and high mechanical dampening. The lowest energy state for two immiscible liquids is a bilayer separated by a planar interface, minimizing interfacial area. If the liquids could be shaped and locked into bicontinuous structures, entirely new paradigms emerge for controlling energy transduction in materials. The impact of such a new materials platform would be far reaching. All-liquid batteries with very high ion transport and low impedance, circuitry not confined to the rigid device architectures, flow-through catalyst platforms, and ultra-low frictional materials can be envisioned. Kahn, Baker and coworkers recognized the importance of structuring liquids for energy applications by self-assembling networks of fumed silica nanoparticles to provide structural support in a polyelectrolyte medium for battery applications.[15-17] Though promising, the structure of the fumed silica was poorly defined and not responsive. So, realizing the dream of structuring liquids has been elusive.

There have been numerous studies on the use of surfactants or compatibilizers to stabilize one liquid (small molecule or polymer) in another but, at equilibrium, the domains *always* revert to a spherical shape to minimize interfacial area. Colloidal particles have been shown to be interfacially active, forming monolayers at the interface between two fluids,[8, 18] but, in the absence of an active external field, the fluids assume a spherical shape. Colloids are also large, so the time to assemble and organize at the interface is long. Since the reduction in the interfacial energy per particle is large,[19] the colloidal assemblies often form 2-D crystals, solidifying the assemblies.[8, 18] With NPs, on the other hand, time scale for assembly is shortened, the assemblies are disordered, but the energy holding the NP at the interface is small.[20, 21] Consequently, any in-plane compressive force will eject the NP from the interface and the fluids will assume spherical shapes. Locating the NPs at the interface requires that the contact angle between the NPs and *both* fluids be 90^{o}, i.e. the interactions between the NPs and both fluids must be balanced.[22-24] Achieving this is exceptionally difficult. Micron-sized Janus-type particles have been studied, where the two halves of the particle interact favorably with either fluid.[25-27] Preparing large quantities of Janus-type colloidal particles is a formidable task, which is made even more difficult for NPs.

Cates and coworkers theoretically developed the concept of *bijels*, bicontinuous interfacially jammed emulsion gels, and experimentally realized this behavior with mixtures of water, lutidine and colloidal particles that undergo spinodal decomposition.[28-31] As domains of water and lutidine developed, the colloids segregated to the interface between the fluids and, as phase separation progressed,

the reduction in the interfacial area jammed the colloids at the interface, arresting phase separation. Bicontinuous domains of water and lutidine, separated by a layer of colloidal particles, were kinetically trapped. However, producing bijels by this route, is *very restrictive*. The fluids must spinodal phase separate to ensure bicontinuity of the phases, the temperature dependence of interaction energies must be large, and colloidal particles are required to locate the particles at the interface. While the concept of bijels is elegant and their applications are many, due to the restrictions described, they have remained an academic exercise.

Recently, it was found that if functionalized NPs are dispersed in one fluid and polymers having a complementary functionality at one end are dispersed in a second fluid, the NPs and polymers interact at the interface, forming NP surfactants, a NP head with multiple polymer tails.[32] The number of polymer chains attached to the NP is self-regulated, to maximize the reduction in the interfacial energy. The NP surfactant assemblies are disordered, forming a liquid monolayer at the interface. By deforming the liquids (with shear, electric or magnetic fields), the interfacial area increases, exposing bare interface, and more NP surfactants form and assemble at the interface. When the external field is removed, the systems attempt to reduce interfacial area causing the NP surfactants to jam, locking-in the shape of the liquids *indefinitely*.

These initial studies have opened an entirely new concept in materials design, *structured liquids*, where any two immiscible fluids can be shaped and the structure lock-in by the interfacial jamming of the NP surfactants. If an external field is applied to the structured liquids, the load-bearing percolated pathways of the NPs at the interface are broken, returning the NP assemblies to a liquid state that will again jam when the field is removed. Consequently, these structured liquids are responsive to external fields. These initial findings, while very promising, have raised numerous fundamental scientific questions.

1.3 Interfacial Tension

If two homogeneous bulk phases are in contact, there is a region of finite thickness where the properties change, that region is called interface. The density profile across the interface (measured normal to the interface) establishes and interfacial width that depends on the degree of immiscibility between the components, the more immiscible, the sharper is the interface. Figure 1.1, for example, shows that the interface between water and decane is only a few angstroms.[33] The interface between the two phases is in tension, due to an imbalance of molecular forces at the interface. The forces on the molecules located at the interface differ from those in the bulk, as shown in Figure 1.2. Therefore, interfacial area is minimized. Interfacial tension is defined as the work required to

impose an increase in the surface area. Commonly, interfacial tension has dimensions of force per unit length, or of energy per unit area. The two are equivalent, but when referring to energy per unit of area, it is common to use the term surface energy.

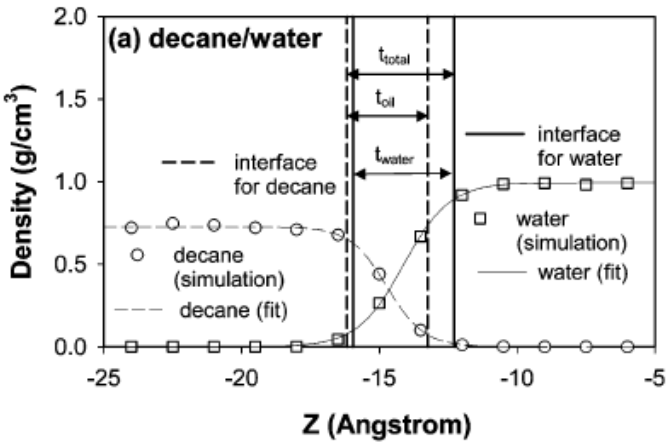

Figure1.1 Definition of interfacial thickness between water and decane via density profile.[33]

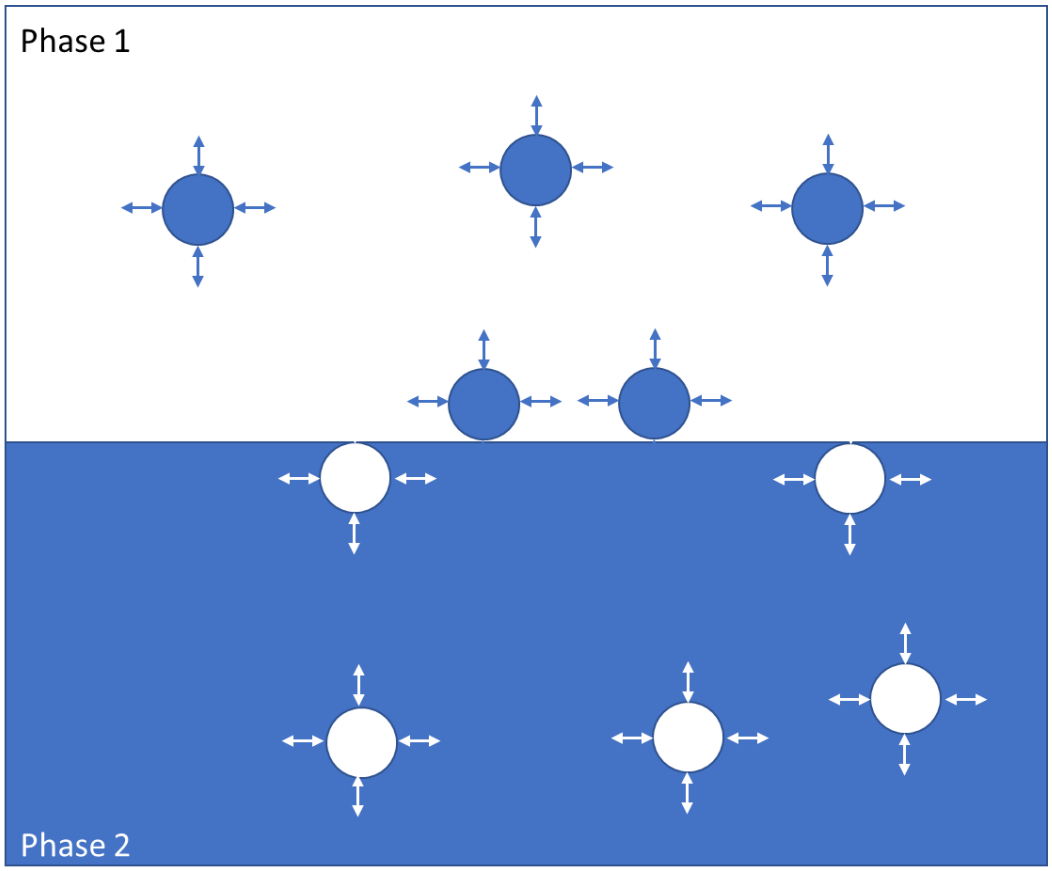

Figure 1.2 Diagram of molecular force in solution and at interface when two immiscible liquids contact.

Techniques to measure surface and interfacial tension are separated here into two main categories: (1) force tensiometry, where the force the surface imparts on a probe is directly measured, including Du Nouy ring, Wilhelmy plate, and platinum rod methods, (2) optical tensiometry, where the shape of a drop or bubble extracted from an image is fit to a theoretical equation, this technique is commonly referred to as axisymmetric drop shape analysis (DSA). A pendant drop tensiometer uses DSA, where a liquid droplet is suspended from a needle in another liquid and the shape of the droplet is imaged, as shown in Figure 1.3a. The measured shape parameters are used to determine the droplet shape that is then fit with the Young-Laplace equation to calculate interfacial tension. This method is used extensively throughout this dissertation.

Pendant drop tensiometry was first proposed by Worthington over a century ago, where he hypothesized the shape of the drop results from the relationship between interfacial tension and gravity.[34] As a consequence, interfacial tension can be determined from the drop shape, based on the Young-Laplace equation[35], which relates the Laplace pressure across an interface to the curvature of the interface and the interfacial tension γ:

$$\gamma\left(\frac{1}{R_1}+\frac{1}{R_2}\right)=\Delta P=P_0-\Delta\rho g z \tag{1}$$

where R_1 and R_2 are the principal radii of curvature; $\Delta P = P_{in} - P_{out}$ is the Laplace pressure across the interface; $\Delta\rho = \rho_d - \rho$ is the density difference between the droplet and continuous phase. For a pendant drop the principal radii of curvature at the vertex (lowest point of the drop) are: R1=R2=R (shown in Figure 1.3b). Thus, it is convenient to place the reference plane at this point. For every point above this, $R_2 = \frac{x}{\sin\phi}$. This leads to:

$$\frac{1}{R_1}+\frac{\sin\phi}{x}=\frac{2}{R}-\frac{\Delta\rho g z}{\gamma} \tag{2}$$

The introduction of a parametrization using the arc length s of the drop shape results in the following set of three first-order differential equations with three boundary values, which is solvable by numerical procedures:

$$\frac{d\phi}{ds}=-\frac{\sin\phi}{x}+\frac{2}{R}-\frac{\Delta\rho g z}{\gamma} \tag{3}$$

$$\frac{dx}{ds} = cos\phi \tag{4}$$

$$\frac{dz}{ds} = sin\phi \tag{5}$$

$$0 = x(s = 0) = z(s = 0) = \phi(z = 0) \tag{6}$$

Interfacial tension is the work (energy) required to generate interface. Effective reduction of interfacial tension is the key to realize the stabilization of large interfacial areas and structuring and locking-in non-equilibrium liquid shapes. Surface active materials are meant to reduce interfacial tension between two liquids, which will be discussed in the next section.

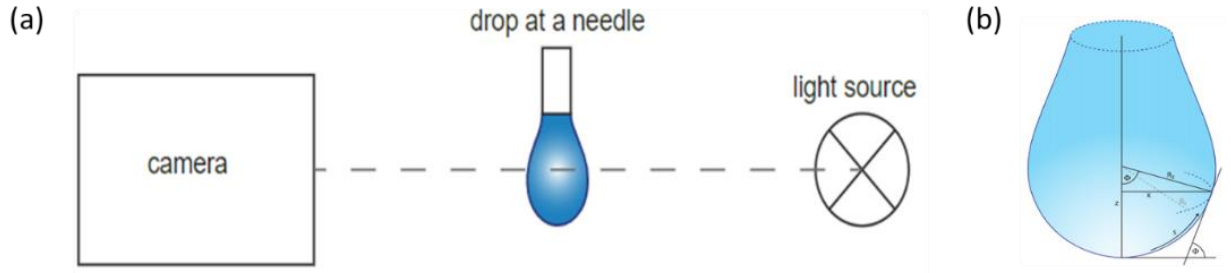

Figure 1.3 (a)Schematic setup for pendent drop method (b) associated variables used for Young-Laplace fit on a pendant drop

1.4 Interfacially active materials

There are mainly three types of materials that can reduce interfacial tension between two immersible liquids: (1) *surfactants* (**surf**ace **acti**ve **a**ge**nts**), molecules that have hydrophilic and hydrophobic parts, are the most commonly used and can be easily found in nature or synthesized; (2) *colloids*, which are not amphiphilic, but the interactions between the liquids and the colloid are less the interactions of the two fluids with each other and the colloids reside at the interface to reduce the total energy of the system, [36] and (3) *nanoparticle surfactants (NPSs)*, formed at the interface by the anchoring of ligands dissolved in one liquids to the surface of functionalized nanoparticles dispersed in the second liquid, forming effectively a supersurfactant, where the binding energy of the NPS is markedly greater than the one holds the NP or the ligand. We will discuss these interfacially active materials, their similarities and differences, in the following sections. We will discuss why Janus nanoparticles (JNPs), nanoparticles with part of the surface being hydrophilic and the remaining part being hydrophobic, afford new pathway to stabilize one liquid domain in another and also structure liquids.

1.4.1 Surfactants

A surfactant is defined as a substance which has the property of adsorbing onto the interfaces of a system and tends to reduce the interfacial tension between two phases. Commonly, surfactant molecules, either small molecules or polymers, are amphiphilic, having both hydrophilic (water-loving, polar) and lipophilic (fat-loving) properties. When a small amount of surfactant is dissolved in one liquid phase of a two liquids system, such as water/oil, the molecules segregate to the interface with their hydrophilic heads in the water phase and the hydrophobic tail facing in the oil phase to reduce interfacial tension. The hydrophilic-lipophilic balance(HLB) of a surfactant is a measure of the degree to which it is hydrophilic or lipophilic, determined by calculating values for the different regions of the molecule, as described by Griffin: [37, 38]

$$\mathrm{HLB} = 20 * \frac{M_h}{M} \tag{7}$$

where M_h is the molecular mass of the hydrophilic portion of the molecule, and M is the molecular mass of the whole molecule. As shown in Figure 1.4, the HLB system is particularly useful to identify surfactants for oil and water emulsification. Water in oil (W/O) emulsions require low HLB surfactants, Oil in Water (O/W) emulsions require higher HLB surfactants. Increasing the surfactant concentration in the bulk would lead to saturation of surfactants at interface and the remaining molecules in bulk form aggregates such as micelles. The interface saturation concentration is called critical micelle concentration (CMC), which can be used as a measure of surfactant efficiency.[39]

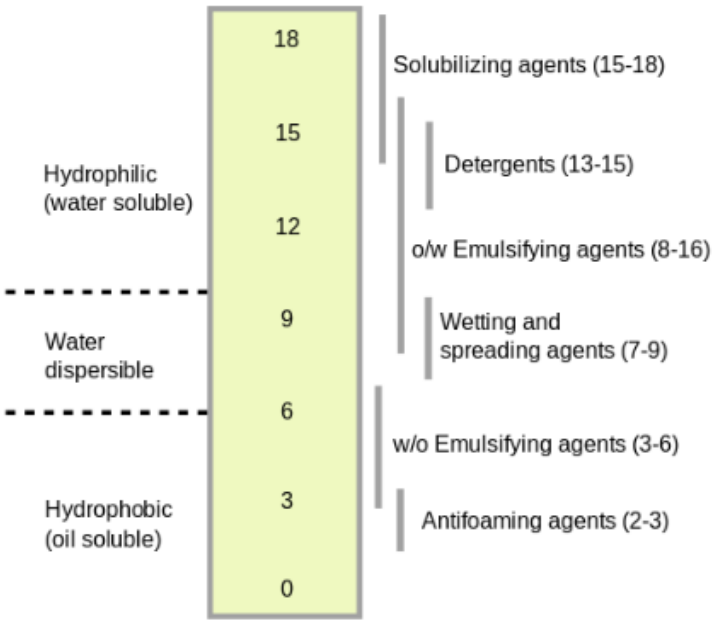

Figure 1.4 HLB scale showing classification of surfactant function. [37]

The reduction of the interfacial tension by surfactants has been used in many applications, including oil recovery, food additives, emulsification, encapsulation for pharmaceuticals, foaming for purification and, of course, for making bubbles, that has entertained us for centuries.[40-45] Despite the great success, structuring the liquids into non-equilibrium, i.e. non-spherical, shapes cannot be achieved solely with surfactants, since the driving force to return to the equilibrium spherical shapes is driven by a reduction in the total energy and, therefore interfacial area. This reduction in the interfacial area exerts a compressive force on materials assembled at the interface and the binding energy of simple surfactants is small and the surfactants are ejected from the interface.

1.4.2 Colloids

Colloids are particles that range in size from tenths to tens or hundreds of microns. Colloids can be hard, as for example metal, silica or carbon, or "soft", as for example microgels and bacteria. Colloidal particles, similar to surfactant molecules, will segregate to the interface between two immiscible fluids (liquid–gas or liquid–liquid) to reduce interfacial tension and form a monolayer at interface. As mentioned in 1.3.1, the tendency of a surfactant is quantified in terms of the HLB. In the case of spherical particles which adsorb to interfaces (fluid-fluid) the relevant parameter is thought to be the contact angle θ which the particle makes with the interface.[46] If particles are hydrophilic, such as metal oxides, the contact angle into aqueous phase is smaller than 90 degrees with the majority of the particle residing in water, and O/W emulsions may form as a consequence. For hydrophobic particles, the contact angle is generally greater than 90 degrees and the particle resides more in oil, forming W/O emulsions (shown in Figure 1.5).

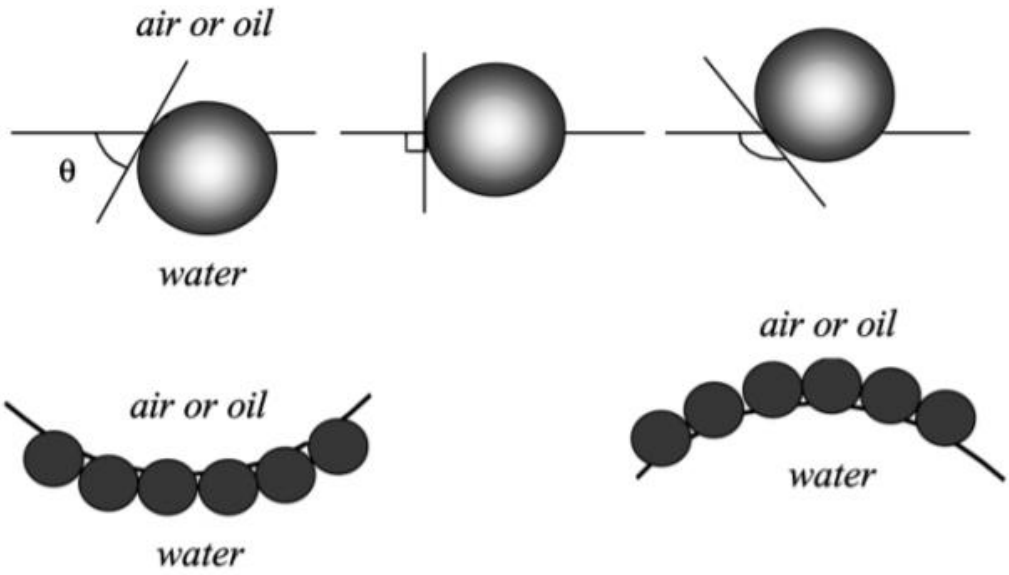

Figure 1.5. (Upper) Position of a small spherical particle at a planar fluid/water interface with contact angle θ less than(left), equals to(middle), greater than(right) 90 degrees. (Lower) Corresponding probable positioning of particles at a curved fluid/water interface. O/W emulsions may form if θ < 90 degree and W/O emulsions may form if θ > 90 degree.[46]

As shown in Figure 1.6, the stabilization of emulsions can be achieved not only by classical surfactants, but also by solid particles that adsorb to the interface between two immiscible liquid phases. This behavior, first reported by Pickering, were not well-understood energetically.[36]. In 1980, Pieranski argued that there is an interfacial energy well is produced when the particle sits at the interface. For a spherical particle (radius=r) at an interface having a contact angle θ (see Figuure1.7), the interfacial energy can be calculated as:

$$\mathrm{E(z)} = \pi r^2 [\left(\frac{z}{r}\right)^2 + 2\left(\frac{\gamma_{p/o}}{\gamma_{o/w}} - \frac{\gamma_{p/w}}{\gamma_{o/w}}\right)\left(\frac{z}{r}\right) + 2\left(\frac{\gamma_{p/o}}{\gamma_{o/w}} + \frac{\gamma_{p/w}}{\gamma_{o/w}}\right) - 1] \ , \qquad (8)$$

where $\mathrm{E(z)_{min}}$ at $\mathrm{z} = \frac{\gamma_{p/w} - \gamma_{p/o}}{\gamma_{o/w}} * r$. The change in the interfacial energy, ΔE, by placing one spherical particle of radius at interface is given by:

$$\Delta E = -\frac{\pi r^2}{\gamma_{o/w}}[\gamma_{o/w} - (\gamma_{p/w} - r_{p/o})]^2 \quad (9)$$

where$\gamma_{o/w}$, $\gamma_{p/w}$,and $\gamma_{p/o}$ are the interfacial tensions between oil and water, the particle and water, and the particle and oil, respectively.[19] Since $\sin\theta = \frac{z}{r}$, equation (9) can be written with contact angle θ:

$$\Delta E = -\pi r^2 \gamma_{o/w}(1 - |cos\theta|)^2 \quad (10)$$

$\Delta E_{max}\ at\ \theta = 90°$ means, particles with neutral wettability to water and oil are most stable at an interface. It also indicates that larger particles are held at the interface more strongly. A 0.5 mm particle can reduce interfacial energy by 10^4 k_bT.[47] This is a very important difference between the colloids and surfactants as interfacially active materials, that the energy holding particles at an interface depends upon the both contact angle of particle at interface and size of the particles, whereas the energy holding small molecular surfactants at interface solely depends on their amphiphilicity. For micro-sized particles, the substantial reduction of interfacial tension per particle and the uniformity of particle size can lead to 2D particle crystallization, solidifying the interfacial assembly, and possibly locking a non-spherical shape under applied external field.[22, 23, 46]

The concept of **bijel**s (bicontinuous interfacially jammed emulsion gels) was introduced by Cates, Clegg and coworkers.[29] The concept has been experimentally realized with the immiscible water/lutidine system with colloidal particles.[28, 30, 48, 49] Under spinodal decomposition in response to change of temperature, domains of water and lutidine form with colloids segregate to the interface to reduce interfacial energy. As the phase separation continues, reduction of interfacial area leads to jamming of the colloidal particle assembly at the interface, and the system is arrested from further phase separation. The bicontinuous domains of water and lutidine were produced by the interfacial jamming of the colloidal particles. Producing bijels by this route, though, is restrictive. First one needs to have two fluids that undergo spinodal phase separation to produce the bicontinuous fluids. Second, the interactions of the particles with both fluids must be balanced, to locate the particles at the interface without a tendency of being drawn into either fluid or impart a curvature to the interface. Third, the interaction energies between the fluids must be large, to strongly bind the colloidal particles to the interface so that the compressive force exerted on the particles as the interfacial area is reduced does not

eject the particles from the interface. Furthermore, the large size of colloidal particles results in lengthy assembly time. Re-shaping the liquids leads to fracturing of assemblies, thus rapid responsiveness and rapid reconfigurability are difficult to achieve.[50]

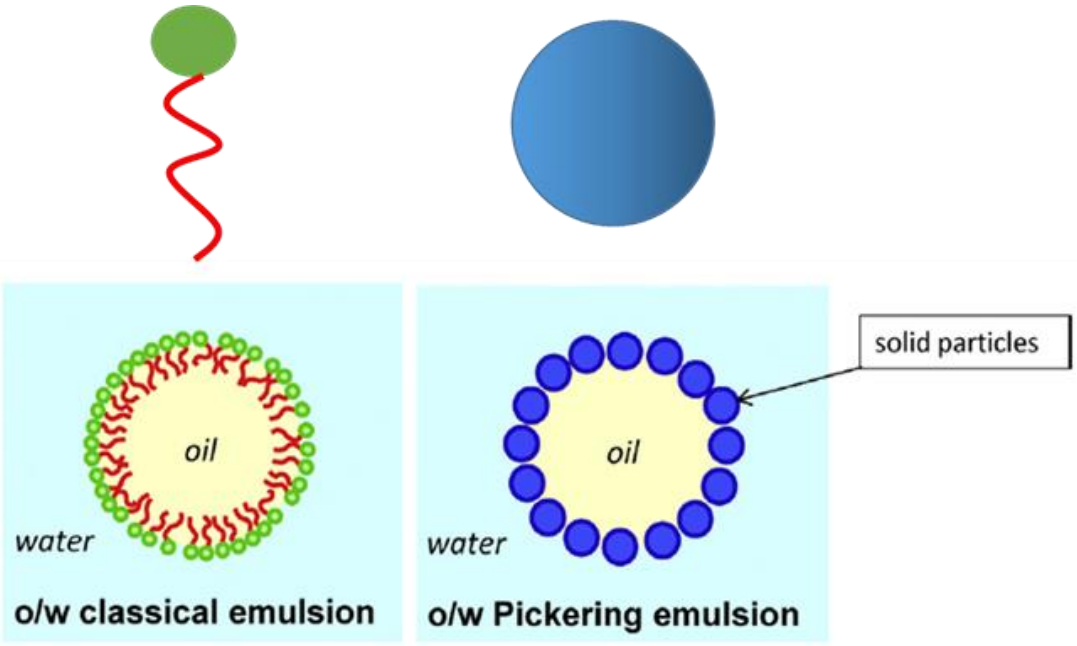

Figure1.6 Comparison of classical emulsion caused by surfactant and Pickering emulsion that solid particles segregate at interface.

In comparison to colloidal particles, the time scale for assembly of nanoparticle(NPs) is reduced by a factor of ~10^4 (base on diffusion coefficients in solution). The thermal energy and size distribution of NPs results in assemblies that are disordered and liquid-like. Also, as discussed by Pieranski, the energy binding the NPs to the interface is substantially smaller, due to their size, allowing[20, 21] the NPs assembled at interface to readily exchange with the NPs in the bulk liquid. Any type of compressive force will eject NPs from the interface, making structuring liquids with NPs impossible. There are two major pathways that can successfully structure liquids with NPs at interface. One is to coupling NPs with polymer ligands at interface and the other is to produce Janus type NPs.

1.4.3 Nanoparticle-ligand surfactants

Since the energy holding NPs are interface is close to thermal energy, that any compressive force can eject NPs from interface.[44] When under external field, droplet can deform into non-spherical shapes, once the field is removed, system ultimately relaxes to a monolayer of NPs assembled on spherical droplets, leading structuring liquids with solely NPs not possible. To circumvent this, Russell and

coworkers developed the idea of nanoparticle surfactants(NPSs), where functionalized NPs are dispersed in water and end-functionalized polymer ligands that have complementary functionality are dissolved in oil. The end-functionalized ligands are interfacially active such that they can assembled at the interface with the functional end-group sticking out to water phase. NPs in the aqueous phase move to interface by diffusion and can interact the polymer ligands, forming NPSs where the NP polar associates with multiple hydrophobic polymer tails in the oil (Figure 1.8).[45] Like NPs assembled at an interface, the system forms a disordered monolayer of NPSs at interface, however, the reduction of interfacial tension by NPSs is substantial. If the shape of water droplet is distorted by electric field, interfacial area increases with constant volume of droplet that allows more NPSs to form at interface. Once the external field is removed, the droplets try to relax back to the spherical shape to minimize interfacial area, placing a compressive force on NPSs assembled at the interface. Since the binding energy of each NPS is large, the NPS will not leave the interface but laterally jam, locking-in a non-equilibrium shape of the liquid phases.(Figure 1.8)[45]

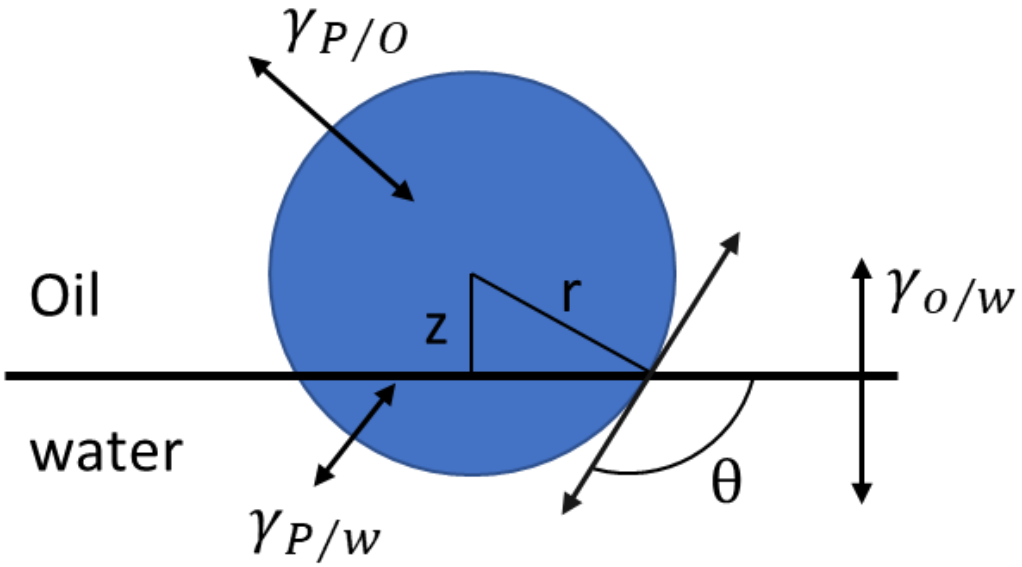

Figure 1.7 Schematic of a spherical particle with radius of r absorbs onto oil/water interface with contact angle of θ.

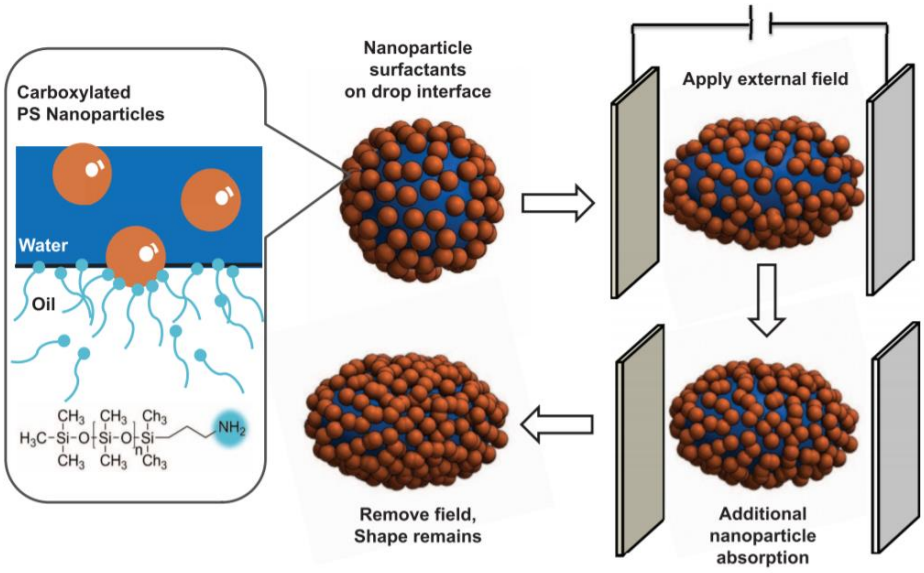

Figure 1.8 Schematic representation of the deformation of a spherical drop, cladded with nanoparticle surfactants, by an electric field, into an ellipsoid whose shape is maintained after the removal of the field by the interfacial jamming of the nanoparticle surfactants.[32]

1.4.4 Janus Nanoparticles

Apart from NPSs, amphiphilic Janus nanoparticles (JNPs), having one hydrophobic and one hydrophilic hemisphere, represent another strategy to promote the interfacial assembly of nanoparticles.[51] De Gennes originally proposed that JNPs would adsorb to the liquid/liquid or liquid/air interface to form a monolayer.[52] The interfacial activity of JNPs is markedly increased in comparison to uniformly functionalized nanoparticles, due to the amphiphilic nature of the particles as the two halves of the particles interact favorably with either liquid.[27, 53, 54] It is useful to distinguish two different characteristics of JNPs, surface activity and amphiphilicity. Surface activity is the tendency of particles to adsorb at surfaces, whereas amphiphilic means the two parts of the particle have different affinities for the solvent(s). Homogeneous particles with a 90 of contact angle at a oil-water interface are strongly surface active but not amphiphilic. Janus particles are both surface active and amphiphilic, which enables JNPs to strongly bind at an interface without having contact angles near 90 degrees.[55] Like surfactants, JNPs are held strongly at the interface but will not be ejected from the interface when compressive forces are applied. The interfacial assembly of JNPs is very effective for stabilizing emulsions.[56]

Many studies have shown that inorganic JNPs can reduce interfacial tension and stabilize emulsions yet preparing large quantities of precisely defined Janus type

colloids or inorganic nanoparticles is non-trivial. [25, 57-59] Soft JNPs, on the other hand, can be prepared in reasonable quantities from triblock copolymers and have been shown to be interfacially active.[60-62] However, their behavior, such as their assembly, jamming, and reconfiguration at liquid interfaces have not been well studied in the past. Thus, we focus on the study of these soft polymeric Janus particles and their assemblies at liquid interfaces, as well as their potentials to structure liquids.

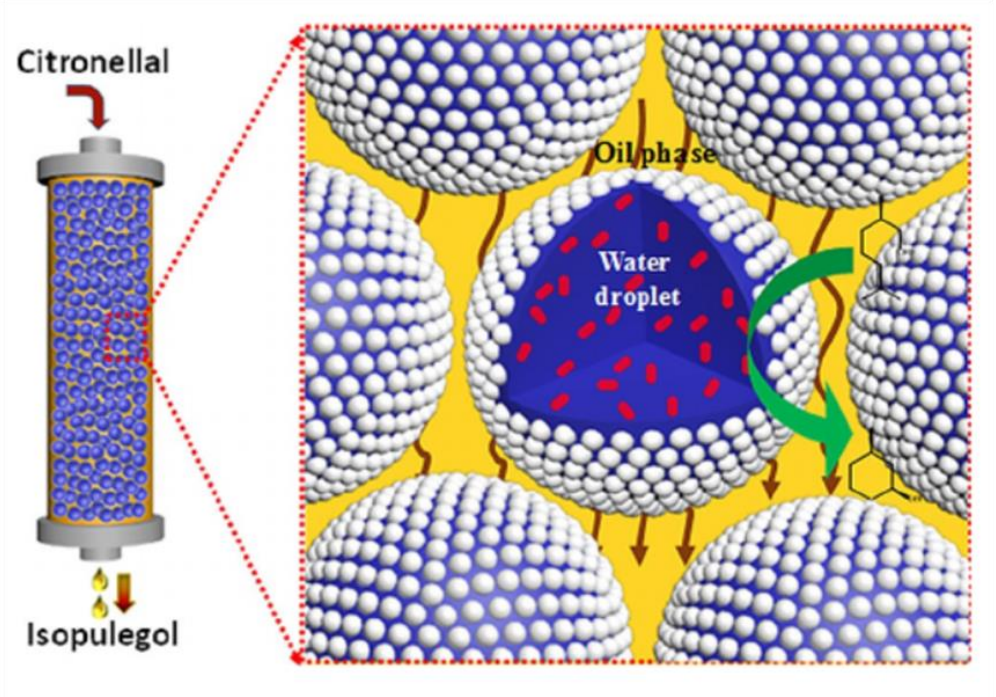

Figure 1.9 A flow-through Pickering Emulsion system for catalytically accelerated oil–water biphasic reactions.[63]

1.5 All liquids systems and devices

Liquid–fluid interfaces provide a platform both for structuring liquids into complex shapes and assembly of confined, multi-functional nanomaterials. Much attention has focused on stabilizing emulsions and foams, in which surface-active materials, as described in the previous sections, stabilize structures against liquid droplet coalescence and alter the mechanical properties of the liquid interfaces.[64-69] Recently, new research areas have begun to demonstrate the full potential of the assembly of nanomaterials at liquid–liquid interfaces to generate all liquid, functionally complex, biomimetic systems.[70] Pickering emulsions, with one liquid dispersed within another where colloidal particles (typically micrometer-sized) adsorb to the liquid–liquid interface, have been used to construct all-liquid devices. Yang and co-workers have successfully developed a Pickering emulsion system with applications as biphasic chemical synthesis reactors (Figure 1.9).[63, 71-73] The

applications rely on particles irreversibly absorbing onto interfaces of droplets that are closely packed, which enables the droplets to be highly resistant to coalescence and Ostwald ripening. The catalyst placed inside of silica NP-stabilized water droplets which are stacked and immobilized within a column reactor. As an organic phase flows through the system that contains an oil-soluble reactant, reactions could be performed at the oil–water interface with reactant molecules and reaction products continuously flowing through. Such systems can significantly reduce reaction times that are typically required in batch processes, and no further removal of catalyst is needed post-reaction.

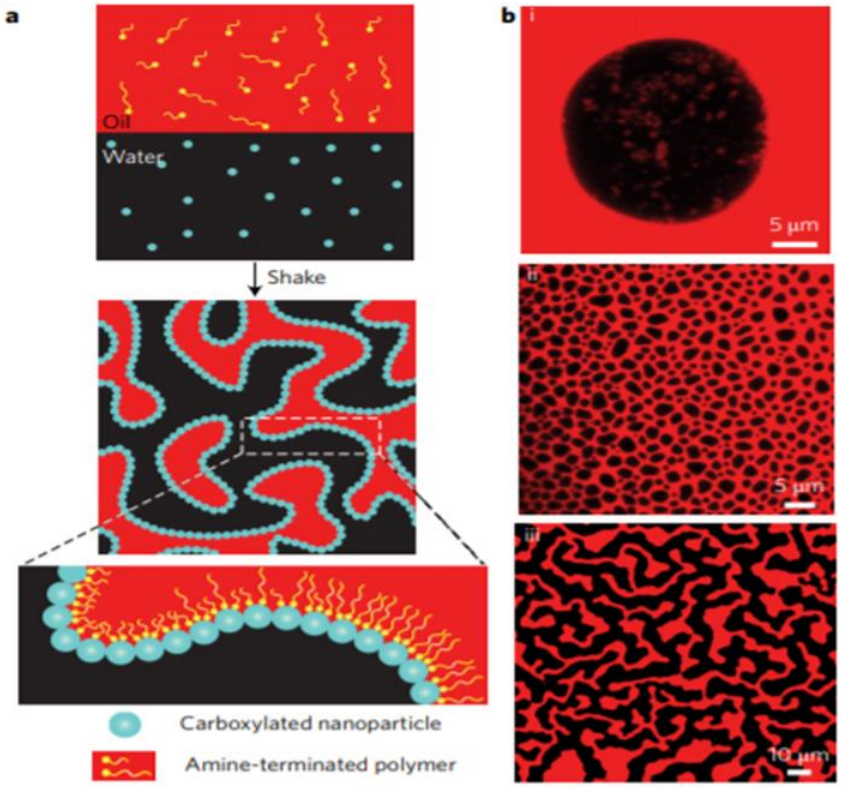

Figure 1.10 (a) Schematic showing the formation of bijels formed by the jamming of nanoparticle surfactants at the oil–water interface. (b) Emulsions stabilized by a single molecular weight of PDMS-NH_2 in toluene (i) M_w = 1,000 g/mol, (ii) M_w = 3,000 g/mol; water contains 1 mg/mL nanoparticles. (iii) Bicontinuous system stabilized by nanoparticle surfactants consisting of an equimolar mixture of 1,000 g/mol and 3,000 g/mol PDMS-NH_2 and nanoparticles (0.5 mg/mL).[31]

Huang and co-workers generated bijel structures with sub-micrometer domains via NPSs assembly at water/oil interface.[31] As shown in Figure 1.10a, ligands(shown in yellow) with amine groups are dispersed throughout the oil or solvent, and nanoparticles coated with carboxylic acids (shown as blue dots) are

scattered in the water. With vigorous shaking, the nanoparticles and ligands form NPSs that get trapped and jammed at the interface of the two liquids(Figure1.10b). The bijel formation can be achieved when nanoparticles bonds to two ligands that have the same functionality but different molecular weight, while W/O emulsions were formed if all the ligands in oil have the same molecular weight. The generation of bijel is greatly simplified, in comparison with bijels produced via spinodal decomposition which requires the fulfilment of several stringent criteria.

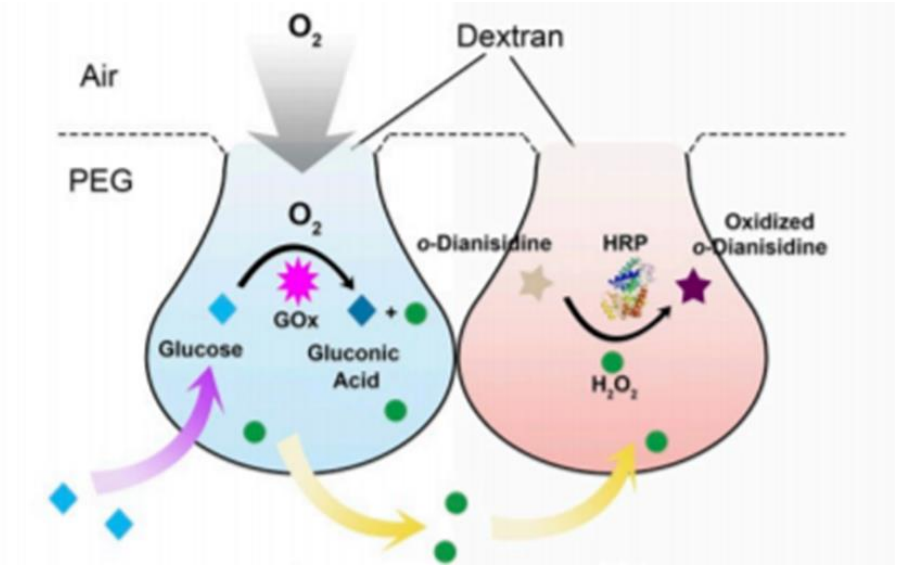

Figure1.11 Schematic of the bioinspired hanging microreactor system. A hanging droplet absorbs glucose from the PEG solution and takes in oxygen from the air to oxidize the glucose. The hydrogen peroxide produced diffuses into and fuels the reaction in the neighboring hanging droplet.[77]

An aqueous two phase system (ATPS) is generated when a pair of hydrophilic polymers (such as polyethylene glycol (PEG) and dextran) are immiscible with one another.[74] Such ATPS presents have properties like a near-zero interfacial tension and excellent biocompatibility.[74-76] Xie and co-workers have extended the application of nanomaterials assembly at liquid interfaces to structure liquid to ATPSs.[77] When dense droplets of dextran solution containing polycations are dropped into a PEG solution (less dense) containing polyanions droplets can hang from an interface by surface tension to build two-dimensional assemblies of structurally complex droplets as a polyelectrolyte coacervate forms at the interface between the two aqueous phases that prevents the droplet from sinking. Selective ion diffusion between the hanging droplets and the bulk solution was also observed, which enables the development of smart reactors where reagents can be selectively exchanged between compartmentalized hanging droplets.[78, 79] As an example, One of these droplets contained glucose oxidase (GOx), which was shown to react

with oxygen from the surrounding air, after absorbing glucose from the bulk PEG phase to produce hydrogen peroxides which later diffuse into a neighboring droplet to initiate horseradish peroxidase (HRP)-catalyzed o-dianisidine oxidation. (Figure 1.11).

These examples clearly show great potential to generate and construct all liquid devices and systems via self-assembly of materials at complex liquid interfaces. A variety of materials can be assembled at liquid–fluid interfaces, from NPSs, to polyelectrolyte–polyelectrolyte complexes, to nanocrystals and colloidal particles, all of which have a promising future.

1.6 General approach and synopsis of subsequent chapters

The work described in this dissertation has been a natural progression, starting with a fundamental understanding of soft JNPs assembled at water/oil interfaces. In Chapter 2, the concept is demonstrated that soft type polymeric JNPs are interfacially active and can assembled at W/O interfaces, while the kinetics of JNPs assembled at the interface is studied and the mechanism of soft JNPs assembly at the interface is proposed in difference to any hard-type materials. The search for fundamental understanding of the soft polymeric JNPs led to a rational design that optimized the interfacial activity. In chapters 3 and 4, further tailoring of JNPs interfacial activity, under the framework from chapter 2, was successfully demonstrated by varying the softness and anchoring JNPs by complementary ions from water phase. In Chapter 4, understanding developed in the early chapters was applied toward the ability of JNPs with different ion complexity to stabilize water in oil emulsions and their stabilities was demonstrated. With more ion complexations with JNPs at interface, the JNPs holding onto interfacial with more dense packing and better stabilize emulsions droplets. In chapter 5, preliminary results show some rational prospective of designing JNPs such as having more arbitrary shapes and increasing amphiphilicity to further tune their interfacial activities. In all, a comprehensive understanding of soft JNPs at interface is presented, which benefit further design and application of soft JNPs in structuring liquids.

Chapter 2

Understanding the Assembly of Janus Particles at Liquid Interfaces

In this chapter, the self-assembly and interfacial jamming of soft spherical Janus nanoparticles (JNPs) at the water/oil interface are discussed. We use polymeric JNPs, made by cross-linking triblock copolymers of polystyrene-block-polybutadiene-block-poly(methyl methacrylate) (PS-PB-PMMA), as a model Janus type material to exam their interfacial activity at the water/oil interface. We find that these soft JNPs are highly interfacially active, even though none of the components of the triblock copolymer is water soluble. The JNPs self-assemble at the interface, reducing the interfacial energy, but the interfacial assembly is dynamic, responsive to changes in the pH of the aqueous phase. Unlike hard particles, JNPs composed of polymer chains can spread at the liquid− liquid interface to maximize coverage at relatively low areal densities. In pendant drop geometry, the interfacial area of a water droplet in oil is significantly decreased and the JNPs are forced to pack more closely. Entanglements of the polymer chains cause the JNPs to form a solid-like interfacial assembly, resulting in the formation of wrinkles when the interfacial area is decreased. The wrinkling behavior, the retention of the wrinkles, or the slow relaxation of the liquid drop back to its original equilibrium shape were found to depend upon pH. The results demonstrate a unique behavior of polymer-functionalized JNP assemblies at liquid-liquid interfaces, establishing a framework for tailoring the interfacial activity and assembly of JNPs.

2.1 Introduction

JNPs can be used to reduce interfacial energy. Much progress has been made to embed a Janus character to synthetic nanoparticles, such as emulsion-based methods, particle replication with templates, and microfluidic methods.[1-4] Various types of JNPs have been designed and their interfacial activity have been investigated.[5-11] However, preparing large quantities of precisely defined JNPs is non-trivial. Recently, the controlled cross-linking of microphase separated multi-compartment micelles of ABC triblock terpolymers was shown to provide a simple, scalable route to generate polymeric JNPs.[12-14] Here, the volume fraction and molecular weights of the blocks can be varied over a broad range, providing simple routes to control the size and nature of the JNPs. In addition to the chemistry of the polymer blocks, the Janus balance can also be precisely tailored to achieve tunable interfacial activity. The interfacial assembly of polystyrene-block-polybutadiene-block-poly(methyl methacrylate) (PS-PB-PMMA, SBM) JNPs at polymer/polymer interfaces has been demonstrated, where a monolayer of the JNPs assembles at homopolymer/homopolymer interfaces, reducing the interfacial energy and size of the domains. Even at high shear forces in a twin-screw extruder the JNPs remained at the interface and droplet deformation, rather than droplet coalescence, was

observed. These results underscore the high interfacial activity of these types of polymeric JNPs.[15-17] The JNPs consist of a cross-linked PB core with a corona consisting of two hemispheres of immiscible polymer chains, polystyrene (PS) and poly(methyl methacrylate) (PMMA), anchored to the cross-linked PB core. The interfacial behavior of JNPs and the influence of JNP shape (i.e., spherical, cylindrical, and disk-like) to reduce interfacial energy between immiscible liquids have been reported.[7, 18] However, their interfacial jamming behavior at liquid−liquid interfaces is less understood. In contrast to static, nondeformable colloids, these JNPs consist of flexible chains that can interpenetrate when the two JNPs are compressed. This should dramatically influence the packing of the JNPs at fluid interfaces and their characteristic packing transitions. Tunability can be provided by a range of solvents, since the interactions with the two coronas dictate the configuration of the chains, and the cross-sectional area of each corona at the interface. The asymmetry of the corona at the interface will influence the curvature of the droplet. Temperature and pH, in the case of water-soluble blocks, should also influence the interfacial behavior of the JNPs. We focused on the interfacial jamming of these soft polymeric JNPs at the water/toluene interface, aiming to gain a comprehensive understanding of the kinetics and mechanism of their assembly and the role of pH.

2.2 Results and Discussion

Here, the soft JNPs were generated from the self-assembly of linear tri-block copolymer in solution.[12, 13, 19] First, linear triblock SBM copolymers were synthesized by anionic polymerization , yielding SMB copolymers with narrow molecular weight distributions (PDI<1.1).[20] The detailed synthetic route for SBM linear triblock copolymers synthesis can be found in Figure 2.1. As shown in Figure 2.2, the copolymers were dispersed in a good solvent for PS and PMMA but a non-solvent for the middle PB block, to form core-corona micelles. Subsequently, the solvent was exchanged for a selective solvent for PMMA. With the selective solvent, the PS chains segregate, forming multicompartment micelles. The number of subunits is determined by the volume ratio of PS and PB. The PB cores within multicompartment micelles are crosslinked by applying Ultra Violet (UV) light, to lock-in the core-shell structure. Finally, the micelles were dissolved in a good solvent for all the three blocks, and soft JNPs are produced. The final shape of JNPs is determined by weight ratio between PS and PB. In this chapter, the weight ratio between each polymers is fixed at PS:PB:PMMA = 40:20:40 and total molecular weight to be 108k Daltons, to generate spherical soft JNPs. The morphology of the JNPs was confirmed by transmission electron microscopy, as shown in Figure 2.3.

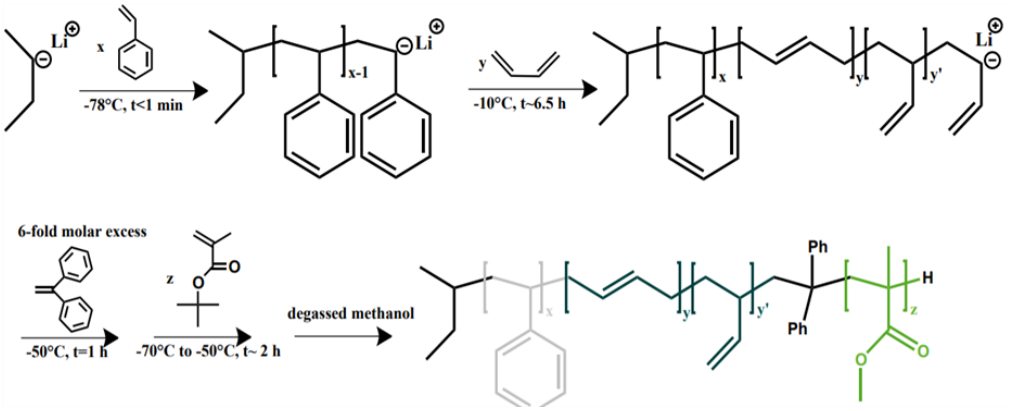

Figure 2.1 Synthetic route of SBM linear triblock copolymer

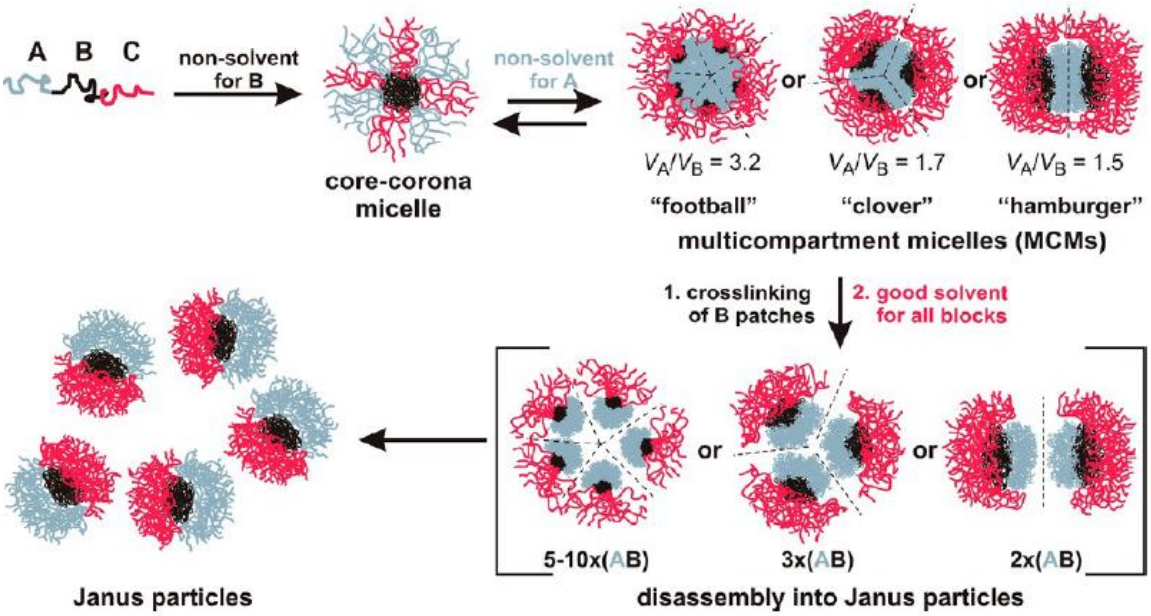

Figure 2.2 Schematic of self-assembly of ABC triblock terpolymers into mlticompartment micelles and subsequent disassembly into Janus particles.[12]

The water/toluene system was used since toluene is one of few solvents that are good solvents for all three polymer blocks of the JNPs. The average hydrodynamic diameter of the JNPs, as determined by dynamic light scattering, was ~64 nm (A.1.1(a)), this is consistent with the fact that toluene is a good solvent for all components and that no larger aggregates or micelles are involved in the interfacial assembly. As shown in A.1.1(b), these solutions were stable, showing no sign of aggregation, for at least 6 days after preparation. The size distribution of JNPs dispersed in dimethylacetamide(DMA). a good solvent for PS and PMMA but a non-solvent for PB, showed no significant difference compared to the toluene dispersion.(A.1.2) The results suggested that, the PB cores of JNPs does not swell

even in a good solvent of PB, i.e., the crosslink density is high, and serve as a hard particles with separated PS/PMMA coronae.

The interfacial tension, γ, between toluene and de-ionized water was measured by pendant drop tensiometry of a water droplet immersed in pure toluene or a solution of the JNPs in toluene. The droplet profile was fit with the Young−Laplace equation to determine γ. For the pure toluene/water system, the interfacial tension (IFT) is $\gamma \approx 35$ mN/m. Similar results were found for acidic (pH = 3.4) and basic (pH = 11.9) water against pure toluene, indicating that pH did not influence the IFT(A.1.3).

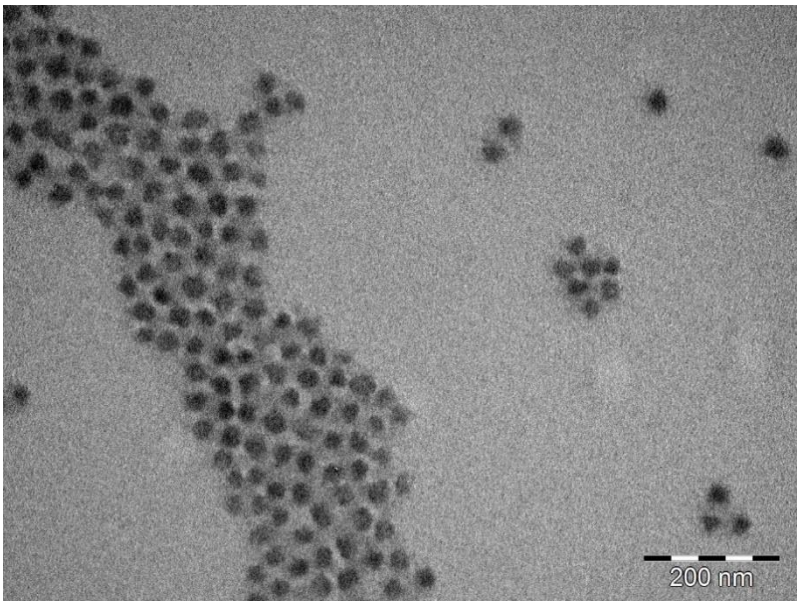

Figure 2.3 TEM image of S40B20M40, sample was stained by OsO4 prior to measurement.

Time-dependent IFT measurements at the water/toluene interface were performed with different concentrations of SBM JNPs dispersed in the toluene phase. An interface was created by injecting a pendant drop of water into a toluene solution containing SBM JNPs. Figure 2.4a shows that the dynamic IFT decreases with time, approaching a quasi-equilibrium value over a wide range of concentrations. The dynamic IFT profile composes two distinct regions: a fast early decay (first few hundred seconds), followed by a much slower reduction (over 6000 seconds). The fast decay corresponds to the initial recruitment of the JNPs to the interface, where the JNPs diffuse to and adsorb at the interface, and configurationally re-arrange to minimize the IFT with the constraint of stretching of the corona chains. As more JNPs adsorb, those JNPs already at interface must undergo further configurational changes to generate more space to recruit more JNPs. Such configurational change would lead the center of JNPs displaced from the interface into the toluene phase,

and PMMA are stretched parallel to the interface to maintain contact and coverage with water phase. A balance between the PMMA reconfiguration and the redutionn the IFT limit the number of JNPs that can adsorb to the interface at equilibrium. With increasing concentration of JNPs, the initial adsorption of the JNPs to the interface is too rapid to measure and the gradual reduction observed at longer times represents the rearrangement and reconfiguration of the JNPs. The equilibrium interfacial tensions at different concentrations are shown in Figure 2.4b. At low JNP concentrations the interface was not saturated by JNPs and the equilibrium IFT between the toluene solution of JNPs and water decreased with increasing JNP concentration. When the concentration was higher than ~0.027 mg/mL (A.1.4), the IFT decreased much more slowly with increasing JNP concentration. This transition in the concentration dependence of the interfacial tension, instead of reaching a plateau of IFT when the concentration is above the critical micelle concentration (CMC), suggests that the JNPs at the interface are dynamic and undergo configurational changes to accommodate other JNPs at the interface, forming a monolayer at interface.[20] Since PMMA is more polar, it is expected that the PMMA side of the JNPs faces the aqueous phase

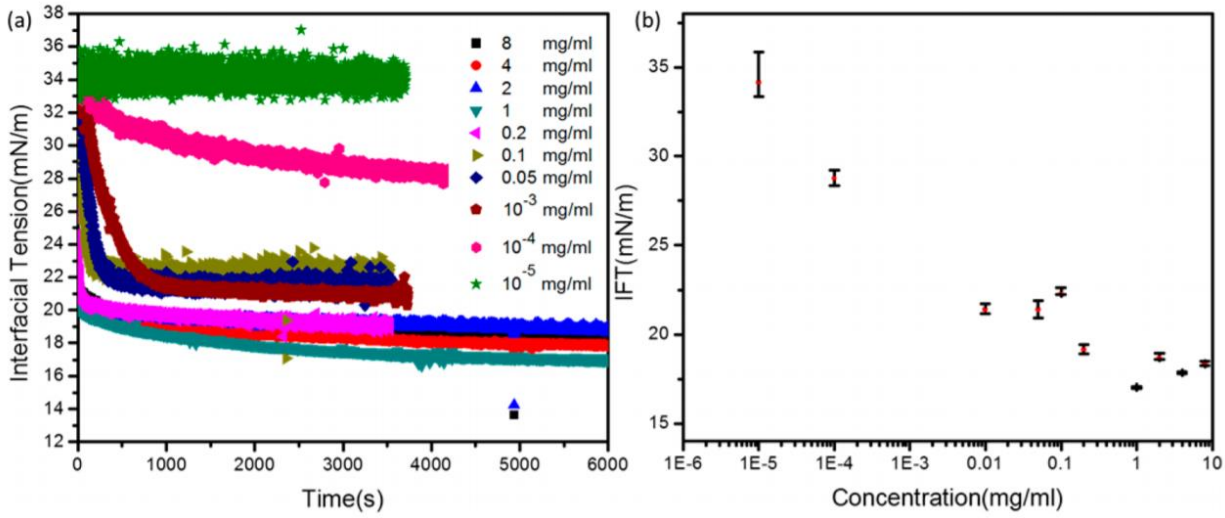

Figure 2.4 (a) IFT isotherms of deionized water against Janus particles in toluene solution at different concentrations. (b) Quasi-equilibrium IFT versus concentration.

The interfacial area was reduced by decreasing the volume of the droplet by retracting the aqueous phase into the syringe. This compresses the JNPs at the interface, forcing the JNPs to closely pack and, eventually, jamming of the JNPs at the interface. A further reduction in the interfacial area results in the formation of wrinkles at the interface.(Figure 2.5 a) Such wrinkling was found only for high JNPs concentrations (≥6 mg/mL), indicating the energetic gain for locating the JNPs at

the interface increases with increasing JNP concentration. Before the wrinkling experiment, water droplets (15 μL) were immersed in toluene solutions containing JNPs to allow them to assemble at the interface and to reach a constant interfacial tension, as shown in Figure 2.5 a. After 6000 seconds of aging, the droplet volume was reduced at a constant rate of 50 μL/min to decrease the interfacial area and compress the JNPs at the interface until wrinkling occurred, as shown in Figure 2.5 b. To observe wrinkling, the volume of the droplet had to be reduced by ~90%. In contrast, wrinkling is observed with only 9% droplet volume reduction for 50 nm silica nanoparticles with PDMS-NH2 ligands (Figure 2.6). The remarkable difference in the compression ratio to induce wrinkling arises from the initial spreading of the PMMA at the toluene−water interface. Both PS and PMMA are soluble in toluene. However, the interaction between PMMA and water is less costly energetically than the interaction of PS/water and toluene/ water, since PMMA is less hydrophobic than PS. Consequently, the PMMA chains will spread to cover the interface between toluene and water to minimize toluene/water and PS/water contacts. The extent to which the spreading occurs depends on the balance between the entropy required to stretch the chains at the interface and the gain in interfacial energy. As the volume of the droplet and surface area is decreased, the stretched PMMA chains can undergo a configurational change, even though the JNPs are in contact. As the surface area decreases further, the PMMA chains at the interface contract, with the center of mass of the JNPs being pushed away from the liquid−liquid interface and further into the toluene phase. It is expected that PMMA chains of neighboring JNPs will overlap. Upon further reduction of the interfacial area (droplet size) wrinkling occurs when it becomes energetically too costly for the JNPs to further compress and recede into the toluene phase. This type of behavior is far different from that observed for hard-spherical NPs where the transition from a liquid state to a jammed or vitrified state occurs over a much narrower range in the reduction of the interfacial area. When the droplet was suspended in toluene for longer times, e.g. 12 h, the wrinkling began at a smaller compression ratio (67%), which indicates that more JPs have adsorbed to and assembled at the interface (Figure 2.5 c). This behavior demonstrates the high interfacial activity of the JNPs, although there was no significant reduction in the interfacial tension. This result would be expected if the PMMA chains that spread on the surface were efficient in minimizing the non-favorable interactions of water/toluene and water/PS.

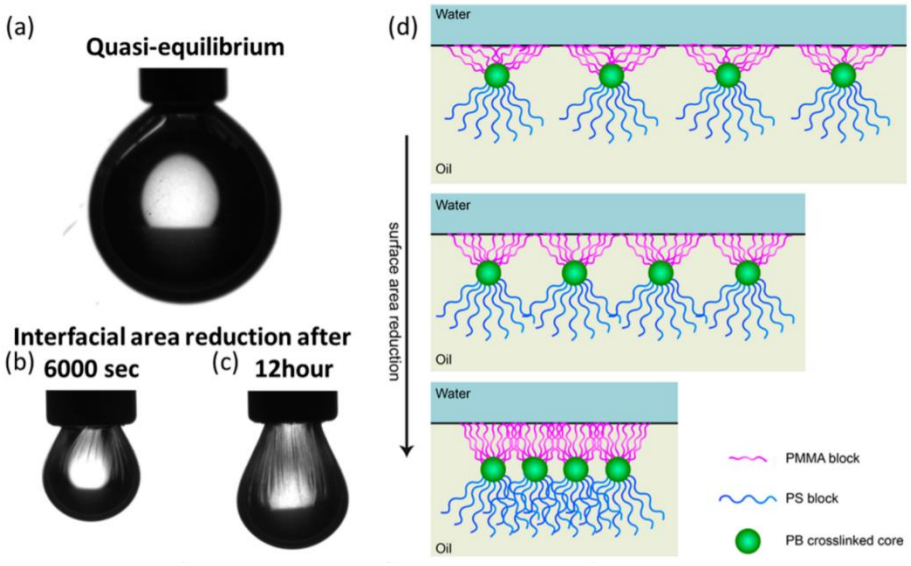

Figure 2.5 (a) Droplet after the IFT reaches quasi-equilibrium. (b and c) Droplet in toluene with interfacial area reduction until wrinkling with aging time of 6000 s and 12 h. For a−c droplet is water and environment is JNPs in toluene with a concentration of 8 mg/mL. (d) Schematic of wrinkling with reduction of interfacial area. (Top) PMMA chains spread out to cover the water/oil interface. (Middle) When the interfacial area starts to reduce, JNPs get close to neighboring particles and chains get stretched normal to the interface. (Bottom) On further reduction of interfacial area, it wrinkles when JNPs are closely packed to each other.

Figure 2.5(d) shows a schematic illustration of the JNPs adsorbed at the interface for different periods of time and the response of the JNPs to an applied compression. The assembly of the JNPs at the interface must occur in at least two distinct stages. The first is the migration of the JNP to the interface and a reorientation of the JNPs to place the more hydrophilic PMMA block toward the water phase. For a low surface coverage, the PMMA chains of the JNPs then stretch to cover the interface as effectively as possible. As more JNPs approach the interface, those JNPs at the interface will relax and reorganize at the interface, recovering some stored elastic energy in the stretched chains, allowing the additional JNPs to adsorb at the interface. Since the total number of PMMA segments at the interface does not change, the measured IFT is constant, although the total amount of JNPs increases. Interpenetration of PMMA chains of the JNPs facilitates the adsorption to the interface. Consequently, the number of adsorbed JNPs will increase over time, and the compression ratio to induce wrinkling will decrease.

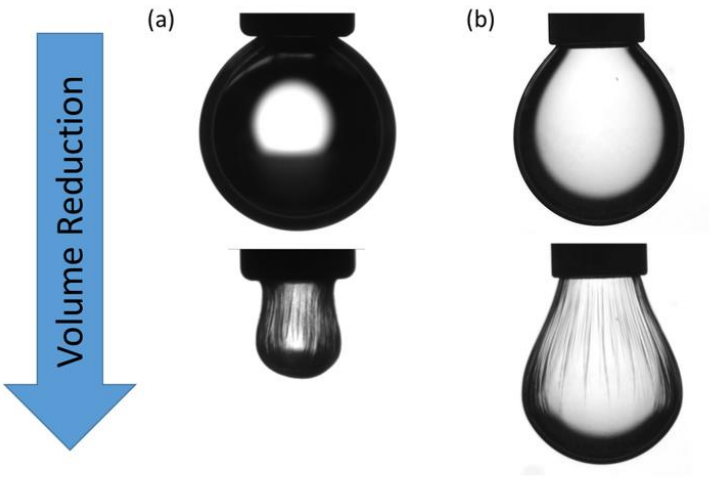

Figure 2.6 Volume reduction of (a) water droplet (15 µl) in 8 mg/ml JNPs toluene solution.(b) carboxyl functionalized silica nanoparticle (d= 50nm) aqueous droplet in silicone oil contains 5wt% PDMS-NH_2(M_w=2k)

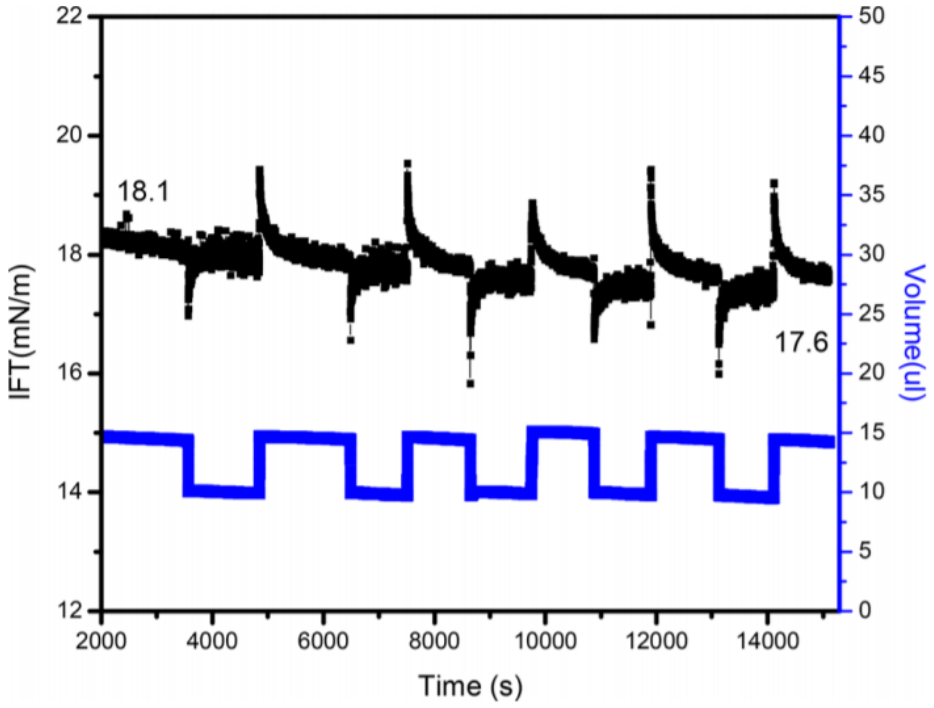

Figure 2.7 IFT profile (black) between water/ JNPs toluene solution in response to fluctuation of droplet volume (blue).

The IFT between water/toluene is also tunable with compression/expansion cycles of interfacial area. Figure 2.7 shows the IFT as a function of time after the

droplet volume was decreased or increased between 15 and 10 µL under constant rate of 50 µL/min. When the total interfacial area of the droplet is reduced, the JNPs assembled at the interface are forced to pack more closely, which leads to a decrease of the IFT. Once the reduction of interfacial area stopped, the IFT slowly relaxed to almost the initial value. During the relaxation, the rearrangement of JNPs took place at the interface. As the packing of JNPs at interface becomes much more crowded, the center of mass of the JNPs will have to move towards to toluene phase while PMMA chains are still attached to the interface. Such out-of-plane rearrangement dispatches the as increased repulsive force arise from the denser packing of JNPs at interface. As the droplet is re-inflated to the original volume, the IFT rapidly increases. The result indicates that the kinetics of the in-plane redistribution of JNPs that were already assembled at interface is rather slow, and that the spreading of PMMA chains already at interface is not as fast as the generation of bare water/toluene interface, causing the increase in IFT on re-expansion of interfacial area. Thus, there are two factors contributing to the relaxation of IFT: (1) absorption of more JNPs from the bulk toluene phase to the water/toluene interface generated by the expansion in the interfacial area, and (2) reorganization of the JNPs at the interface, typically the spreading and stretching of PMMA chains to cover more interface. On fitting these data with a single-exponential function (A.1.5), characteristic decay times of 108 and 273 s are obtained for the relaxation of the IFT after a step decrease or increase in the volume of the droplet, respectively. Since more JNPs can absorb to the interface during the re-expansion of water droplet. As expected, the areal density of JNPs at the interface increased and the IFT decreased slightly from 18.1 to 17.6 mN/m after five compression/re-expansion cycles, as shown in Figure 2.7. This provides a pathway where the packing of the JNPs at the interface can be mechanically improved.

The interfacial activity of the JNPs also depends on the pH of the aqueous phase even though pH does not influence the IFT of the water/toluene interface (A.1.3). Figure 2.8 shows the time-dependent IFT of a water droplet in toluene containing 8 mg/mL JNPs where the pH of the aqueous phase was decreased from 7 to 3.6 with increment ~1 by addition of HCl. For $7 > pH > 5.9$, the dynamic IFT profiles were similar to the one of pH 7, only subtle drops of the IFT at equilibrium was found. However, for $pH < 5$ a marked reduction and leveling off in the IFT is seen within 2000 seconds for $pH = 4.8$ and 1000 seconds for $pH = 3.6$. Since PMMA can be viewed as a weak Lewis base, the increased interfacial activity with decreasing pH of the aqueous phase is understandable. As the water phase becomes more acidic, the contact of PMMA segments with water phase is more favorable, promoting PMMA to assemble at the interface with less in-plane spreading.

Eventually, a higher packing density of JNPs at the interface is achieved by making water more acidic.

When the pH is increased by adding NaOH to the aqueous phase, the IFT gradually decreases with time until very basic conditions are used where at a pH of 11.9, a very rapid decrease is seen in the IFT (Figure 2.8 b). It is known that alkali metal ions can complex with the carbonyl group of PMMA, where the binding increases with increasing pH. Figure 2.8 shows the pH-dependent IFT measured after 6000 seconds where, as the pH is increased, the IFT reaches a maximum value.[21] Then, with a further increase in pH, the IFT decreases. NaOH was used to increase the pH from 7. Consequently, the reduction in the IFT at elevated pH values can be understood. The asymmetry in the maximum (Figure 2.9) simply reflects the different interactions at low and high pH values. The difference in the interactions of PMMA at the interface is also seen in the jamming behavior of the assemblies. In particular, at pH 3.6, the wrinkles on the surface of the droplets, induced by compressing the assemblies, relaxed slowly, while at higher pH values, no significant change in the wrinkling pattern was observed after 30 min.

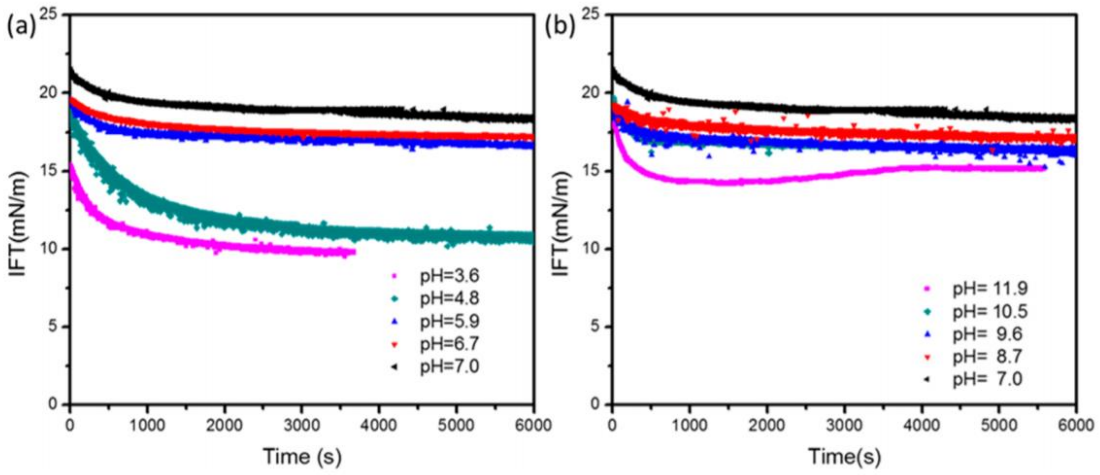

Figure 2.8 Influence of pH in water phase on the interfacial tension reduction. Interfacial tension isotherms of solutions of Janus particles in toluene (8 mg/mL) against (a) acidic and (b) basic water at different pH values.

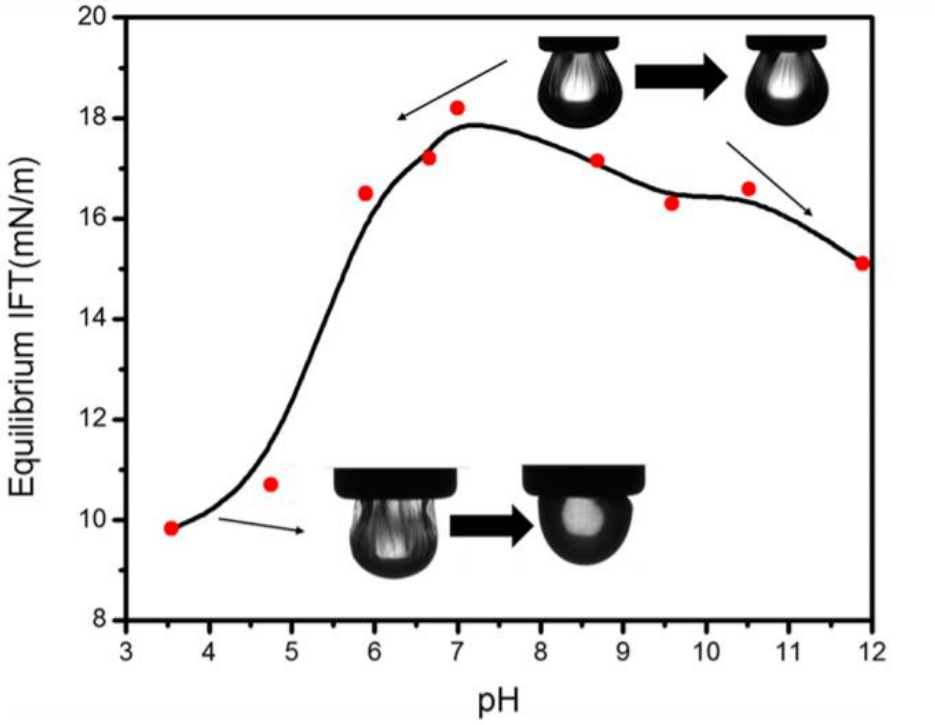

Figure 2.9 Quasi-equilibrium interfacial tension as a function of pH (values obtained after 6000 s), and wrinkle behavior corresponding to different pH. Only when pH < 4, the wrinkle undergoes slow relaxation; otherwise, the wrinkle remains unrelaxed. Line is a guide to the eye.

2.3 Conclusion

In summary, the assembly and interfacial jamming of spherical JNPs at the water/oil interface, as a new class of soft materials, was investigated. The soft nature of the JNPs with hemispheres of PMMA and PS chains that can entangle and stretch normal to the interface only leads to jamming at the interface when the interfacial area is significantly reduced, which has not been seen for hard spherical nanoparticles assemblies at liquid interface. IFT reduction and jamming by this type of Janus nanoparticles can be tailored by changing the pH of the water phase. When the water phase is more acidic or basic, the IFT between water and toluene can be significantly reduced, when compared to that at a pH of 7 (neutral). The wrinkling at the interface has been observed to relax only for low pH values; otherwise, it remains unchanged. Soft JNPs presented here clearly shows great promise as a new avenue of materials for interfacial active and structuring liquid.

2.4 Experimental section

2.4.1 Synthesis of Polymeric JNPs

2.4.1.1 Synthesis of linear triblock copolymer precursors

Linear triblock copolymers were synthesized by anionic polymerization with a modified method of a procedures described in the past.[20] All monomers and 1,1-diphenylethylene were reagent grade materials. Di-n-butylmagnesium ($MgBu_2$) was used as 0.5M solution in heptane, ($AIEt_3$) as 1M solution in hexane. THF was technical grade and purified first by distillation under nitrogen from CaH_2 and then refluxing over potassium. Styrene was pre-dried with CaH_2 and condensed from $MgBu_2$ under high vacuum into Teflon stoppered ampoules. Butadiene was condensed onto $MgBu_2$, stirred for several hours and then directly condensed into the reactor. MMA was pre-dried with CaH_2, carefully degassed by freeze-thaw cycles in high vacuum, mixed with $AIEt_3$ solution until a yellow color persisted and then condensed into ampoules. The glass ampoules with the purified liquid monomers were stored at liquid nitrogen temperature until use. 1,1-Diphenylethylene was purified by distillation from the deep red initiator solution with n-BuLi under nitrogen and handled with syringes.

In a typical procedure 20ml n-BuLi (1.4M in hexane) were added to 1200ml purified THF and aged at room temperature overnight. On the next day, styrene was introduced and cooled to -80 ℃. The polymerization was initiated with n-BuLi under vigorous stirring to give the orange solution of living PS. After 30 mins, butadiene was condensed into the reactor and the colorless solution warmed up to -10℃. Depending on the molecular weight of the midblock, butadiene was polymerized during 4-6h. Under these conditions most of the butadiene (> 90%) had reacted. After this time an excess of 1,1-diphenylethylene was added to the solution. The red color gradually developed within minutes. After cooling down to -60℃ for 1 hour, MMA monomers were slowly added. The colorless solution was warmed to -40 ℃ and stirred for 2 hours to complete the reaction. The triblock copolymer was terminated and isolated by precipitation into MeOH. During the synthesis, aliquots of the PS block and the end capped PS-*b*-PB intermediate were isolated for analytical purposes.

2.4.1.2 Synthesis of SBM JNPs

SBM JNPs were generated via following procedure. First, 500 mg of the polymer of S40B20M40 was dispersed in 50 ml of DMAc and left in the oven at 70°C overnight. The solution was then dialyzed against 2 liters of acetone/isopropanol (v/v 60/40) mixture to form multicompartment micelles. After three hours, the dialysis bath was changed. Meanwhile, a TPO solution was prepared

in 10 ml acetone/isopropanol (v/v 60/40) mixture with TPO concentrations matching a 1: 1 molar ratio to butadiene double bonds. After mixing TPO and SBM, the solutions were wrapped in aluminum foil and stirred for 2 hours for homogenization and then subsequently irradiated for one hour with a UV LED lamp (λmax = 365 nm) to crosslink butadiene core.

To purify the crosslinked JNPs from remaining TPO, the polymer solution was slowly added dropwise to 2 liters of methanol with a dropping funnel. The SBM JNPs showed greatly enhanced stability in methanol as compared to the triblock terpolymer. Thus, 10 vol% water was added to methanol to induce precipitation. Finally, the product was filtered and washed several times and dried.

2.4.2 Transmission electron microscopy (TEM) of JNPs

Bright-field TEM images were obtained by Transmission Electron Microscopy (TEM) measurements were performed on a JEOL JEM-1400 Plus TEM, operating at an accelerating voltage of 120 kV and a point resolution of 0.38 nm as well as a line resolution of 0.2 nm. Images were recorded with 16-bit 4096 × 4096 pixels CMOS digital camera and processed with FIJI open-source software package. For sample preparation, one drop of the particle dispersion (c = 0.5 g·L^{-1}) was deposited on a carbon-coated copper grid (200 mesh, Science Services, Germany). All samples were stained with OsO_4 vapor for 3 h prior to measurements.

2.4.3 Dynamic interfacial tension measurement

The IFT between water and the organic solvent (toluene) was measured with a pendant drop tensiometer (Krüss), that water droplet is dispensed from 1mL syringe and hanging vertically on the needle tip (diameter= 1.27 mm), the hanging droplet was immersed in toluene in a glass cuvette. The shape of water droplet immersed in toluene was captured by CCD camera, which used to fit Young-Laplace equation to give interfacial tension. For each measurement, the volume of each droplet was ~15 µL. The shape parameter was captured and recorded once every second for 6000 sec starting from droplet formed. The densities of DI water and toluene were 1.00 and 0.865 kg/m^3, respectively. pH dependence of IFT between water/ JNPs toluene solution were measured by tuning pH of the aqueous phase was adjusted using 1 M hydrochloric acid (HCl) or sodium hydroxide (NaOH). Value of pH was measured with an Accumet model 20 pH/conductivity meter.

2.4.4 Wrinkling/relaxation experiment

After the system was equilibrated, the droplet was retracted back to the syringe with a constant retraction rate at 0.4 or 50 µL. Retraction/re-inflation experiment was done by retracting the droplet at constant rate of retraction followed by re-inflation of the droplet to the initial volume at the same rate. A video was

recorded during the retraction/re-inflation process at 15 frame/sec. As each frame can provide real-time shape parameter, the profile was later used to calculate dynamic IFT during the process.

2.4.5 Size distribution of the JNPs

The size distribution of the JNPs in toluene was determined by dynamic light scattering (DLS) measurements, performed on a Malvern Zetasizer Nano-ZS equipped with a 633 nm laser at a scattering angle of 90°, and fixed JNPs concentration at 1 mg/mL. DLS measurements were conducted upon preparation of JNPs solution and 6 days after preparation to probe solution stability. JNPs in DMA solution was also made with 1mg/mL of concentration for DLS measurement under the same condition.

Chapter 3

Effect of Softness of Soft Janus Nanoparticles on their Interfacial Assemblies at Liquid Interface

Soft polymeric Janus nanoparticles (JNPs) made from linear tri-block copolymer polystyrene-b-polybutadiene-b-poly meth methacrylic (PS-PB-PMMA, SBM) have shown promise as an effective interfacial active material that can reduce water/toluene interfacial tension and jam at the interface. JNPs first assemble onto the water/toluene interface by diffusion. Particles translate and rotate to let PMMA chains face the water phase to minimize interfacial energy. Given the soft nature of JNPs, PMMA chains spread and extend to cover as much as interfacial area as possible, which leads to rearrangement of JNPs at interface. The assembly of such soft type JNPs has shown far different assembly kinetics and mechanisms than hard spherical particles. Also, the packing density of soft JNPs is far less than hard spherical nanoparticles, including nanoparticle-ligand surfactants (NPSs), assembled at liquid interface over the same time frame. The low packing density of JNPs at interface impedes their use as structuring liquid materials, which makes fabricating 3-dimensional (3D) printing all liquid structures and patterns impossible. To fully develop soft JNPs potential to enable effective structuring liquids, there is a need to tailor the packing of soft JNPs at liquid interface. In this chapter, we will start from manipulation of JNPs with controlled softness to tune their interfacial assembly behavior. The results show that the packing density of JNPs made with smaller ratio of PS and PMMA domains in the coronae can be increased by ~20%. The results provide a pathway for tailoring JNPs interfacial assembly by solely changing the softness while the sizes and chemistry remain the same.

3.1 Introduction

A tremendous amount of work has been done with particle assembly at liquid interfaces, such as liquid marbles, specific encapsulations, and droplets with heterogeneous surface properties etc.[1-5] Recently, more work has focused on all-liquid materials and complex devices that are generated via interfacial assemblies and jamming of nanoparticles which maintain metastable structures that are reconfigurable in response to external stimulus. All liquid 3-dimensional (3D) printing, where ink solutions can be printed into another liquid where the ink can still maintain the customized shape, has drawn specific interest.[6-11] Forth et al. developed a way to print 3D structures composed entirely of liquids where threads of water are injected into silicone oil (Figure 3.1). [12] Here, nanoparticle-ligand surfactants (NPSs) form, assemble and jam at oil-water that prevent the tubes from breaking up into droplets and locks-in the printed constructs. Water soluble active matters can be encapsulated or transported through the as printed liquid tubes.

To realize structuring liquids, like 3D printing of all liquids structures using NPSs assembly at liquid-liquid interfaces, two conditions are required: (1) the absorption rate of NPSs onto the interface need to be compatible to the flow rate, so

that interface can be saturated with NPSs immediately once created, and (2) as assembled NPSs are bound strongly and closely packed at the interface, therefore NPSs can jam to resist ink fluid relax back to discrete droplets.[13] Feng et al. used this concept to fabricate 3D all-liquid fluidic devices by the strong binding of nano-clay platelets and polymer ligands at water/oil interface. These devices are infinitely reconfigurable and endowed with spatially programmable functions.[6]

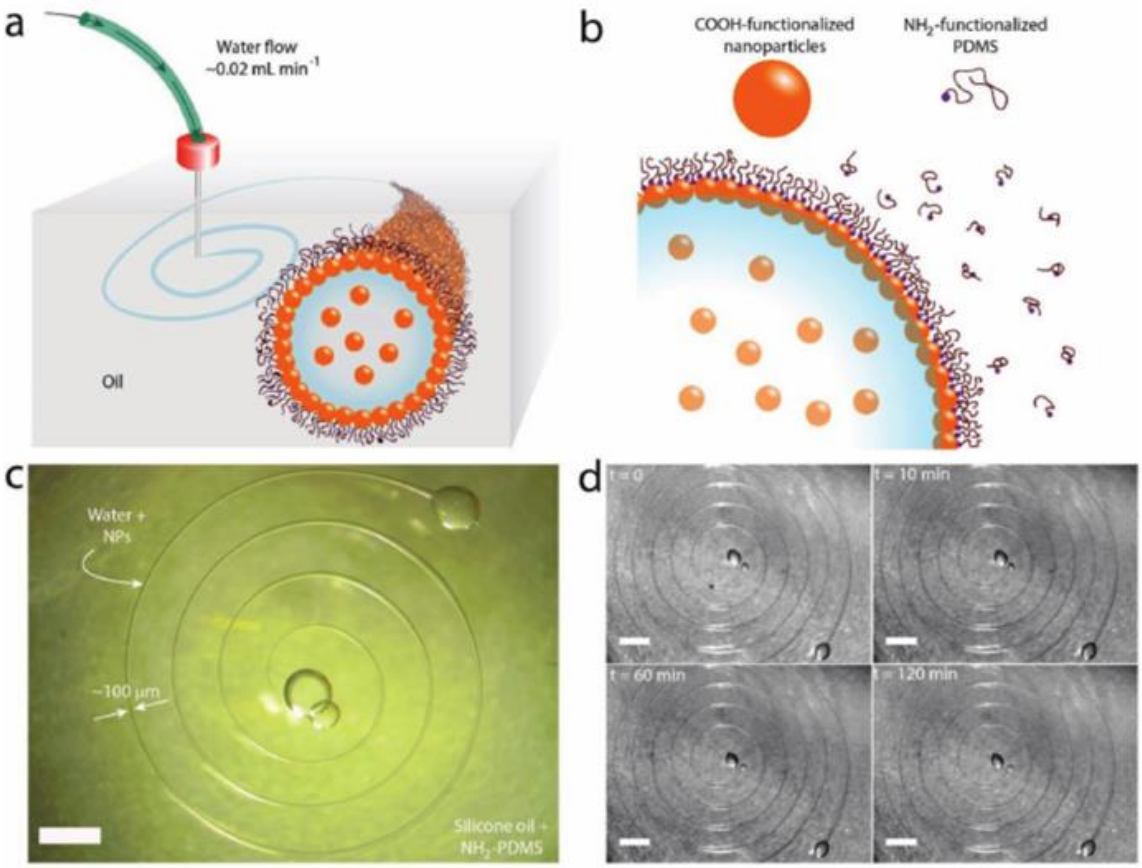

Figure 3.1 Printing of water in oil using 2D NPS assemblies. a) Schematic of the 3D printing of NPS-stabilized aqueous threads in a silicone oil. b) Schematic of the interfacial assembly of NPSs and the elastic films they form. c) An aqueous spiral, 6.8 cm long, thread thickness 100 µm, in silicone oil. d) Time-lapse showing a 13.5 cm long spiral 0, 10, 60, and 120 min after printing. [NP] = 1 mg mL^{-1}, [PDMS-NH2] = 5% w/w. All scale bars, 2 mm [12]

From the previous discuss in chapter 2, polymeric soft JNPs can assemble at water/oil interface and interfacial energy can be reduced. However, due to the soft nature of polymeric JNPs, the assembly has an inherent low areal density of particles. Upon compression, JNPs first get closer to each other and finally closely pack at interface and jam at very high compressions, making it impossible to 3D printing all

liquid systems with the interfacial JNPs assemblies. To explore the full potential of JNPs to structure liquid, the packing density of JNPs must be improved to the level of hard NPs. In this chapter, we will discuss the methods that were developed to improve the packing of JNPs at water/oil interface. The interfacial activity of JNPs can be tuned by decreasing the softness of the particles so as to reduce the routes for the assemblies to relax, or by the complexation of the PMMA chains with lithium ions, to increase the binding energy of the particles to the interface. The results provide a fundamental understanding of soft JNPs packing at the water/oil interface and provides a strategy to tailor the areal density of soft JNPs at liquid/liquid interface, enabling the design of smart responsive structured-liquid systems.

3.2 Results and discussion

First, the molecular structure-interfacial assembly relationship and the manipulation of the interfacial activity of soft JNPs at water/oil interface were examined. Since PB core of JNPs is incompressible where phase-separated PS and PMMA chains form the coronae, softness is determined by the PS and PMMA chains. The longer the PS and PMMA chains, the softer are the JNPs. Different softness of JNPs can be achieved by keeping PB core size constant while increasing the chain length of PS/PMMA coronae. With this method, the overall size of JNP will increase when increasing the softness. To exclude the influence of size, JNPs with different softness were synthesized by increase PB weight fraction of SBM terpolymers with constant overall molecular weight. Three different JNPs were made with SBM terpolymers where the weight fraction of the polybutadiene core are varied from 10-20-30%, while the total molecular weight and the Janus balance were kept about constant, in the following discussion we will refer to these as Janus-10, Janus-20, and Janus-30. The synthesis of SBM and formation of JNPs have been discussed in detail in chapter 2. Table 3.2 provides the molecular weights and weight fractions of each component.

Sample #	f_{PS} wt%	f_{PB} wt%	f_{PMMA} wt%	M_n [kg/mol]
SBM-10	46	10	44	80
SBM-20	39	20	41	90
SBM-30	33	32	34	88

Table 3.2 Details of weight fractions and over molecular weight of SBM-10, SBM-20 and SBM-30

Since the crosslinked PB core is stiffer than the PS and PMMA corona, the softness of the JNPs decreases with increasing core size. The core size was characterized by bright field TEM to 22nm (Janus-10), 27nm (Janus-20), 55nm (Janus-30) as inserted images of Figure3.3 (a,b,c) with negative staining by OsO_4. OsO4 is a selective staining agent for double bonds and preferentially reacts with remaining double bonds in the PB core that appear dark under bright field TEM mode, PS can be slightly stained appear grayish due to its own contrast from aromatic side groups. On closer examination, one can recognize the PS corona as either grey phase for the JNPs aggregates on the TEM grid as the typical pattern in Figure 3.3(a). PMMA is not visible due to electron beam degradation. Given that the two PS and PMMA hemispheres of the JNPs are solubilized corona chains that do not dry as a compact phase on the TEM grid, so they were shown as a diffuse area of chains under TEM. The contrast of this diffuse area is usually very low, which makes visualization of the Janus character itself by TEM challenging.

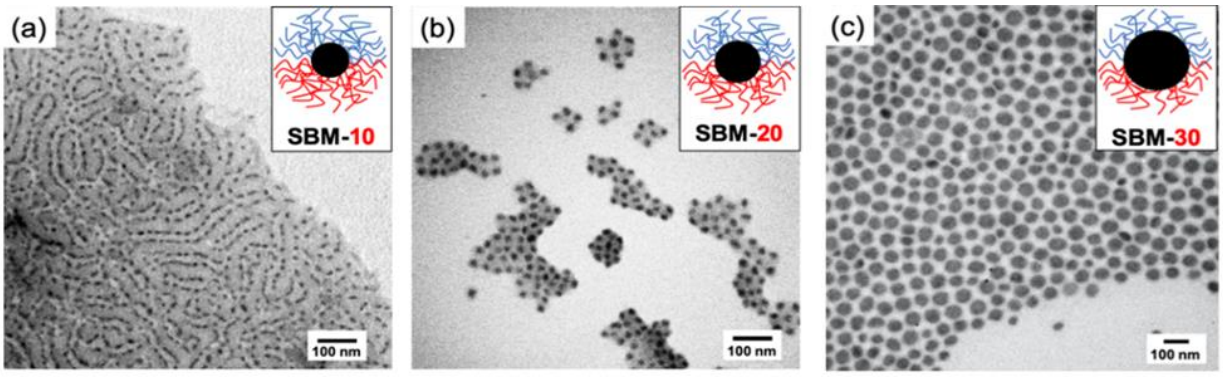

Figure 3.3 TEM imgaes of JNPs made with (a) SBM-10 (fPB=10%) (b) SBM-20(fPB=20%) and (c) SBM-30(fPB=30%), samples were stained by OsO4. PB: black PS: grey PMMA: not visible. Insert images on top-right are the schematic drawings of SBM-10 SBM-20 and SBM-30, PB core: black, PS: blue, PMMA: red.

Since the particle assembly takes place in an all-liquid environment, DLS measurements were made to obtain the hydrodynamic diameter of JNPs in solution, shown in Figure 3.4. The number of chains that compose each JNP can be calculated from the PB core volume based on the following equation:

$$N_{agg} = \frac{m_{core}}{M_{PB}} = \frac{4\pi N_A \rho_{PB} R_{core}^3}{3M_{PB}} \quad \text{(Eq. 3.1)}$$

The number of chains per particle is 403, 331, and 1940 for Janus-10, Janus-20, and Janus-30 respectively.

The softness is defined numerically by

$$\text{Softness}=1-\frac{Size_{core}}{Size_{total}}. \quad \text{(Eq. 3.2)}$$

For Janus-10, Janus-20, Janus-30, the softness decreases from 77% to 64% to 46%, which clearly indicates decreasing softness. The number PMMA chains per volume of JNPs can also be calculated to be $2.06\text{x}10^{24}$ chain/meter^3, $7.42\text{x}10^{24}$ chain/meter^3, and $2.11\text{x}10^{25}$ chain/meter^3 for Janus-10, Janu-20, and Janus-30 respectively, showing clear increase of chain density by decreasing the softness.

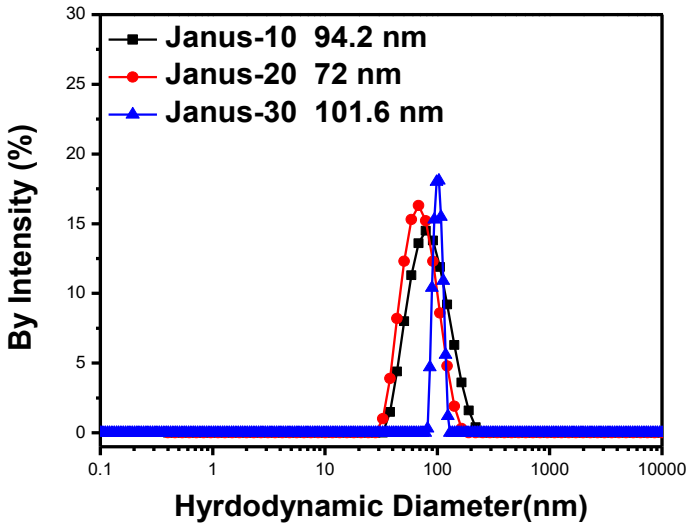

Figure 3.4 Dynamic light scattering of Janus-10 Janus-20 and Janus-30 in toluene (1mg/mL)

A pure 15 µL water droplet was immersed in toluene solutions of the SBM JNPs to measure the dynamic interfacial tension (IFT) between water and toluene as SBM assembled onto the interface. As shown in Figure 3.5(a-c), the IFT initially decreased due to the assembly of the SBM JNPs at the interface. The equilibrium IFT was found to decrease with increasing SBM JNP concentration. For low concentrations of JNPs (0.08 mg/ml), the time evolution of IFT shows an initial rapid decrease, followed by a period where the IFT decreases much more slowly. The fast decay corresponds to the initial recruitment of the JNPs to the interface where the JNPs adsorb and configurationally re-arrange to minimize the IFT with the constraint of stretching of the corona chains. The JNPs already at the interface must undergo further configurational changes to generate more space to let more JNPs from the solution absorb onto interface. During the process, the corona chains must stretch and push the core of the JNPs away from the interface, which limits the

overall number of JNPs that can adsorb to the interface at equilibrium. With increasing concentration of JNPs, the initial adsorption of the JNPs to the interface is too rapid to measure, thus the initial fast decay of IFT has been greatly suppressed. The gradual reduction observed after the initial fast decay represents the rearrangement and reconfiguration of the JNPs.

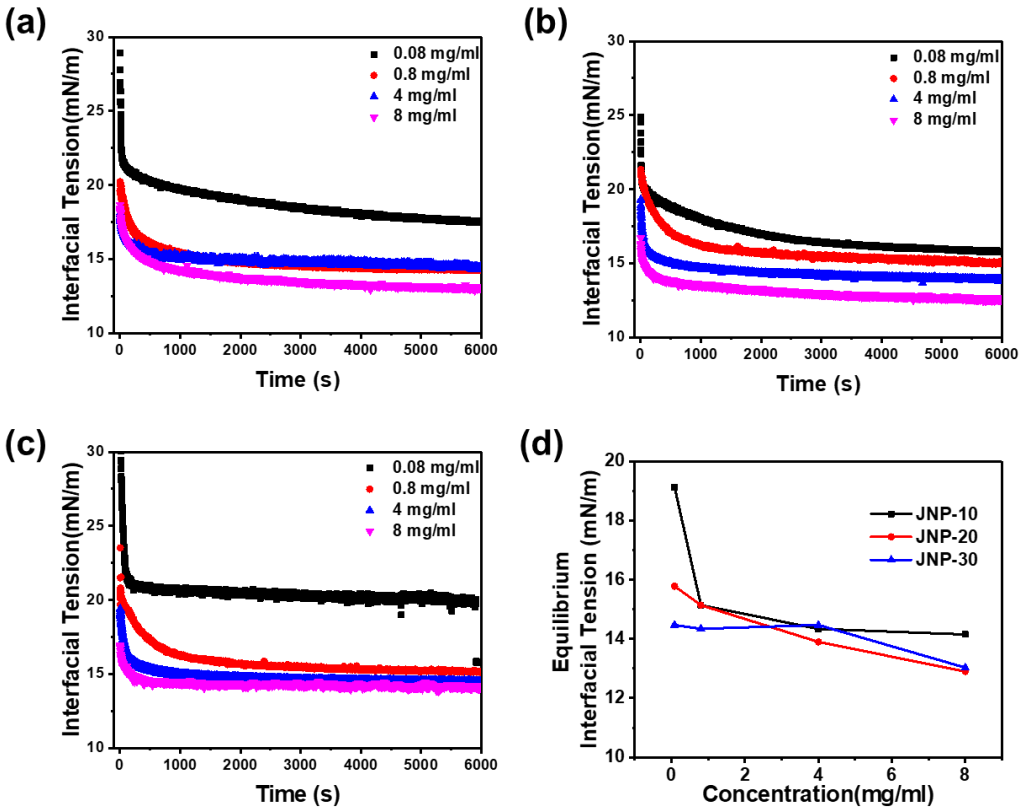

Figure 3.5 Time evolution of interfacial tension between water and JNPs toluene solutions at different JNPs concentrations of (a) Janus-10 (b) Janus-20 (c) Janus-30;(d) Equilibrium interfacial tension for JNPs at different concentrations

In Figure 3.5(d), the concentration dependence of the equilibrium IFT for each JNPs were summarized. Janus-30 behaves more like hard NPs since it has the largest core and shortest corona chains. The degrees of freedom of the corona chains are much reduced, therefore a very rapid approach to an equilibrium IFT was observed. At equilibrium, the packing of Janus-30 is denser compared to Janus-20 and Janus-10. For Janus-20 and Janus-10, the corona chains can be stretched much further, so the PMMA chains can extend along the interface to maximize coverage. With increasing JNPs concentration, more chains adsorb onto the interface if the PMMA chains of those JNPs that already adsorbed onto interface can relax, however, the coverage does not increase substantially.

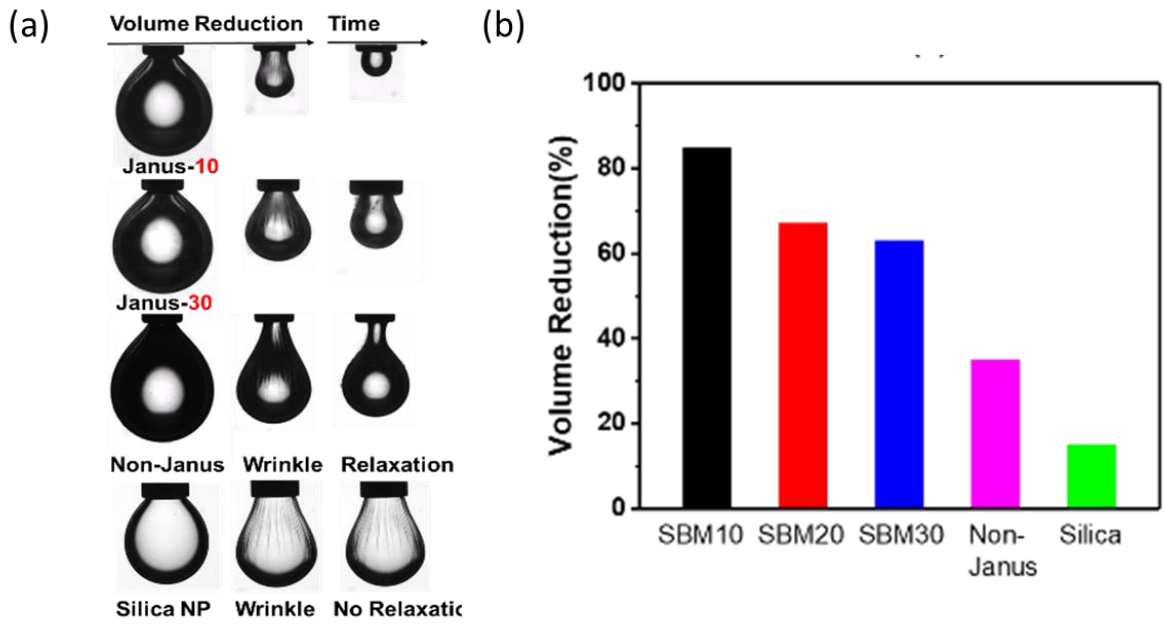

Figure 3.6 (a) From top to bottom: Wrinkling/Relaxation of Water droplet immersed in toluene solution with 8 mg/ml JNP-10, Janus-30, non-Janus and Silica NP in water with PDMS-NH2 ligand in silicone oil. (b) Summary of volume reduction ratio to induce wrinkling.

To differentiate the packing and jamming behavior of the JNPs with different softness, the droplet volume was decreased at a rate of 100 µl/min after the system has equilibrated and the droplet shape and appearance were recorded with a CCD camera at 12.5 frames/second which captures the wrinkling if it happens. The volume reduction causes reduction in the interfacial area, applies a constant compressive force on the JNPs assembled at the interface, forcing JNPs at interface to get closer to each other. As the assembly gets denser, the particles eventually wrinkle when no more JNPs can accommodate the stress and the structure buckles instead as the JNPs have jammed. In Figure 3.6(a), a clear difference of wrinkling behavior was found between soft JNPs to hard spherical NPs that, with soft JNPs, the jamming occurs but only after a significant reduction in the interfacial area (60-80%) of the volume had been retracted and the wrinkles rapidly relax to reduce the applied stress. In comparison, hard silica NPs of comparable size show wrinkling after only 15% of the volume is removed and the wrinkles do not relax. As shown in A.2.1, at a concentration of 8 mg/ml of Janu-10, Janus-20 and Janus-30, the interfacial tension was reduced from 35 mN/m to 13 mN/m, 12.5 mN/m and 13.9 mN/m respectively, indicating similar interfacial activity. The Janus-30system requires the least volume retraction to obverse the wrinkles with 63% of volume

reduction, while 67% and 85% value reduction is measured for the Janus-20 and Janus-10 Consequently, as the weight fraction of the PB core decreases, the PMMA chains can more effectively cover the interface initially, but as the compressive force is applied, since the density of chains at the interface also decreases, the chains adsorbed to the interface can retract more easily, causing a reduction in the volume at which wrinkling occurs to be the greatest. The Janus-20 falls between Janus-10 and Janus-30 as would be expected. In all cases, the rate of compression is still rapid in comparison to the relaxation of the soft JNPs and a reconfiguration occurs allowing the stress buildup to relax in the form of wrinkling. However, if the rate of volume reduction was decreased, the JNP coronae would have time to relax and reconfigure, and wrinkling would only be observed at an extremely large volume reduction. As shown in A.2.2, for Janus-30 that requires the least volume retraction, wrinkling was observed when the volume was reduced by 98% at a volume reduction rate of 0.4 µl/min, in comparison a 63% volume was required when the reduction rate was 100 µl/min. The rate of relaxation will decrease with decreasing corona length, as is observed. As the corona chains are compressed, the separation distance between the cores decreases and the separation distance between the interface and the core increases. In addition, the PS chains that are dissolved in the toluene will become further entangled as the JNPs are pushed closer together, further lengthening the relaxation of the soft JNP corona chains.

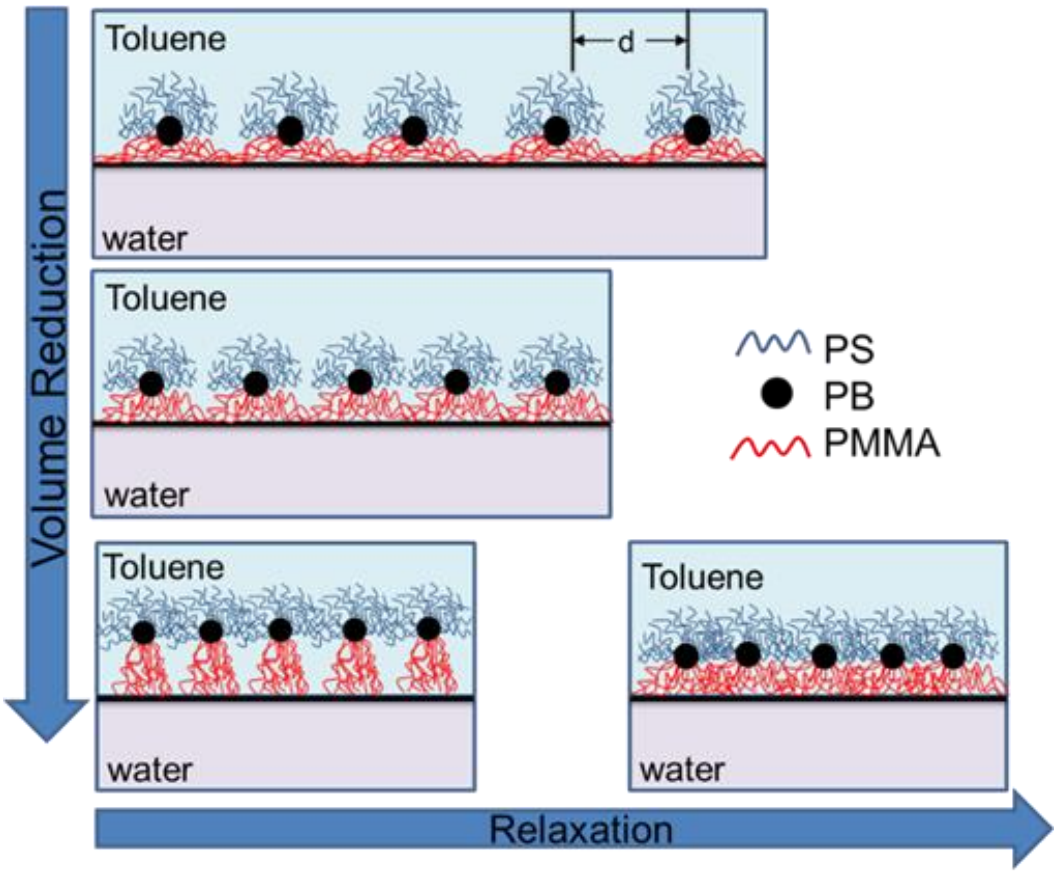

Figure 3.7 Schematic of JNPs assembling under volume reduction and later relaxation.

The unusual wrinkling-relaxation behavior of the JNPs can be attributed to the spreading of PMMA chains at the interface. This was confirmed by varying the weight ratio of the core to the corona while keeping the total molecular weight the same. With decreasing core size, the lengths of the corona chains increased. The packing density of the JNPs decreased with higher molecular weight, since the chains spread out onto the interface and cover more interfacial area. The inter-particle distance, defined as core-to-core distance between particles, varies with $d_{Janus\text{-}10} > d_{Janus\text{-}20} > d_{Janus\text{-}30}$ as softness deceases. Consequently, the volume reduction to induce wrinkling varies in a similar manner and corresponds to the extent to which the corona chains of adjacent soft NPs can interpenetrate, but also the extent to which the corona chains must stretch out-of-plane during compression, and the amount that the chains can reconfigure and relax after wrinkling. Such characteristics are schematized in Figure 3.7.

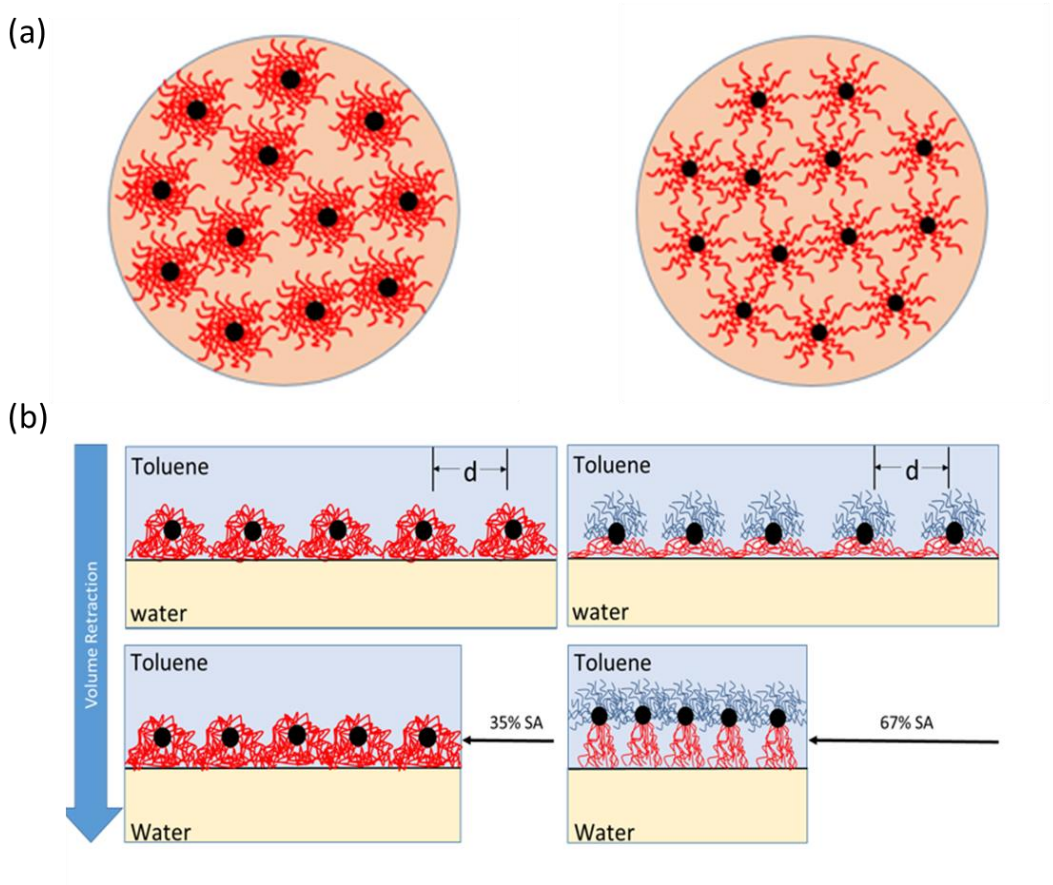

Figure 3.8 (a) schematic bottom-view of Non-Janus nanoparticles (lhs) and Janus nanoparticles (rhs) assembling at interfafce. Only the PMMA chains are shown in the schematic. PS chain are out-of-plane pointing into the toluene;(b) schemetic of Non-Janus (lhs) and Janus (rhs) nanoparticles at interface under compression. Black dots: PB core, Red chains: PMMA, Blue chains: PS

To distinguish how the Janus character influences the jamming behavior of JNPs, non-Janus NPs were made from PB-PMMA diblock copolymers that have molecular weight of the PMMA corona chains is 90k and the weight fraction of PB core is 20%. The non-Janus NPs have similar core size to Janus-20 but a crosslinked PB core with only a homogeneous PMMA corona. Pendent drop tensiometry showed that these non-JNPs reduce the water/toluene interfacial tension as effectively as Janus-20 (magenta curve in A.2.1), since the PMMA chains segregate to the interface to minimize water/toluene contact since interfacial tension of water/PMMA is much lower in than water/toluene. During the volume reduction, much less reduction was required (35%) to wrinkle the non-JNP assembly (Figure 3.6(b)). This arises from the reconfiguration of the non-JNP, placing more PMMA chains (per particle) at the interface for the non-JNPs in comparison to the JNP as

schematized in Figure 3.8(a). Consequently, the number of chains per NP that stretched across the interface is more, causing the wrinkling to occur with less compression (Figure 3.8(b)).

As it has been discussed above, the packing density of soft JNPs is determined by the extent of chain spreading at interface and the hydrophobic interactions between PMMA chains to their nearest neighbors. To achieve higher packing density of soft JNPs at interface to make the assembly more like a solid, the spreading of chains at interface must be suppressed. One possible method is to enhance the Janus balance, such as substitution of PMMA block by Poly (methacrylic acid) (PMAA). PMAA is a hydrophilic polymer and can be solubilized in water, thus chains of PMAA can point into water phase and such JNPs should be more densely packed at water/oil interface. However, such a method requires change of the chemical nature of SBM JNPs, and the PMMA to PMAA hydrolysis cannot be realized in-situ. Instead, lithium ions were added to water phase that can complex with the PMMA corona chains. This complexation strongly increases the polarity of the PMMA and its affinity to the aqueous phase, making the soft JNPs behave more like traditional amphiphilic JNPs with chains of one hemisphere being solubilized in one liquid while the chains of the opposing hemisphere are solubilized in the second fluid. Such complexation can tailor the interfacial activity of SBM JNPs without changing its own chemical composition. For SBM JNPs, the chains of the PMMA corona would partially extend into the aqueous phase, alleviating stretching at the interface initially. This reduces the spacing between the JNPs at the interface, enabling a denser interfacial packing (Schematically shown in Figure 3.9).

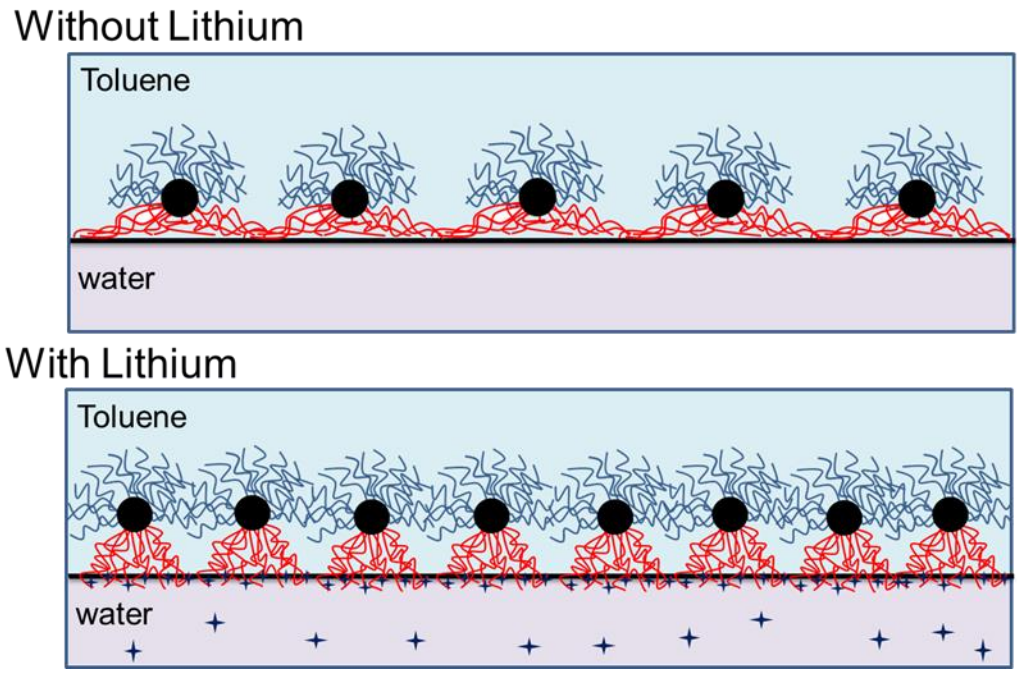

Figure 3.9. Schematic of JNPs assembly at water/toluene interface with or without lithium ion in the aqueous phase.

To confirm the complexation of the PMMA to lithium has taken place at the interface, Janus-30 toluene solution and 100 mM LiCl water solution were put in the glass vial and vigorously shaken to form emulsions. After 12 hours the emulsion layer was drop cast onto a substrate and dried under vacuum, the resulting film was characterized by Fourier-transform infrared spectroscopy (FT-IR). As shown in A.2.3, the characteristic peak for C=O stretching absorption at 1725 cm^{-1} in PMMA has shifted to 1634cm^{-1} after Lithium complexation. For all the SBM soft JNPs, the IFT were found to further decrease with increasing lithium chloride concentration in the aqueous phase, indicating an increased solubility of the PMMA in the aqueous phase and enhanced interfacial activity of SBM JNPs (Figure 3.10(a)). Wrinkling of the soft JNP assemblies with the addition of LiCl to the aqueous phase occurs at a smaller reduction in the droplet volume, which indicates higher equilibrium packing density has been achieved (Figure 3.10(b)). The reduction volume when wrinkling occurs decreases with increasing salt concentration (Figure 3.10(c)). Typically, with 50 mM lithium ions added to aqueous phase, the volume at which wrinkling was observed for SBM30 decreased from 62% to 35% of the initial volume, indicating that the packing density nearly doubled. After complexation with Li ions, the chains are also positively charged. So, when the JNPs were forced closer together, the electrostatic repulsion also weakens the chain reconfiguration and interpenetration. Increasing the lithium ion concentration further decreased the equilibrium interfacial tension of the system (<10 mN/m). The complexation of lithium ions to JNPs at water/toluene interface was further assessed by inductively coupled plasma-optical emission spectrometry (ICP-OES). For a 100 mM lithium chloride solution, there were 56.3 mM, 56.8 mM and 58 mM left in the water phase after complexing with SBM10, SBM20 and SBM30 at the interface, respectively.

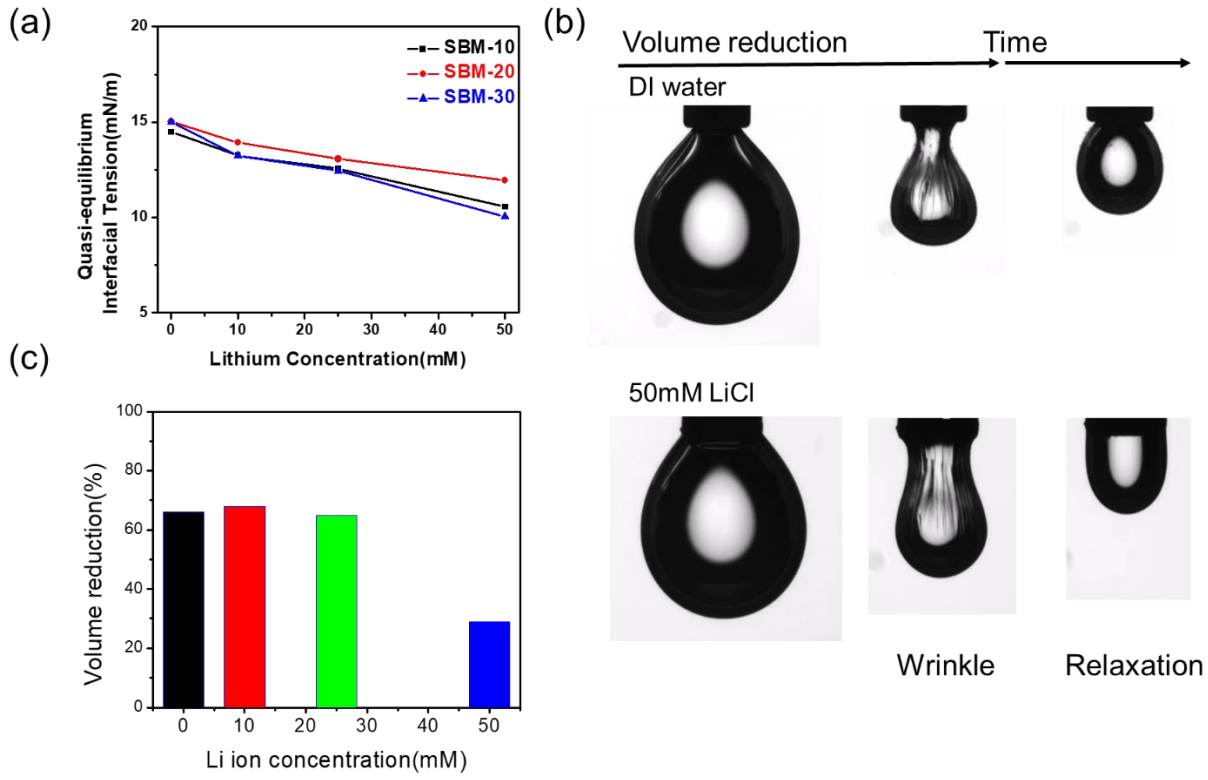

Figure 3.10 (a) Summary of equilibrium interfacial tension with 0.8 mg/mL JNPs in toluene and increasing concentrations of lithium chloride in water. (b) Snapshots of DI water and 50 mM LiCl droplet immersed in JNPs toluene solution, wrinkles under constant volume reduction rate, and the relaxation of wrinkle after reduction stopped. (c) Volume reduction ratio to observe wrinkles with different concentration of lithium ion in water

After interacting with Li ions at the interface, the size of JNPs is expected to increase as the JNPs would swell. DLS were used to measure the size before and after the complexations. From A.2.4(a) the size increase caused by the complexation is subtle. Typically, for SBM10 in contact with water containing 0, 50, 100, 250, and 500 mM LiCl, the average size increased from 95.2 to 95.4, 98.2, 99 and 101.3 nm respectively. In A.2.4(b), all three JNPs show a similar increase in size by ~10% upon exposure to 500 mM LiCl. The results indicate that the interaction only happen at the interface.

3.3 Conclusion

In summary, we have demonstrated that soft JNPs can assemble at a liquid/liquid interface, even though the corona chains are not soluble in one of the two liquids. The corona chains are seen to spread at the interface to reduce the interfacial tension balanced against an elastic recovery force. The softness of JNPs was shown to influence the packing density at the interface and was shown to be far different in comparison to hard spherical NPs. The coverage of JNPs is also related to the softness of JNPs. The shorter the corona chains, the harder are the particles are, resulting from less chain stretching. Thus, a denser coverage can be achieved. Upon compression, the soft JNPs can undergo a reconfiguration, relaxing the imposed stress. The extent to which this occurs decreases with decreasing molecular weight of the corona chains. Complexation with salt ions, in the case of PMMA against water, can promote the solubilization of the PMMA in the aqueous phase, eliminating the need to stretch the chains to cover the interface. With complexation, the area density of soft JNPs at the interface increases with the corresponding changes in the response of the assemblies to compression. This provides a convenient means of controlling the density of JNPs at the interface and tailoring the interfacial properties.

3.4 Experimental Methods

3.4.1 Synthesis of Polymeric JNPs

3.4.1.1 Synthesis of linear triblock copolymer precursors

Linear triblock copolymers were synthesized by anionic polymerization with a modified method of a procedures described in the past and has been described in detail in 2.4.1.2 of chapter two.

In this chapter, three different weight ratios of PS, PB, PMMA were designed in respect to give them different softness. The JNPs were named as SBM-10, SBM-20 and SBM-30 in respect to the weight fraction of PB core. Details of weight fractions and over molecular weight of JNPs can be found in table 3.1

3.4.1.2 Synthesis of SBM JNPs

All 3 SBM JNPs were synthesized following the same procedure. First, 500 mg of the polymer was dispersed in 50 ml of DMAc and left in the oven at 70°C overnight. The solution was then dialyzed against 2 liters of acetone/isopropanol (v/v 60/40) mixture to form multicompartment micelles. After three hours, the dialysis bath was changed. Overall, three changes were made. After dialysis and for crosslinking, a TPO solution was prepared in 10 ml acetone/isopropanol (v/v 60/40) mixture with TPO concentrations matching a 1: 1 molar ratio to butadiene double

bonds. For SBM10 with 10 wt% PB, 322 mg TPO was dissolved in 10 mL acetone/isopropanol (60:40), while for SBM20 with 20 wt% PB, 640 mg TPO and for SBM30 with 32 wt% a total of 1030 mg TPO was added. After mixing TPO and SBM, the solutions were wrapped in aluminum foil and stirred for 2 hours for homogenization and then subsequently irradiated for one hour with a UV LED lamp (max = 365 nm).

To purify the crosslinked JNPs from remaining TPO, the polymer solution was slowly added dropwise to 2 liters of methanol with a dropping funnel. The SBM JNPs showed greatly enhanced stability in methanol as compared to the triblock terpolymer. Thus, 10 vol% water was added to methanol to induce precipitation. Finally, the product was filtered and washed several times.

3.4.2 Characterization of JNPs

Size distribution of JNPs in toluene was measured by Dynamic Light scattering performed on a Malvern Zetasizer with Laser nm with a scattering angle of 167°. TEM images were obtained by Transmission Electron Microscopy (TEM) measurements were performed on a JEOL JEM-1400 Plus TEM, operating at an accelerating voltage of 120 kV and a point resolution of 0.38 nm as well as a line resolution of 0.2 nm. Images were recorded with 16-bit 4096 × 4096 pixels CMOS digital camera and processed with FIJI open-source software package. For sample preparation, one drop of the particle dispersion (c = 0.5 g·L−1) was deposited on a carbon-coated copper grid (200 mesh, Science Services, Germany). All samples were stained with OsO4 vapor for 3 h prior to measurements.

3.4.3 Dynamic interfacial tension measurement

The IFT between water and the organic solvent (toluene) was measured with a pendant drop tensiometer (Krüss), that water droplet is dispensed from 1mL syringe and hanging vertically on the needle tip (diameter= 1.27 mm), the hanging droplet was immersed in toluene in a glass cuvette. The shape of water droplet immersed in toluene was captured by CCD camera, which used to fit Young-Laplace equation to give interfacial tension. For each measurement, the volume of each droplet was ∼15 μL. The shape parameter was captured and recorded once every second for 6000 sec starting from droplet formed. The densities of DI water and toluene were 1.00 and 0.865 kg/m3, respectively. pH dependence of IFT between water/ JNPs toluene solution were measured by tuning pH of the aqueous phase was adjusted using 1 M hydrochloric acid (HCl) or sodium hydroxide (NaOH). Value of pH was measured with an Accumet model 20 pH/conductivity meter.

3.4.4 Wrinkling/relaxation experiment

After the system was equilibrated after 6000seconds, the droplet was retracted back to the syringe with a constant retraction rate at 0.4 or 50 µL. Retraction/re-inflation experiment was done by retracting the droplet at constant rate of retraction followed by re-inflate the droplet to the initial volume at the same rate. A video was recorded during the retraction/re-inflation process at 15 frame/sec. As each frame can provide real-time shape parameter, the profile was later used to calculate dynamic IFT during the process**.**

3.4.5 FT-IR Measurement

Janus-30 toluene solution and 100 mM LiCl water solution were put in the glass vial and vigorously shaken to form emulsions. After 12 hours the emulsion layer was drop cast onto a glass substrate and dried under vacuum, the remaining drop cast film was characterized by Fourier-transform infrared spectroscopy (FT-IR) with wavenumber range from 1200 to 2000 cm^{-1}.

3.4.6 ICP-OES measurement

An 8 mg/ml JNP solution in toluene was prepared and placed on top of a 100 mM aqueous solution of lithium chloride. After gentle shaking by hand, large micro-emulsion droplets formed that subsequently relaxed to two separate phases. The water-phase was then diluted 1000x to bring the solution into the detection range for ICP-OES.

Chapter 4

Pickering emulsion and its Stabilization by Janus Nanoparticles

An emulsion is defined as a dispersion of one immiscible liquid in another that has been stabilized with an interfacially active component that reduces the interfacial energy, thereby preventing the coalescence, maintaining the dispersion. Emulsions have been widely used in areas including oil recovery, paints, food science, and drug delivery. In general, an emulsifier is used to stabilize droplets of one fluid in a second, reduce the droplet size, and impart stability. Pickering emulsions are stabilized by solid particles that segregate to the interface between two immiscible liquid phases, where the interactions between the two liquids and the particles is less than the interfacial energy between the liquids, thereby reducing the interfacial energy. By substituting solid particles for traditional surfactants to stabilize the emulsions, one can take advantage of the specific properties of the particles to functionalize the interface. The wide range of possible particles enables different applications of Pickering emulsion. In this chapter, we evaluate the stabilization of Pickering emulsion with Janus nanoparticles, where a fraction of the surface of the particle interacts favorable with one liquid, while the remining surface area interacts favorably with the second, specifically toluene and water. We study the transport and diffusion across the water/toluene interface, and emulsion stability.

4.1 Introduction

4.1.1 Emulsions and their stability

An emulsion consists of two immiscible liquids where one liquid (dispersed phase) is dispersed in another (continuous phase). Interfacial tension (IFT), the free energy penalty of exposing one immiscible liquid to another, is the greatest impediment to the stability of emulsions, since it drives them to phase separate. Consequently, dispersion of one liquid in another is thermodynamically unstable and will rapidly separate into two liquid layers with an interface that is planar, to minimize the interfacial area and, hence, interfacial energy. To counteract this, emulsions can be stabilized by introducing amphiphilic particles, emulsifiers, molecules comprised of two components, each interacting favorably with the two liquids, that segregate to the liquid/liquid interface, reducing the interfacial tension, and the free energy. If water is dispersed phase and oil is the continuous phase, the emulsion, it is called a water-in-oil(W/O) emulsion, and an oil-in-water(O/W) emulsion, if water is the continuous phase.

The process of dispersing two immiscible liquids together to form mixture requires inputting sufficient energy to break-up the liquid from bulk to droplets. Generally, the larger the amount of shear force applied to the system, the smaller the droplet size of the dispersed phase generated. [1] Emulsifying agents, commonly referred as surfactants, are critical for stabilizing the emulsion droplets. Surfactants commonly contains a hydrophilic part, that favorably interacts with water, and a

hydrophobic part that preferentially interacts with oil. Because of their special chemical structure, surfactants assemble at the oil/water interface and form an interfacial film. This leads to a reduction in the interfacial tension and, consequently, stabilizes the droplets. The composition and concentration of the surfactants determine the type and stability of the emulsions. In general, the liquid phase containing the surfactant is the continuous phase. For O/W emulsion, the surfactant is usually soluble in water, whereas for W/O emulsion, the surfactant is usually soluble in oil.

Emulsions are often categorized by the size of the dispersed droplets: macroemulsions and microemulsions.[2] During the emulsification, the dispersed phase is broken-up into small droplets dispersed in the continuous phase, creating a large interfacial area between the two phases An emulsions is categorized as a macro-emulsion if the droplets are bigger than 0.2μm. The droplets of range from 0.2 to 50 micrometers (μm) in size can be easily visible with an optical microscope. Those emulsions are generally thermodynamically unstable as the droplets tend to coalesce and minimize interfacial area. Surfactants reduce the interfacial tension between two liquids to an amount that depends on the solubility and preferential interactions with the two liquids, and stabilize the emulsion, preventing droplet coalescence. Emulsions that preserved large quantity of droplets have size ranging from 0.01 to 0.2 μm is labelled as micro-emulsion, also specifically refer to thermodynamically stable emulsions.

Emulsion stability refers to the ability of emulsions to resist changes in their physicochemical properties over time. Emulsions are usually thermodynamically unstable system due to its natural tendency to minimize its interfacial interactions (interfacial energies) but mostly demonstrate kinetic stability. In the absence of surfactants, once the droplets are created, they begin to change due to different time-dependent processes, such as sedimentation, and creaming, flocculation, Ostwald ripening, and coalescence. Sedimentation or creaming result from density difference between the dispersed droplets and the continuous phase. Under the influence of gravity, the droplets either float or sink depending on the density difference with the continuous phase. Flocculation is the process where droplets in an emulsion form clusters as the result of universal van der Waals attraction. With Ostwald ripening larger droplets increase in size at the expense of the smaller droplets, driven by the minimization of the interfacial area, by the diffusion of the liquid in the dispersed phase through the continuous phase. With coalescence smaller droplets diffuse to the larger droplets, meld into a larger droplet, reducing the interfacial area while keep the volume constant.

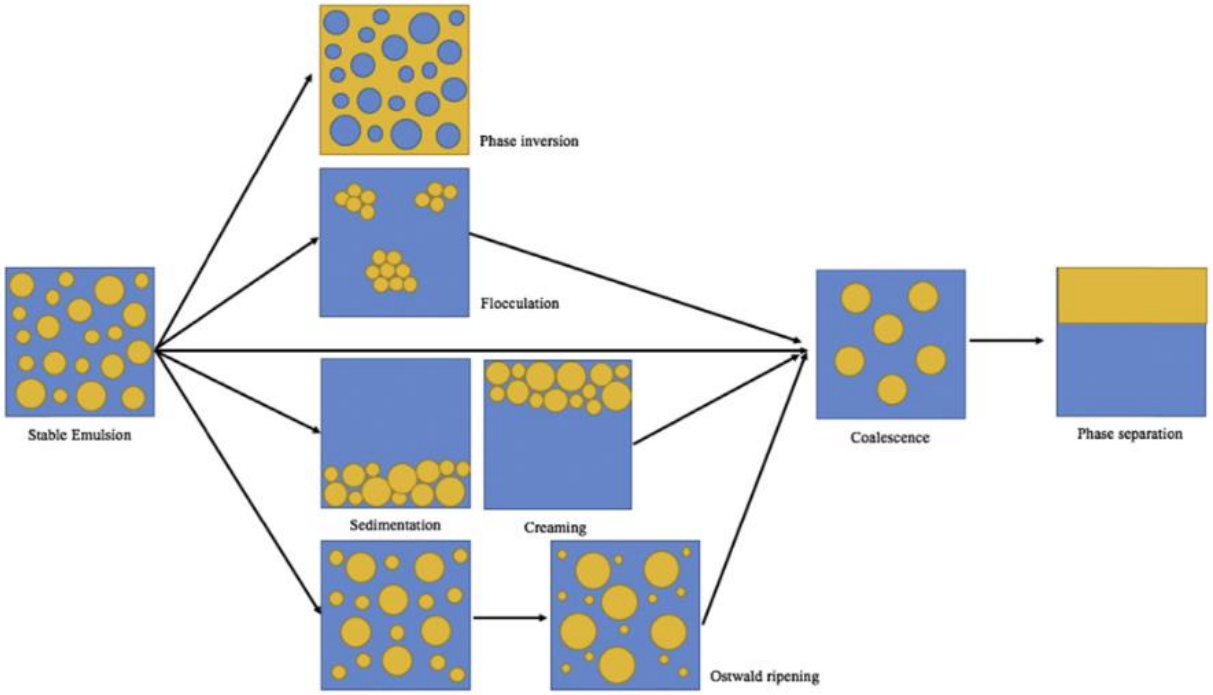

Figure4.1 Schematic representation of instability mechanisms in the emulsion system.[3]

In general, there are three main interaction forces between emulsion droplets that can prevent the droplet growth, therefore enhance emulsion stability: van der Waals, electrostatic repulsion, and steric repulsion which can be tuned with the engineering of the emulsifiers.

4.1.2 Pickering Emulsion, Nanoparticle-Ligand Surfactant, and Janus nanoparticles

Solid particles have been present in emulsion formulations for many years. Such emulsions often categorized as Pickering emulsion, in recognition of Pickering who found that particles wetted more by water than by oil acted as an emulsifier for O/W emulsions by locating the particle at water/oil interface. The relationship between the type of solid and emulsion type (o/w or w/o) was recognized Finkle et al. who showed the importance of wettability of particles at the water/oil interface, quantified by the contact angle that gives rise to the stability of a Pickering emulsion [4] In an emulsion containing solid particles, one of the liquids would wet the solid more than the other liquid, with the more poorly wetting liquid becoming the dispersed phase. That explains why silica particles can stabilize o/w emulsions and carbon black can stabilize w/o emulsions. Particles were absorbed at the interface between two immiscible liquids to stabilize droplets against coalescence. There are certain advantages of Pickering emulsions (i) solid particles reduce the possibility

of coalescence, bringing about higher stability to emulsions; (ii) many solid particles have unique characteristics such as conductivity, porosity to achieve transport and conducting purposes, and (iii) some food-grade solid particles have lower toxicity, thus leading to higher safety for in vivo use. It has been demonstrated that numerous types of inorganic particles, including silica, clay, and hydroxyapatite (Hap), as well as some organic particles, can effectively serve as Pickering emulsifiers. For Pickering emulsions, solid particles at the interface between two liquid phases serve as the stabilizing agent. Thus, the stability, type (O/W or W/O), morphology and characteristics of Pickering emulsions are highly depended on the properties of the solid particles.

Binks and Fletcher have done a series theoretical studies that show the ability of solid particles to assemble at liquid-liquid interface to reduce interfacial tension and stabilize Pickering emulsions, similar to surfactants.[5-8] The water or oil-liking tendency of a surfactant is defined in terms of the hydrophile–lipophile balance (HLB) number which is often used to quantitatively correlate their adsorption at interfaces, the wettability by contact angle and the radius of solid particles would determine energy holding the particles to the liquid interface. For particles that have a contact angle in an alkane/water system (interfacial tension is ~ 50 mN m^{-1}), the energy holding a particle, with radius less than 0.5 nm, is comparable to most surfactant molecules, several k_BT, (k_B is the Boltzmann constant, and T is the absolute temperature). Therefore, particles are easily detached from the interface due to subtle thermo-fluctuations and are not effective emulsion stabilizers. The limits on the size of particles also constrain the sizes of the emulsion droplets to a minimu of several hundreds of nanometers. Russell and coworkers introduced nanoparticle surfactants (NPSs), where functionalized NPs dispersed in one liquid and polymer/oligomer ligands dissolved in the second liquid interact at the interface between the liquids.[9-12] The energy holding each NP at the interface can be significantly increased by the self-regulated number of ligands anchored to the NPs. The broad selection of nanoparticle characteristics and functionalities and the interactions between NPs and the ligands makes NPS as effective emulsifier to be applicable for variety of scientific and engineering purposes.[13]

In 2012, Aveyard raised the question “Can Janus particles give thermodynamically stable Pickering emulsions?”[14] The desorption energy, theoretically, of Janus particles from interface should be up to 3-times greater than homogeneous particles. However, precisely tuning the surface properties of Janus particles is extremely challenging. Janus particles, consisting of a nanparticle core and two or more different polymer anchored to the nanoparticle core can integrate the performances of polymers and the unique properties of nanoparticles, which have desirable optical, magnetic, and electronic properties. The Pickering emulsion

stabilized with the JNPs can be manipulated using external stimuli such as pH, temperature.[15-17]

4.1.3 Pickering Emulsion Applications

Pickering emulsions and their applications have attracted much attention due to their rather simple preparation and programmable and prolonged stability. Furthermore, by utilizing particles to stable the interface, Pickering emulsions show higher stability, lower toxicity, controlled permeability, and potential stimuli-responsiveness than emulsions stabilized by surfactants. Toor et al. produced monodispersed aqueous droplets dispersed in oil that encapsulate nanoparticles, dyes, and proteins with diameters in the 2.4–30 nm range. The droplets are stabilized by NP–surfactants of carboxylated-silica nanoparticles and amine-PDMS. The droplets showed a greater resistance to coalescence and could prevent the exchange of materials across the interface, due to the presence of an elastic layer at the interface.[18] Feng et al also studied the assembly of clay surfactants at the oil−water interface to produce all-liquid fluidic devices with a semi-permeable membrane between the liquids that can be used for programmable, reconfigurable microreactors. NOS Pickering emulsions can have responsiveness to different external stimuli. Russell and coworkers reported liquid droplets with adjustable magnetic properties by the jamming of a monolayer of magnetic nanoparticles assembled at the water-oil interface that show a reversible paramagnetic-to-ferromagnetic transformation of ferrofluid droplets. Lee reported wax-based Janus particles as surfactants to provide excellent stability against coalescence for both water-in-oil (W/O) and oil-in-water (O/W) emulsions. The Janus micro-particles surfactants are composed of sections of a hydrophilic acrylate resin and a hydrophobic wax that melt at elevated temperatures and become oil soluble, thus the particle-adsorbed droplets coalesce. Such tunability and responsiveness enabled by Janus particles offer new opportunities in the advancing drug delivery systems. In summary, Pickering emulsions stabilized by colloids, NPSs and Janus particles have shown promising potential for the design and manufacture of smart systems that are adaptive, responsive, reconfigurable features.

Chapter 2 and chapter 3 of this dissertation have thoroughly studied the assembly of soft Janus nanoparticles (JNPs) at water/toluene interface that form a monolayer of JNPs with lateral chain stretching, the tunability of the areal packing density, and reduction of interfacial tension by changing the softness of the JNPs and the portioning pf lithium salts to complex with JNPs at interface. It is important to understand the ability of such soft JNPs to stabilize water/toluene emulsions and their stability.

4.2 Results and Discussions

A high speed tip-rotary homogenizer was chosen over vortex mixer and sonication bath to induce emulsification, since it provides the strongest shear force. Emulsification with different water/toluene volume ratios with JNPs dispersed in toluene phase were studied under the same mixing conditions. As shown in Figure 4.1(a), from left to right, the water content was reduced from 90% to 10%. Typically for system with a 50% water content, the Tyndall effect was observed when passing red laser through the emulsion, as shown in Figure 4.1(b). To identify what type of emulsion was created during the mixing, different fluorescent molecules were added to either the toluene or water, and the sample was imaged by laser scanning fluorescence confocal microscope. After testing several dye molecules, Nile red was chosen to label the toluene phase. Nile red is not soluble in water and only exhibits florescent in toluene. Adding Nile red to the toluene does not interference the assembly of JNPs at water/toluene interface, since the dyes has minimal influence on the water/toluene interfacial tension. As shown in A.3.1, adding 0.1% Nile Red to toluene only reduced water/toluene interfacial tension from 35mN/m to 33 mN/m. In Figure 4.1(c), the emulsion layer was found to be a water/oil emulsion, with small droplets of water dispersed in a continuous toluene phase. Regardless of the water toluene volume ratio, the emulsions were always water/oil and no phase inversion was found, due to that high hydrophobicity and poor solubility of JNPs in water.

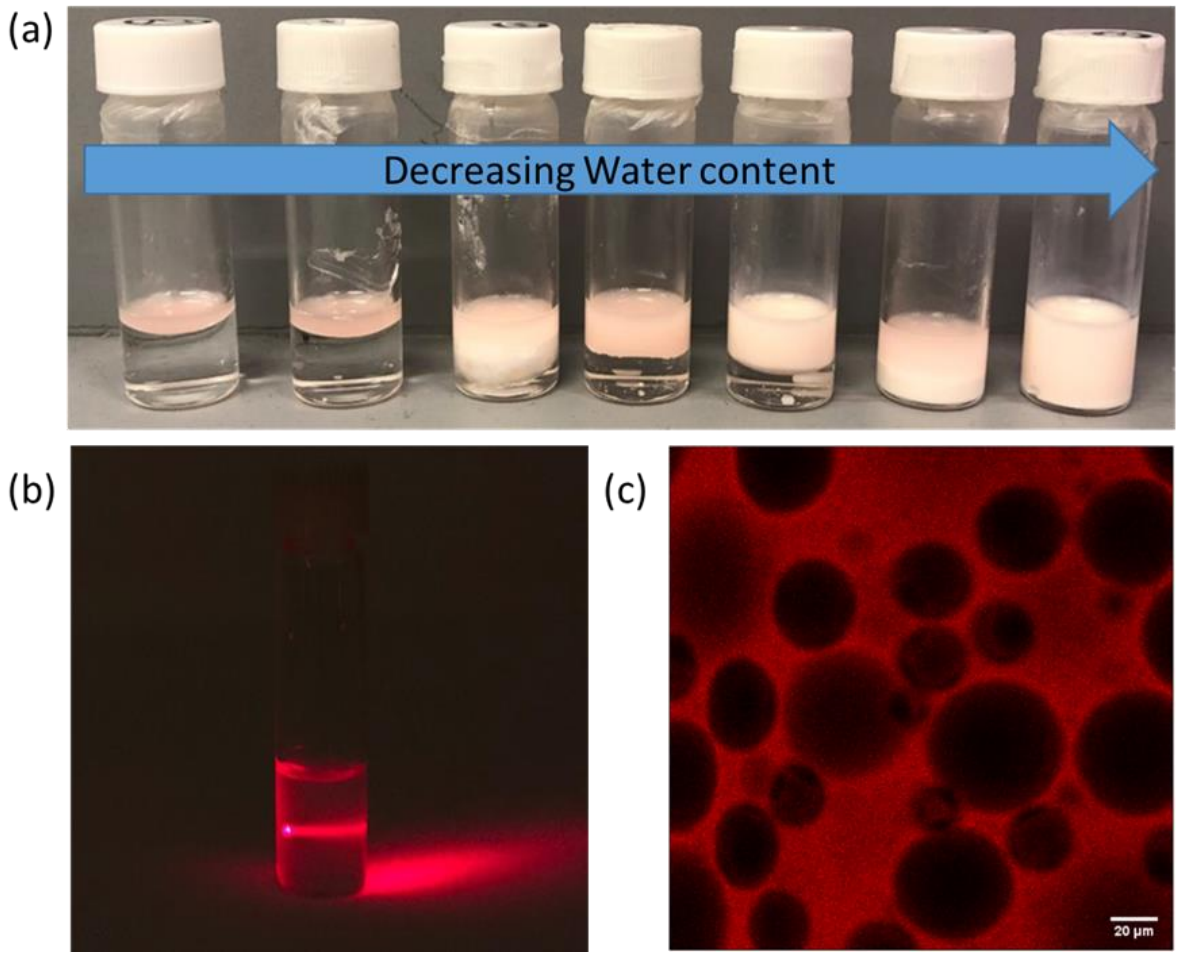

Figure 4.2 (a)Pictures of emulsions generated by high power homogenizer with 500 mM LiCl water and 8mg/ml JNPs in toluene. From left to right water content are 90%, 70%, 60%, 50%, 40%, 30%, 10% (b)Tyndall effect when laser pass through emulsion (c) Confocal Microscope Image of W/O emulsion with 50% water content.

The freshly generated emulsions were diluted with pure toluene so that the size distribution of the droplets could be measured with dynamic light scattering. The results shown in A.3.2 indicate droplets sizes of ~100 and ~500 nm. However, the emulsion droplet sizes after 30 min of homogenization were found to be a broad distribution around 20 µm. The droplets size increased and some of the droplet coalesced to form larger droplets.

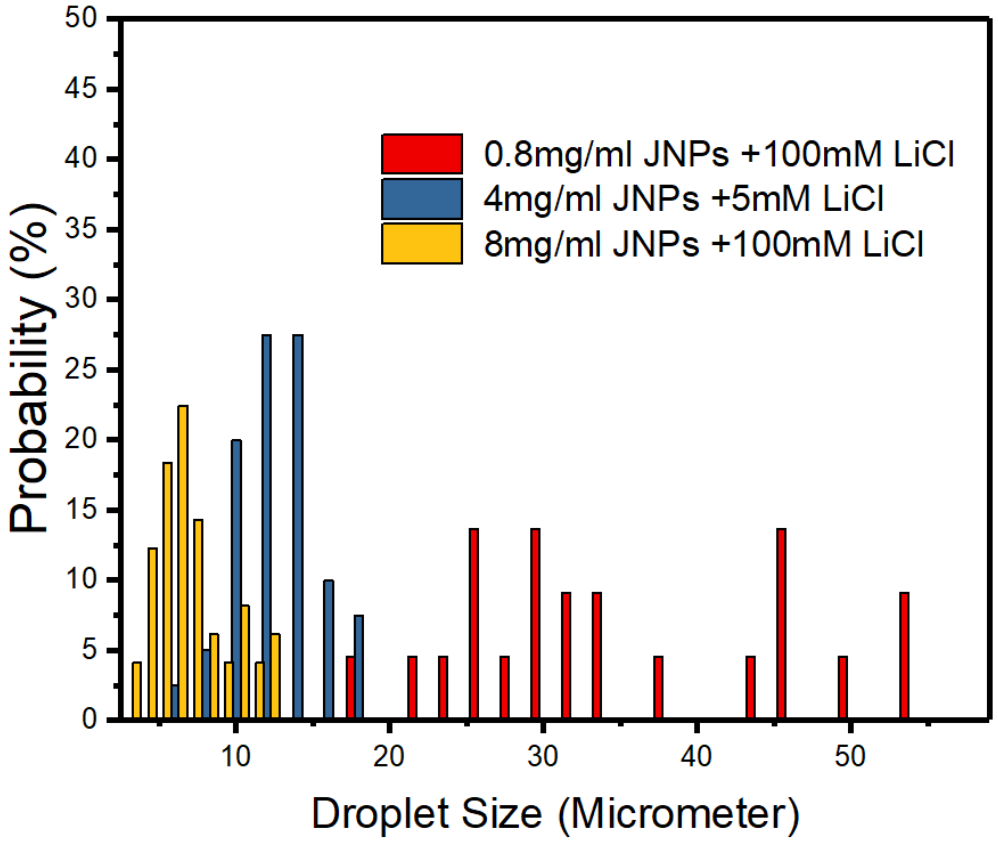

Figure 4.3 Size distrubtion of emulsion droplets stablized by (red) 0.8mg/mL JNPs +100mM LiCl (blue) 4 mg/mL JNPs +5mM LiCl (yellow) 8mg/mL JNPs+100mM LiCl.

Three different concentrations of JNPs and lithium ions were used to probe the stability of emulsions using 1mL water with lithium chloride and 1mL of toluene contains JNPs. The emulsification was done for 90 seconds of homogenizing at constant rate of 25000 rpm. The stability of emulsion droplets was found to be influenced and tuned by the JNPs concentration and concentration of lithium ions that complex with JNPs at the interface. As shown in Figure 4.3, the droplets are polydisperse with sizes ranging from 15 to 60 μm when the concentration of JNPs is low(0.8mg/ml) even with the complexation of lithium ion (100 mM) that promotes the interaction of PMMA and water, making the JNPs more amphiphilic. At this stage, the key limitation is the surface coverage of JNPs at interface. The assumption is made that shearing water into droplets ~500 nm in diameter, the interfacial area created by that would require at least 10^{16} JNPs to close pack the JNPs at the interface, if the JNPs are considered as nondeformable solid spherical particles with a 60nm diameter. At low concentrations of JNPs, not all the interface created is occupied by JNPs, and, therefore, droplets would merge and coalescence when in contact during

creaming until the interfacial area is reduced to the point where it is covered by a monolayer of JNPs and they jam at interface. When the particle concentration is increased, less reduction of interfacial is required to achieve the same coverage by JNPs. Therefore, the coalescence is arrested earlier, the droplets are smaller, and the size distribution. Typically for 4 mg/mL of JNPs in toluene with only 5mM LiCl in water, the droplet size after stabilization is reduced to ~15 μm. The lithium ions at interface also improves the water/toluene emulsion stability. From the discussion in chapter 2 and 3, we know that the JNPs tend to spread and stretch across the interface, and the spreading can is suppressed by lithium complexation which increases the PMMA wettability with water. For freshly emulsified droplets, the packing density of the JNPs-lithium complex is twice JNPs alone. Therefore, emulsions with JNPs-lithium complex each the jamming state at interface with less droplet coalescence. The complexation also makes the interfacial layer positively charged and overcomes electrostatic repulsive forces that can prevent coalescence when droplets are in contact with each other. For 8 mg/mL of JNPs in toluene with 100 mM LiCl in water, the stabilized emulsion droplet sizes were found to be ~5 μm.

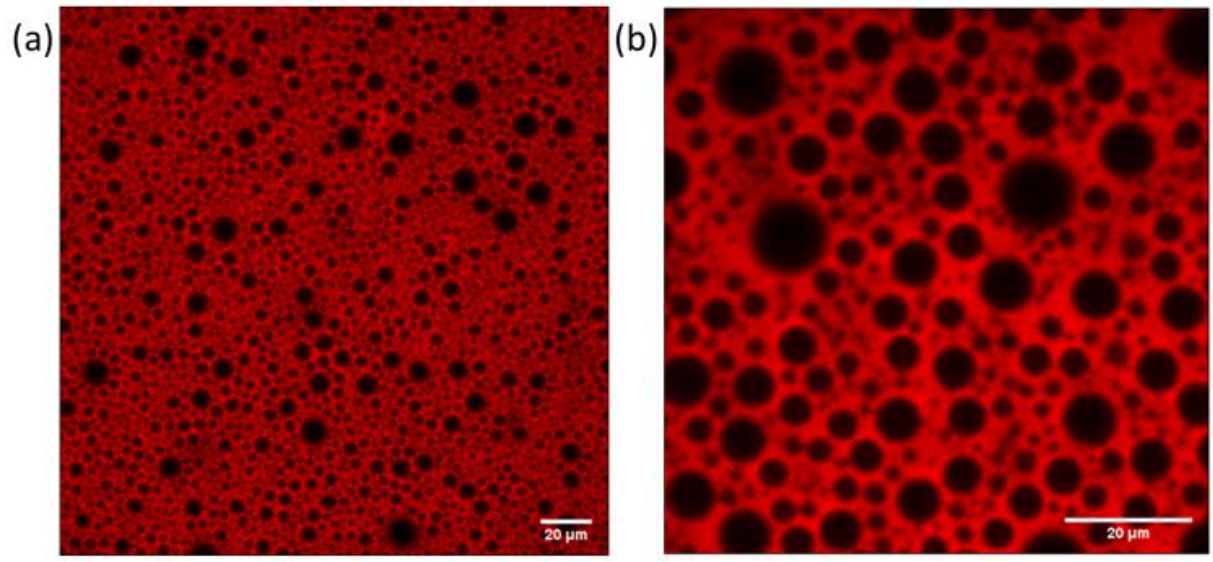

Figure 4.4 confocal images of emulsion droplets after aging of (a) 3 days (b) 6 months.

Once the JNPs-lithium jam at the interface, further droplet coalescence ceases and the emulsion become stable. Figure 4.4 compares the same emulsion made of 1mL of 8 mg/mL of JNPs in toluene and 1mL of 100 mM LiCl in water sealed in glass bottle after 3 days and 6 months under confocal microscope. As shown in Figure 4.5, the size distributions are almost identical to each other, showing long term stability.

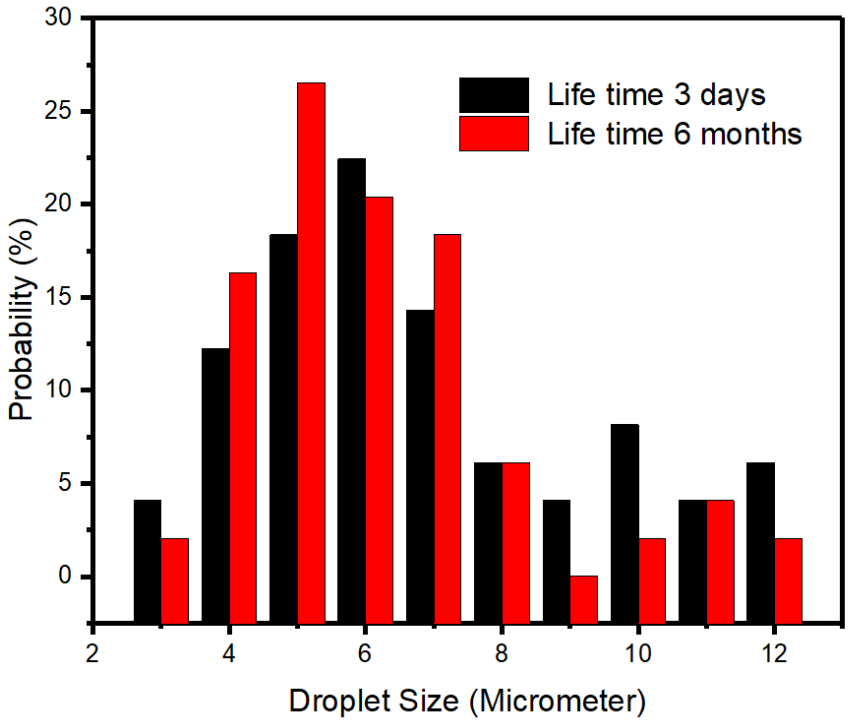

Figure 4.5 Droplet size distribution obtained by analyzing stack images of emulsions of 1mL of 8 mg/mL of JNPs in toluene and 1mL of 100 mM LiCl after 3days and 6months.

Aiming to visualize and quantitively measure droplets coalescence and better understand how JNPs and salt concentrations influence the coalescence, we move forward to microfluidic system to generate emulsion droplets. The advantage of microfluidic system is it can produce monodispersed W/O emulsion droplets. A simple T-Junction microfluidic chip was used, the micrograph of Figure 4.6(a) shows the droplet generation in a T-junction geometry. Toluene was pumped into the horizontal channel as the continuous phase with water was pumped into the vertical channel as dispersed phase. With the right flow rate ratio, controlled by the pumping pressure of both phases, monodispersed droplets were generated at the T-junction. The pump pressures are fixed for the dispersed phase(water) at 220mbar, and the continuous phase (toluene) at 300mbar. The size of droplets exiting the T junction were measured using image-J software, given the channel width of 190 μm. For 8mg/mL JNPs and 500mM LiCl in water the initial droplets were found to be 66.3um, whereas 74.3um for 0.8mg/mL JNPs and 500mM LiCl in water, and 84.5um for 0.8mg/mL JNPs and no LiCl in water, respectively. The emulsion droplets then were transported to collecting vials using a high speed camera to records and capture coalescence. Figure 4.7 shown frame by frame images capture by high speed camera that show two droplets merge to form a larger droplet with 0.8

mg/mL JNPs in toluene and 500 mM LiCl in water (indicated by the red circle in the images). It is notable that, for all concentration combinations, coalescence occurred immediately after droplets were formed by the microfluidic device and stopped in ~300 seconds, which is slightly longer than the adsorption of JNPs to occupy the interface, as indicated indicated in the interfacial reduction profile in chapter 2 and 3. The result suggests there are two scenarios occurring simultaneously during coalescence. First, JNPs adsorb to the droplet interface, and, second, a densification cause by spontaneous interfacial area reduction by droplet coalescence. Once the interface was covered with JNPs-lithium complex which subsequently jammed, the droplets became repulsive, and the coalescence ceased. The stabilized droplets were captured as shown in Figure 4.6 (b,d,f) for different concentrations and summarized in Figure 4.7. In agreement with the previous observations, it is found that the higher concentration of JNPs and lithium used in the bulk liquids, the smaller are the sizes of the stabilized droplets. For 0.8mg/mL JNPs, the droplet sizes at stabilization are polydisperse and range from 300 to 600 μm. When the same concentration of JNPs is complexed with 500 mM LiCl in the water phase, the sizes of droplets at stabilization decreased to ~200 μm. Since the JNPs-lithium complex has a positive charge, the inter-particle repulsion in the plane of the interface would lead JNPs jamming at low areal densities, while the inter-droplets repulsion prevents direct contact between droplets. Overall, the dual repulsions arrested droplet coalescence and resulting in smaller droplet sizes. If further the concentration of JNPs in toluene is increased, most droplets at stabilization are < 100 μm.

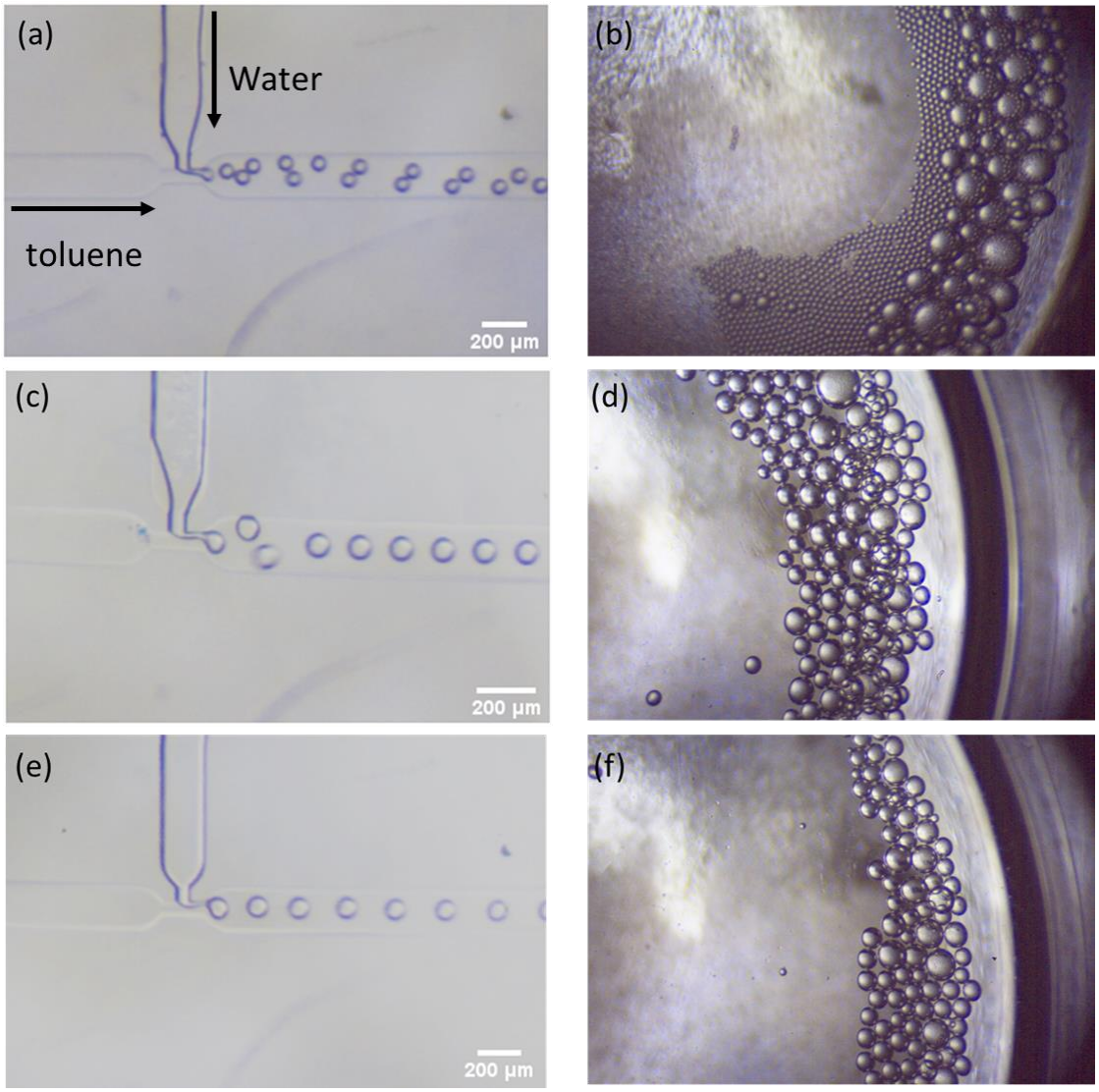

Figure 4.6 Optical images of droplets with 8mg/ml JNPs in toluene and 500mM LiCl in water (a) exit T junction (b)stabilized in collecting vial; 0.8mg/ml JNPs in toluene and 500mM LiCl in water(c) exit T junction (d) stabilized in collecting vial; 0.8mg/ml JNPs in toluene and no LiCl in water (e) exit T junction (f) stabilized in collecting vial.

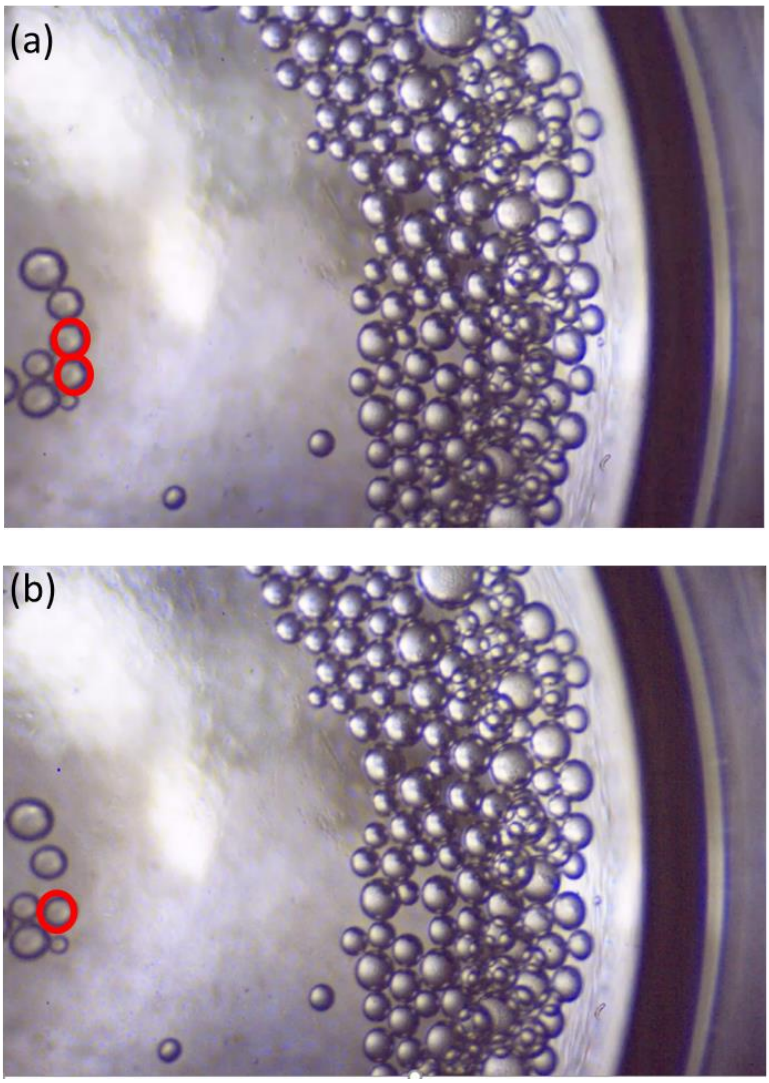

Figure 4.7 Optical images of droplet coalescence with 8mg/ml JNPs in toluene and 500mM LiCl in water.

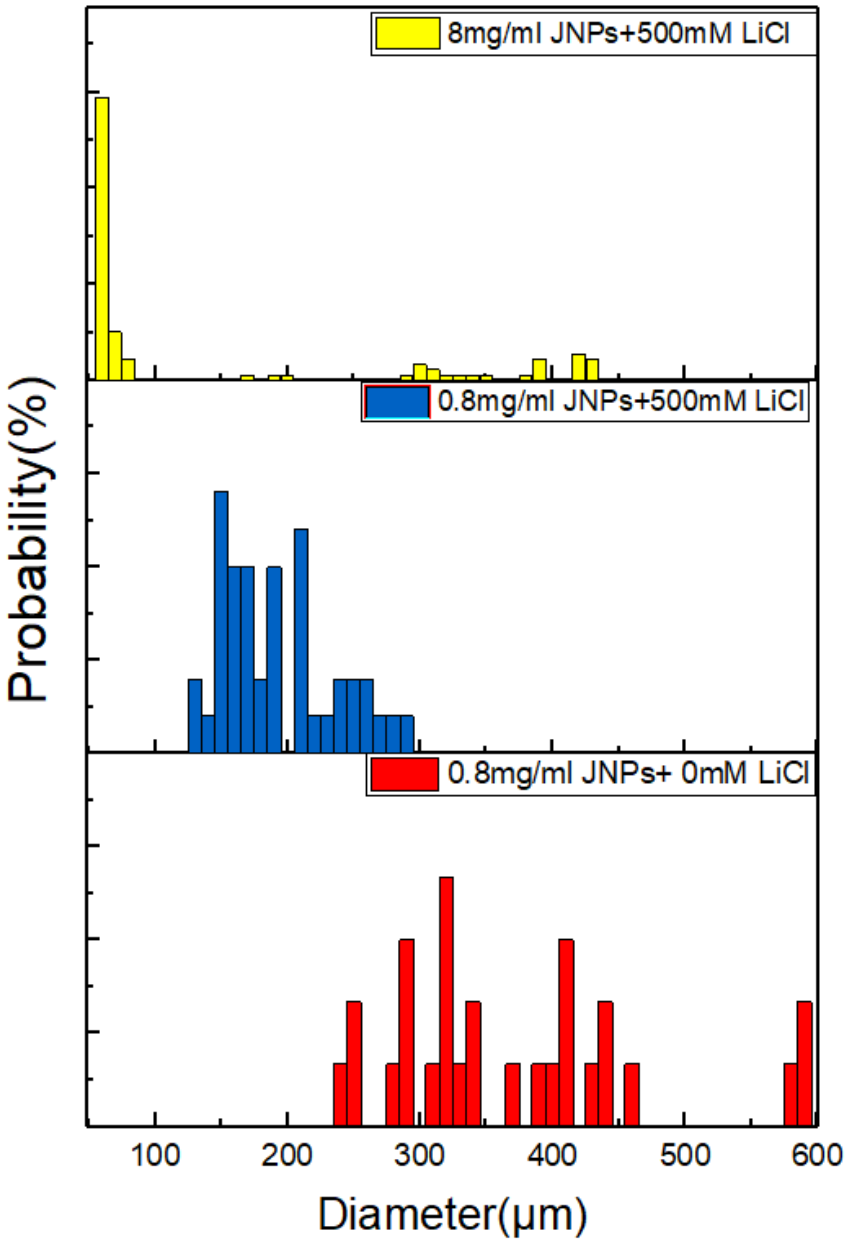

Figure 4.8 Droplets size distribution of different concentration combinations after coalescence. (top) 8mg/mL JNPs +500mM LiCl (middle) 0.8 mg/mL JNPs +500mM LiCl (bottom) 0.8mg/mL JNPs

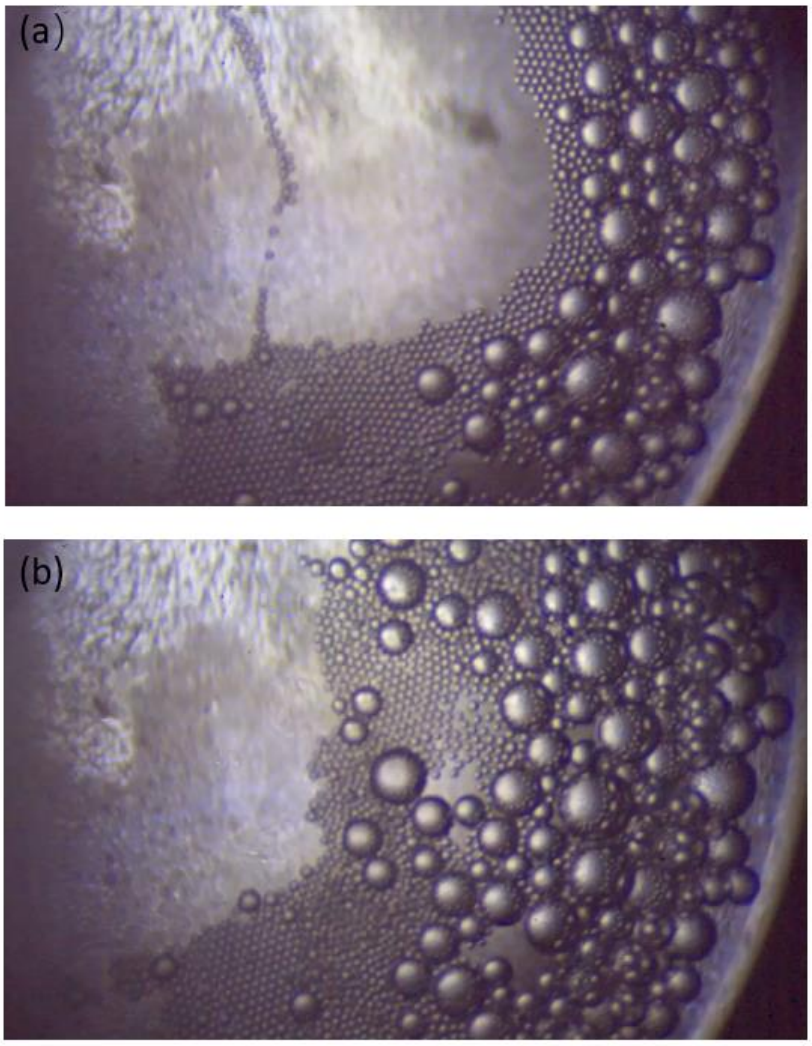

Figure 4.9 Optical images of emulsion droplets (a) after stabilization (b) after 10x dilution of the continuous phase.

When the interface of the collection of droplets is jammed by JNPs, the droplets are stable. With 10x dilution of the continuous phase(toluene), the droplets preserved their shapes and sizes, as shown in Figure 4.9, indicating the irreversible assembly of JNPs at water/toluene interface.

4.3 Conclusions

We discussed the formation of the droplets that are stabilized by JNPs and salt complex at interface. The coalescences were only found at the early stage of droplets formation (a few minutes), which is attributed to the low areal density of JNPs at interface caused by the lateral extension of polymer chains of PMMA. The complexation with lithium salt in water of the JNPs can increase the water solubility of the JNPs only to a limited extent, which cannot prevent coalescence initially.

However, after the complexation, the areal packing density of JNPs-Li is increased, which would arrest coalescence earlier and the final stable emulsion droplet sizes are reduced. Overall, control over emulsion sizes is achieved by manipulation of JNPs and lithium concentration.

4.4 Experimental Methods

4.4.1 Creation of water/toluene emulsions

0.2mL, 0.4mL, 0.6 mL, 0.8mL, 1.0mL, 1.2mL, 1.4mL, 1.6mL, and 1.8mL of water was added separately to glass vials with capacity of 4mL, additional 1.8mL, 1.6mL, 1.4mL, 1.2mL, 1.0mL, 0.8mL, 0.6 mL, 0.4mL, 0.2mL of JNPs toluene solution dyed with 0.1 % (v%) Nile Red was added to make final total volume of 2mL for all vials. The water/ toluene volume ratios were 10%:90% 20%:80% 30%:70%, 40%:60%, 50%:50%, 60%:40%, 70%:30%, 80%:20%, 90%:10% respectively. All samples were then emulsified with T-18 Ultra Turrax Digital Homogenizer at speed of 25,000 rpm for 90 seconds. The emulsions droplets were then transferred onto a cell culture dish with glass bottom(Stellar Scientific) and imaged with Zeiss LSM710 Confocal Microscope with excitation wavelength of 514nm

4.4.2 In-situ imaging droplet coalescence with different concentration of JNPs and lithium chloride

Monodispersed water droplets dispersion in toluene phase were generated by pumping water contains different concentration of lithium chloride and toluene contains different concentration of JNPs through a Dolomite microfluidic chip which offers T-Junction with channel width of 190 micro-meters via two individual mitos P-pump with constant pressure of 220 mbar(water) and 300 mbar(toluene). The droplets created in such way was capture with a high speed camera incorporated with a Zoom Stereo Microscope(AmScope). The coalescence was recorded with droplets in the collection vials.

Reference

Chapter 1

1. Kang, W., et al., *Flocculation, coalescence and migration of dispersed phase droplets and oil–water separation in heavy oil emulsion.* Journal of Petroleum Science and Engineering, 2012. **81**: p. 177-181.
2. Barkat, A., et al., *Basics of pharmaceutical emulsions: A review.* African journal of pharmacy and pharmacology, 2011. **525**: p. 2715-2725.
3. Ye, Y.-S., et al., *High performance composite polymer electrolytes using polymeric ionic liquid-functionalized graphene molecular brushes.* Journal of Materials Chemistry A, 2015. **3**(35): p. 18064-18073.
4. Khan, S.A., G.L. Baker, and S. Colson, *Composite Polymer Electrolytes Using Fumed Silica Fillers: Rheology and Ionic Conductivity.* Chemistry of Materials, 1994. **6**(12): p. 2359-2363.
5. Willard, A.P. and D. Chandler, *Instantaneous Liquid Interfaces.* The Journal of Physical Chemistry B, 2010. **114**(5): p. 1954-1958.
6. Binder, W.H., *Supramolecular Assembly of Nanoparticles at Liquid–Liquid Interfaces.* Angewandte Chemie International Edition, 2005. **44**(33): p. 5172-5175.
7. Thompson, K.L., M. Williams, and S.P. Armes, *Colloidosomes: Synthesis, properties and applications.* Journal of Colloid and Interface Science, 2015. **447**: p. 217-228.
8. Dinsmore, A.D., et al., *Colloidosomes: Selectively Permeable Capsules Composed of Colloidal Particles.* Science, 2002. **298**(5595): p. 1006.
9. Shi, S. and T.P. Russell, *Nanoparticle Assembly at Liquid–Liquid Interfaces: From the Nanoscale to Mesoscale.* Advanced Materials, 2018. **30**(44): p. 1800714.
10. Song, Y., J.-B. Fan, and S. Wang, *Recent progress in interfacial polymerization.* Materials Chemistry Frontiers, 2017. **1**(6): p. 1028-1040.
11. Huang, J., et al., *Nanostructured Polyaniline Sensors.* Chemistry – A European Journal, 2004. **10**(6): p. 1314-1319.
12. Jang, J., M. Chang, and H. Yoon, *Chemical Sensors Based on Highly Conductive Poly(3,4-ethylenedioxythiophene) Nanorods.* Advanced Materials, 2005. **17**(13): p. 1616-1620.
13. Conn, M.M. and J. Rebek, *Self-Assembling Capsules.* Chemical Reviews, 1997. **97**(5): p. 1647-1668.

14. De Koker, S., R. Hoogenboom, and B.G. De Geest, *Polymeric multilayer capsules for drug delivery.* Chemical Society Reviews, 2012. **41**(7): p. 2867-2884.
15. Fan, J., et al., *Composite polymer electrolytes using surface-modified fumed silicas: conductivity and rheology.* Solid State Ionics, 1998. **111**(1): p. 117-123.
16. Walls, H.J., et al., *Fumed silica-based composite polymer electrolytes: synthesis, rheology, and electrochemistry.* Journal of Power Sources, 2000. **89**(2): p. 156-162.
17. Walls, H.J., et al., *Composite electrolytes from self-assembled colloidal networks.* Electrochimica Acta, 2003. **48**(14): p. 2071-2077.
18. Sanz, E., et al., *Colloidal Gels Assembled via a Temporary Interfacial Scaffold.* Physical Review Letters, 2009. **103**(25): p. 255502.
19. Pieranski, P., *Two-Dimensional Interfacial Colloidal Crystals.* Physical Review Letters, 1980. **45**(7): p. 569-572.
20. Lin, Y., et al., *Nanoparticle Assembly and Transport at Liquid-Liquid Interfaces.* Science, 2003. **299**(5604): p. 226.
21. Lin, Y., et al., *Nanoparticle Assembly at Fluid Interfaces: Structure and Dynamics.* Langmuir, 2005. **21**(1): p. 191-194.
22. Binks, B.P. and S.O. Lumsdon, *Influence of Particle Wettability on the Type and Stability of Surfactant-Free Emulsions.* Langmuir, 2000. **16**(23): p. 8622-8631.
23. Binks, B.P. and S.O. Lumsdon, *Pickering Emulsions Stabilized by Monodisperse Latex Particles: Effects of Particle Size.* Langmuir, 2001. **17**(15): p. 4540-4547.
24. Binks, B.P., *Colloidal Particles at a Range of Fluid–Fluid Interfaces.* Langmuir, 2017. **33**(28): p. 6947-6963.
25. Chen, Q., et al., *Supracolloidal Reaction Kinetics of Janus Spheres.* Science, 2011. **331**(6014): p. 199.
26. Walther, A. and A.H.E. Müller, *Janus particles.* Soft Matter, 2008. **4**(4): p. 663-668.
27. Hong, L., S. Jiang, and S. Granick, *Simple Method to Produce Janus Colloidal Particles in Large Quantity.* Langmuir, 2006. **22**(23): p. 9495-9499.
28. Herzig, E.M., et al., *Bicontinuous emulsions stabilized solely by colloidal particles.* Nature Materials, 2007. **6**(12): p. 966-971.
29. Cates, M.E. and P.S. Clegg, *Bijels: a new class of soft materials.* Soft Matter, 2008. **4**(11): p. 2132-2138.
30. Clegg, P.S., *Fluid-bicontinuous gels stabilized by interfacial colloids: low and high molecular weight fluids.* Journal of Physics: Condensed Matter, 2008. **20**(11): p. 113101.

31. Huang, C., et al., *Bicontinuous structured liquids with sub-micrometre domains using nanoparticle surfactants.* Nature Nanotechnology, 2017. **12**(11): p. 1060-1063.
32. Cui, M., T. Emrick, and T.P. Russell, *Stabilizing Liquid Drops in Nonequilibrium Shapes by the Interfacial Jamming of Nanoparticles.* Science, 2013. **342**(6157): p. 460.
33. Jang, S., et al., *Molecular Dynamics Study of a Surfactant-Mediated Decane−Water Interface: Effect of Molecular Architecture of Alkyl Benzene Sulfonate.* Journal of Physical Chemistry B, 2004. **108**: p. 12130-12140.
34. Longmire, M., P.L. Choyke, and H. Kobayashi, *Clearance properties of nano-sized particles and molecules as imaging agents: considerations and caveats.* Nanomedicine (London, England), 2008. **3**(5): p. 703-717.
35. F. Bashforth, J.C.A., *An Attempt to Test the Theories of Capillary Action: By Comparing the Theoretical and Measured Forms of Drops of Fluid.* University Press, 1883.
36. Pickering, S.U., *CXCVI.—Emulsions.* Journal of the Chemical Society, Transactions, 1907. **91**(0): p. 2001-2021.
37. C., G.W., *Classification of Surface-Active Agents by "HLB".* . J. Soc. Cosmet. Chem. , 1949. **1**(311–326)
38. C., G.W., *Calculation of HLB values of non-ionic surfactants* , J. Soc. Cosmet. Chem., 1954. **5**: p. 249-256.
39. Dominguez, A., et al., *Determination of Critical Micelle Concentration of Some Surfactants by Three Techniques.* Journal of Chemical Education, 1997. **74**(10): p. 1227.
40. Iglauer, S., et al., *New surfactant classes for enhanced oil recovery and their tertiary oil recovery potential.* Journal of Petroleum Science and Engineering, 2010. **71**(1): p. 23-29.
41. Abdus, S., Y. Sultana, and M. Aqil, *Liposomal Drug Delivery Systems: An Update Review.* Current Drug Delivery, 2007. **4**(4): p. 297-305.
42. Kralova, I. and J. Sjöblom, *Surfactants Used in Food Industry: A Review.* Journal of Dispersion Science and Technology, 2009. **30**(9): p. 1363-1383.
43. Bouchemal, K., et al., *Nano-emulsion formulation using spontaneous emulsification: solvent, oil and surfactant optimisation.* International Journal of Pharmaceutics, 2004. **280**(1): p. 241-251.
44. Nadeem, M., et al., *Diesel engine performance and emission evaluation using emulsified fuels stabilized by conventional and gemini surfactants.* Fuel, 2006. **85**(14): p. 2111-2119.

45. Duro, R., et al., *Interfacial Adsorption of Polymers and Surfactants: Implications for the Properties of Disperse Systems of Pharmaceutical Interest.* Drug Development and Industrial Pharmacy, 1999. **25**(7): p. 817-829.
46. Binks, B.P., *Particles as surfactants—similarities and differences.* Current Opinion in Colloid & Interface Science, 2002. **7**(1): p. 21-41.
47. Etheridge, M.L., et al., *The big picture on nanomedicine: the state of investigational and approved nanomedicine products.* Nanomedicine: Nanotechnology, Biology and Medicine, 2013. **9**(1): p. 1-14.
48. Stratford, K., et al., *Colloidal Jamming at Interfaces: A Route to Fluid-Bicontinuous Gels.* Science, 2005. **309**(5744): p. 2198.
49. Kim, E., et al., *Arrest of Fluid Demixing by Nanoparticles: A Computer Simulation Study.* Langmuir, 2008. **24**(13): p. 6549-6556.
50. Clegg, P.S., et al., *Emulsification of Partially Miscible Liquids Using Colloidal Particles: Nonspherical and Extended Domain Structures.* Langmuir, 2007. **23**(11): p. 5984-5994.
51. Honciuc, A., *Amphiphilic Janus Particles at Interfaces*, in *Flowing Matter*, F. Toschi and M. Sega, Editors. 2019, Springer International Publishing: Cham. p. 95-136.
52. de Gennes, P.G., *Soft matter.* Reviews of Modern Physics, 1992. **64**(3): p. 645-648.
53. Jiang, S. and S. Granick, *Controlling the Geometry (Janus Balance) of Amphiphilic Colloidal Particles.* Langmuir, 2008. **24**(6): p. 2438-2445.
54. Glaser, N., et al., *Janus Particles at Liquid−Liquid Interfaces.* Langmuir, 2006. **22**(12): p. 5227-5229.
55. Binks, B.P. and P.D.I. Fletcher, *Particles Adsorbed at the Oil−Water Interface: A Theoretical Comparison between Spheres of Uniform Wettability and "Janus" Particles.* Langmuir, 2001. **17**(16): p. 4708-4710.
56. Tu, F. and D. Lee, *One-step encapsulation and triggered release based on Janus particle-stabilized multiple emulsions.* Chemical Communications, 2014. **50**(98): p. 15549-15552.
57. Bradley, L.C., et al., *Janus and patchy colloids at fluid interfaces.* Current Opinion in Colloid & Interface Science, 2017. **30**: p. 25-33.
58. Lattuada, M. and T.A. Hatton, *Synthesis, properties and applications of Janus nanoparticles.* Nano Today, 2011. **6**(3): p. 286-308.
59. Liang, F., et al., *Janus Colloids toward Interfacial Engineering.* Langmuir, 2018. **34**(14): p. 4123-4131.
60. Gröschel, A.H., et al., *Facile, Solution-Based Synthesis of Soft, Nanoscale Janus Particles with Tunable Janus Balance.* Journal of the American Chemical Society, 2012. **134**(33): p. 13850-13860.

61. Ruhland, T.M., et al., *Janus Cylinders at Liquid–Liquid Interfaces.* Langmuir, 2011. **27**(16): p. 9807-9814.
62. Liu, V. Abetz, and A.H.E. Müller, *Janus Cylinders.* Macromolecules, 2003. **36**(21): p. 7894-7898.
63. Chen, H., et al., *Flow Pickering Emulsion Interfaces Enhance Catalysis Efficiency and Selectivity for Cyclization of Citronellal.* ChemSusChem, 2017. **10**(9): p. 1989-1995.
64. Sjöblom, J., et al., *Emulsion Stabilization*, in *Encyclopedia of Colloid and Interface Science*, T. Tadros, Editor. 2013, Springer Berlin Heidelberg: Berlin, Heidelberg. p. 415-454.
65. Leal-Calderon, F. and V. Schmitt, *Solid-stabilized emulsions.* Current Opinion in Colloid & Interface Science, 2008. **13**(4): p. 217-227.
66. Alexis, F., et al., *Factors affecting the clearance and biodistribution of polymeric nanoparticles.* Molecular pharmaceutics, 2008. **5**(4): p. 505-515.
67. Yarranton, H.W., H. Hussein, and J.H. Masliyah, *Water-in-Hydrocarbon Emulsions Stabilized by Asphaltenes at Low Concentrations.* Journal of Colloid and Interface Science, 2000. **228**(1): p. 52-63.
68. Tan, Y., et al., *Fabrication of starch-based nanospheres to stabilize pickering emulsion.* Carbohydrate Polymers, 2012. **88**(4): p. 1358-1363.
69. Lv, G., et al., *Characterization of the addition of lipophilic Span 80 to the hydrophilic Tween 80-stabilized emulsions.* Colloids and Surfaces A: Physicochemical and Engineering Aspects, 2014. **447**: p. 8-13.
70. Forth, J., et al., *Building Reconfigurable Devices Using Complex Liquid–Fluid Interfaces.* Advanced Materials, 2019. **31**(18): p. 1806370.
71. Yang, H., et al., *Compartmentalization of Incompatible Reagents within Pickering Emulsion Droplets for One-Pot Cascade Reactions.* Journal of the American Chemical Society, 2015. **137**(3): p. 1362-1371.
72. Huang, J. and H. Yang, *A pH-switched Pickering emulsion catalytic system: high reaction efficiency and facile catalyst recycling.* Chemical Communications, 2015. **51**(34): p. 7333-7336.
73. Yang, H., T. Zhou, and W. Zhang, *A Strategy for Separating and Recycling Solid Catalysts Based on the pH-Triggered Pickering-Emulsion Inversion.* Angewandte Chemie International Edition, 2013. **52**(29): p. 7455-7459.
74. Hatti-Kaul, R., *Aqueous two-phase systems.* Molecular Biotechnology, 2001. **19**(3): p. 269-277.
75. Keating, C.D., *Aqueous Phase Separation as a Possible Route to Compartmentalization of Biological Molecules.* Accounts of Chemical Research, 2012. **45**(12): p. 2114-2124.
76. Esquena, J., *Water-in-water (W/W) emulsions.* Current Opinion in Colloid & Interface Science, 2016. **25**: p. 109-119.

77. Xie, G., et al., *Hanging droplets from liquid surfaces.* Proceedings of the National Academy of Sciences, 2020: p. 201922045.
78. Xie, G., et al., *Compartmentalized, All-Aqueous Flow-Through-Coordinated Reaction Systems.* Chem, 2019. **5**(10): p. 2678-2690.
79. Liu, Y., R. Lipowsky, and R. Dimova, *Concentration Dependence of the Interfacial Tension for Aqueous Two-Phase Polymer Solutions of Dextran and Polyethylene Glycol.* Langmuir, 2012. **28**(8): p. 3831-3839.

Chapter 2

1. Cayre, O., V.N. Paunov, and O.D. Velev, *Fabrication of asymmetrically coated colloid particles by microcontact printing techniques.* Journal of Materials Chemistry, 2003. **13**(10): p. 2445-2450.
2. Takahara, Y.K., et al., *Asymmetrically Modified Silica Particles: A Simple Particulate Surfactant for Stabilization of Oil Droplets in Water.* Journal of the American Chemical Society, 2005. **127**(17): p. 6271-6275.
3. Hong, L., S. Jiang, and S. Granick, *Simple Method to Produce Janus Colloidal Particles in Large Quantity.* Langmuir, 2006. **22**(23): p. 9495-9499.
4. Jiang, S., et al., *Solvent-Free Synthesis of Janus Colloidal Particles.* Langmuir, 2008. **24**(18): p. 10073-10077.
5. Honciuc, A., *Amphiphilic Janus Particles at Interfaces*, in *Flowing Matter*, F. Toschi and M. Sega, Editors. 2019, Springer International Publishing: Cham. p. 95-136.
6. Bradley, L.C., et al., *Janus and patchy colloids at fluid interfaces.* Current Opinion in Colloid & Interface Science, 2017. **30**: p. 25-33.
7. Ruhland, T.M., et al., *Janus Cylinders at Liquid–Liquid Interfaces.* Langmuir, 2011. **27**(16): p. 9807-9814.
8. Glaser, N., et al., *Janus Particles at Liquid−Liquid Interfaces.* Langmuir, 2006. **22**(12): p. 5227-5229.
9. Tu, F. and D. Lee, *One-step encapsulation and triggered release based on Janus particle-stabilized multiple emulsions.* Chemical Communications, 2014. **50**(98): p. 15549-15552.
10. Binks, B.P. and P.D.I. Fletcher, *Particles Adsorbed at the Oil−Water Interface: A Theoretical Comparison between Spheres of Uniform Wettability and "Janus" Particles.* Langmuir, 2001. **17**(16): p. 4708-4710.
11. Paunov, V.N. and O.J. Cayre, *Supraparticles and "Janus" Particles Fabricated by Replication of Particle Monolayers at Liquid Surfaces Using a Gel Trapping Technique.* Advanced Materials, 2004. **16**(9-10): p. 788-791.

12. Gröschel, A.H., et al., *Facile, Solution-Based Synthesis of Soft, Nanoscale Janus Particles with Tunable Janus Balance.* Journal of the American Chemical Society, 2012. **134**(33): p. 13850-13860.
13. Gröschel, A.H., et al., *Precise hierarchical self-assembly of multicompartment micelles.* Nature communications, 2012. **3**: p. 710-710.
14. Walther, A. and A.H.E. Müller, *Janus Particles: Synthesis, Self-Assembly, Physical Properties, and Applications.* Chemical Reviews, 2013. **113**(7): p. 5194-5261.
15. Bryson, K.C., et al., *Using Janus Nanoparticles To Trap Polymer Blend Morphologies during Solvent-Evaporation-Induced Demixing.* Macromolecules, 2015. **48**(12): p. 4220-4227.
16. Bahrami, R., et al., *The Impact of Janus Nanoparticles on the Compatibilization of Immiscible Polymer Blends under Technologically Relevant Conditions.* ACS Nano, 2014. **8**(10): p. 10048-10056.
17. Walther, A., K. Matussek, and A.H.E. Müller, *Engineering Nanostructured Polymer Blends with Controlled Nanoparticle Location using Janus Particles.* ACS Nano, 2008. **2**(6): p. 1167-1178.
18. Ruhland, T.M., et al., *Influence of Janus Particle Shape on Their Interfacial Behavior at Liquid–Liquid Interfaces.* Langmuir, 2013. **29**(5): p. 1388-1394.
19. Gröschel, A.H. and A.H.E. Müller, *Self-assembly concepts for multicompartment nanostructures.* Nanoscale, 2015. **7**(28): p. 11841-11876.
20. Auschra, C. and R. Stadler, *Synthesis of block copolymers with poly(methyl methacrylate): P(B-b-MMA), P(EB-b-MMA), P(S-b-B-b-MMA) and P(S-b-EB-b-MMA).* Polymer Bulletin, 1993. **30**(3): p. 257-264.
21. Hoberg, A.-M., et al., *The Effect of Counter Ions in Matrix-Assisted Laser Desorption/Ionization of Poly(Methyl Methacrylate).* European Mass Spectrometry, 1998. **4**(6): p. 435-440.

Chapter 3

1. Li, M. and D. Li, *Janus Droplets and Droplets with Multiple Heterogeneous Surface Strips Generated with Nanoparticles under Applied Electric Field*. The Journal of Physical Chemistry C, 2018. **122**(15): p. 8461-8472.
2. Yin, S.-N., et al., *Versatile Bifunctional Magnetic-Fluorescent Responsive Janus Supraballs Towards the Flexible Bead Display.* Advanced Materials, 2011. **23**(26): p. 2915-2919.
3. McHale, G. and M.I. Newton, *Liquid marbles: principles and applications.* Soft Matter, 2011. **7**(12): p. 5473-5481.

4. Bąk, A., et al., *Surface properties ofperfluorodecalin–containing liquid/liquid systems: The influence of Pluronic F-68 dissolved in the aqueous phase.* Journal of Fluorine Chemistry, 2018. **215**: p. 36-43.
5. Toor, A., et al., *Reconfigurable Microfluidic Droplets Stabilized by Nanoparticle Surfactants.* ACS Nano, 2018. **12**(3): p. 2365-2372.
6. Feng, W., et al., *Harnessing liquid-in-liquid printing and micropatterned substrates to fabricate 3-dimensional all-liquid fluidic devices.* Nature Communications, 2019. **10**(1): p. 1095.
7. Forth, J., et al., *Building Reconfigurable Devices Using Complex Liquid–Fluid Interfaces.* Advanced Materials, 2019. **31**(18): p. 1806370.
8. Xie, G., et al., *Compartmentalized, All-Aqueous Flow-Through-Coordinated Reaction Systems.* Chem, 2019. **5**(10): p. 2678-2690.
9. Forth, J., et al., *Hall of Fame Article: Building Reconfigurable Devices Using Complex Liquid–Fluid Interfaces (Adv. Mater. 18/2019).* Advanced Materials, 2019. **31**(18): p. 1970128.
10. Li, Y., et al., *Adaptive Structured Pickering Emulsions and Porous Materials Based on Cellulose Nanocrystal Surfactants.* Angewandte Chemie International Edition, 2018. **57**(41): p. 13560-13564.
11. Shi, S., et al., *Liquid Letters.* Advanced Materials, 2018. **30**(9): p. 1705800.
12. Forth, J., et al., *Reconfigurable Printed Liquids.* Advanced Materials, 2018. **30**(16): p. 1707603.
13. Toor, A., B.A. Helms, and T.P. Russell, *Effect of Nanoparticle Surfactants on the Breakup of Free-Falling Water Jets during Continuous Processing of Reconfigurable Structured Liquid Droplets.* Nano Letters, 2017. **17**(5): p. 3119-3125.

Chapter 4

1. McClements, D.J. and Y. Li, *Structured emulsion-based delivery systems: Controlling the digestion and release of lipophilic food components.* Advances in Colloid and Interface Science, 2010. **159**(2): p. 213-228.
2. Posocco, P., et al., *Interfacial tension of oil/water emulsions with mixed non-ionic surfactants: comparison between experiments and molecular simulations.* RSC Advances, 2016. **6**(6): p. 4723-4729.
3. Hu, Y.-T., et al., *Techniques and methods to study functional characteristics of emulsion systems.* Journal of Food and Drug Analysis, 2017. **25**(1): p. 16-26.
4. Finkle, P., H.D. Draper, and J.H. Hildebrand, *THE THEORY OF EMULSIFICATION1.* Journal of the American Chemical Society, 1923. **45**(12): p. 2780-2788.

5. Binks, B.P. and S.O. Lumsdon, *Influence of Particle Wettability on the Type and Stability of Surfactant-Free Emulsions.* Langmuir, 2000. **16**(23): p. 8622-8631.
6. Binks, B.P. and S.O. Lumsdon, *Pickering Emulsions Stabilized by Monodisperse Latex Particles: Effects of Particle Size.* Langmuir, 2001. **17**(15): p. 4540-4547.
7. Binks, B.P. and P.D.I. Fletcher, *Particles Adsorbed at the Oil−Water Interface: A Theoretical Comparison between Spheres of Uniform Wettability and "Janus" Particles.* Langmuir, 2001. **17**(16): p. 4708-4710.
8. Binks, B.P., *Particles as surfactants—similarities and differences.* Current Opinion in Colloid & Interface Science, 2002. **7**(1): p. 21-41.
9. Huang, C., et al., *Structured Liquids with pH-Triggered Reconfigurability.* Advanced Materials, 2016. **28**(31): p. 6612-6618.
10. Cui, M., T. Emrick, and T.P. Russell, *Stabilizing Liquid Drops in Nonequilibrium Shapes by the Interfacial Jamming of Nanoparticles.* Science, 2013. **342**(6157): p. 460.
11. Lin, Y., et al., *Nanoparticle Assembly at Fluid Interfaces: Structure and Dynamics.* Langmuir, 2005. **21**(1): p. 191-194.
12. Lin, Y., et al., *Nanoparticle Assembly and Transport at Liquid-Liquid Interfaces.* Science, 2003. **299**(5604): p. 226.
13. Shi, S. and T.P. Russell, *Nanoparticle Assembly at Liquid–Liquid Interfaces: From the Nanoscale to Mesoscale.* Advanced Materials, 2018. **30**(44): p. 1800714.
14. Aveyard, R., *Can Janus particles give thermodynamically stable Pickering emulsions?* Soft Matter, 2012. **8**(19): p. 5233-5240.
15. Yang, L., et al., *Responsive Single-Chain/Colloid Composite Janus Nanoparticle.* Macromolecules, 2020. **53**(6): p. 2264-2270.
16. Zhang, L., et al., *Responsive polymeric Janus cage.* Chemical Communications, 2020. **56**(72): p. 10497-10500.
17. Liang, F., et al., *Janus Colloids toward Interfacial Engineering.* Langmuir, 2018. **34**(14): p. 4123-4131.
18. Toor, A., et al., *Reconfigurable Microfluidic Droplets Stabilized by Nanoparticle Surfactants.* ACS Nano, 2018. **12**(3): p. 2365-2372.

Afterword

Motivated by the interest of filling the gap of universal understanding soft matters assemble at liquid interfaces and how their assembly can potentially be employed for structuring liquids, the research work presented by this dissertation achieved to demonstrated Janus type nanoparticle can assemble at liquid interfaces to reduce interfacial tension and was able to harvest membrane at the versatile platform

In chapter 2, discovery has been made that soft nature of the JNPs with hemispheres of PMMA and PS chains can entangle and stretch normal to the interface, which leads to loosely packing of JNPs at interface, which has not been seen for hard spherical nanoparticles assemblies at liquid interface. Varying the pH can influence the ability of JNPs to reduce interfacial tension.

In chapter 3, coverage of JNPs at water oil interface has been proven to be related to the softness of JNPs. The shorter the corona chains, the harder are the particles are, resulting from less chain stretching. Thus, a denser coverage can be achieved. Upon compression, the soft JNPs can undergo a reconfiguration, relaxing the imposed stress. The extent to which this occurs decreases with decreasing molecular weight of the corona chains.

Furthermore, complexation with salt ions, in the case of PMMA against water, can promote the solubilization of the PMMA in the aqueous phase, eliminating the need to stretch the chains to cover the interface, therefore making these soft JNPs behave more like classic surfactants, reducing the stretching of the PMMA chains in the plane of the interface, reducing the footprint of the JNP on the interface, and enabling a higher packing density of JNPs at interface. With complexation, the area density of soft JNPs at the interface increases with the corresponding changes in the response of the assemblies to compression

In Chapter 4, the ability of JNPs particle assemble at interface to stabilize water/oil emulsions has been demonstrated with different ion complexations. The emulsions are kinetically stable over period over 6 months. The soft polymeric JNPs show great potential as Pickering emulsifier that can provide long term emulsion stability.

Overall, soft polymeric JNPs present great potential as effective emulsifier and structuring liquid agent. To explore their full potential, two directions are proposed in the following sections.

Appendix

A.1 Supporting information for Chapter 2

A.1.1

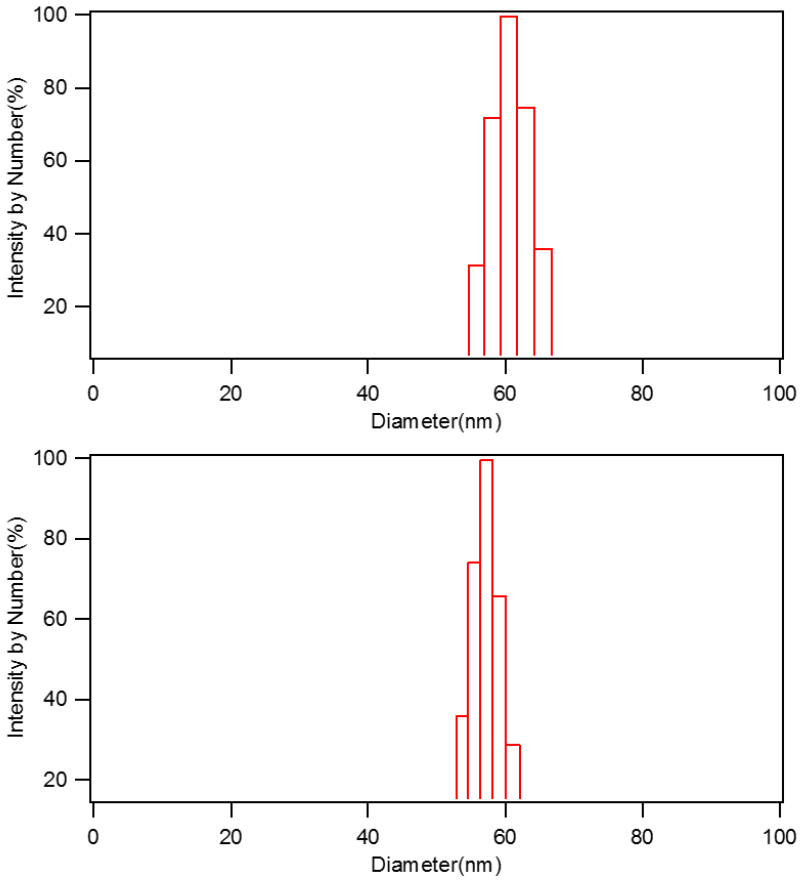

A.1. Dynamic light scattering of Janus particles (8mg/ml) solution in toluene (a) right after preparation of solution (b) 6 days after preparation

A.1.2

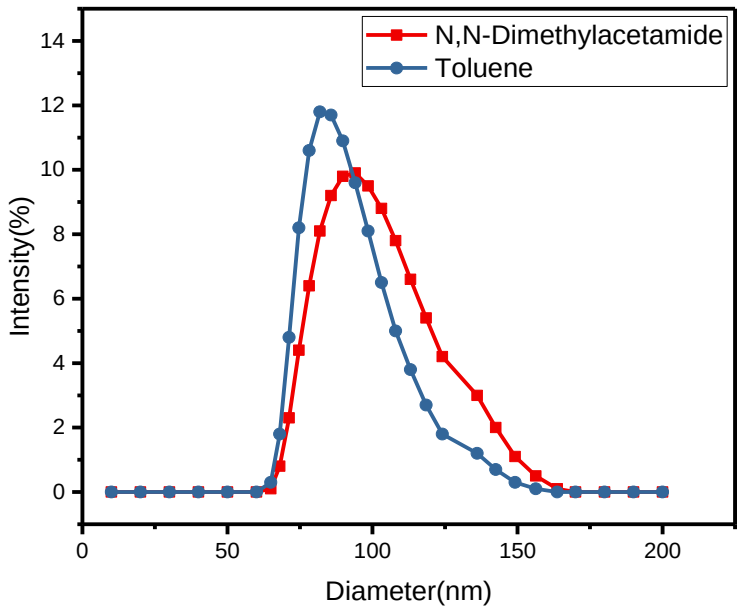

A.1.2 DLS of JNPs in toluene and N,N-Dimethylacetamide

A.1.3

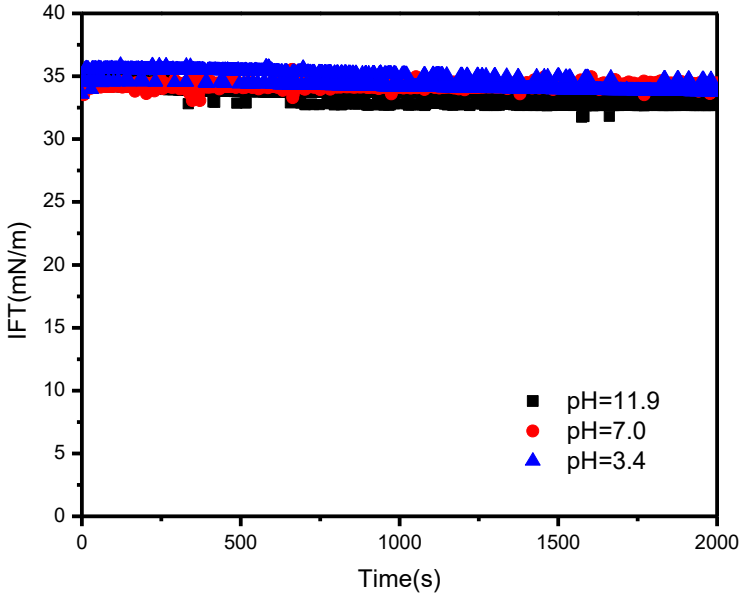

A.1.3 Time dependence of interfacial tension isotherms of pure water/ toluene interface at different pH in water phase

A.1.4

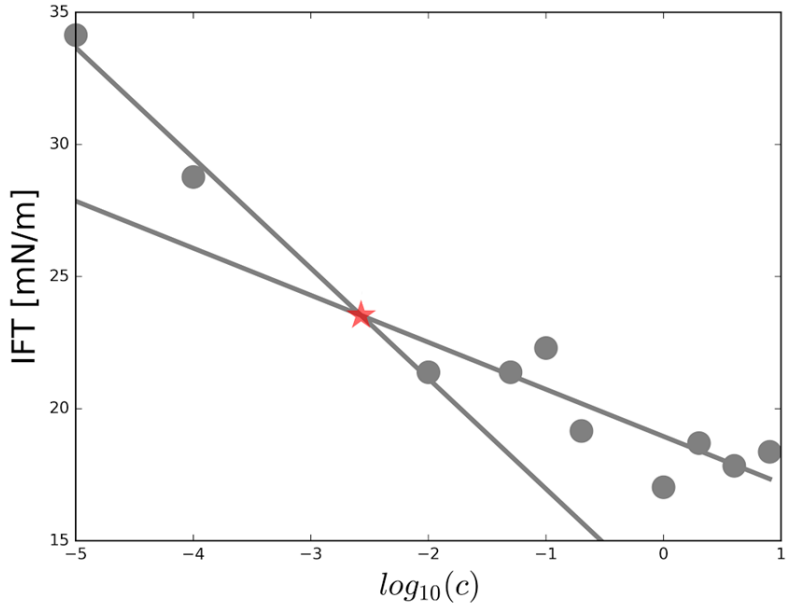

A.1.4 Data fitting of interfacial tension between water/toluene with different concentration of JNPs in toluene

A.1.5

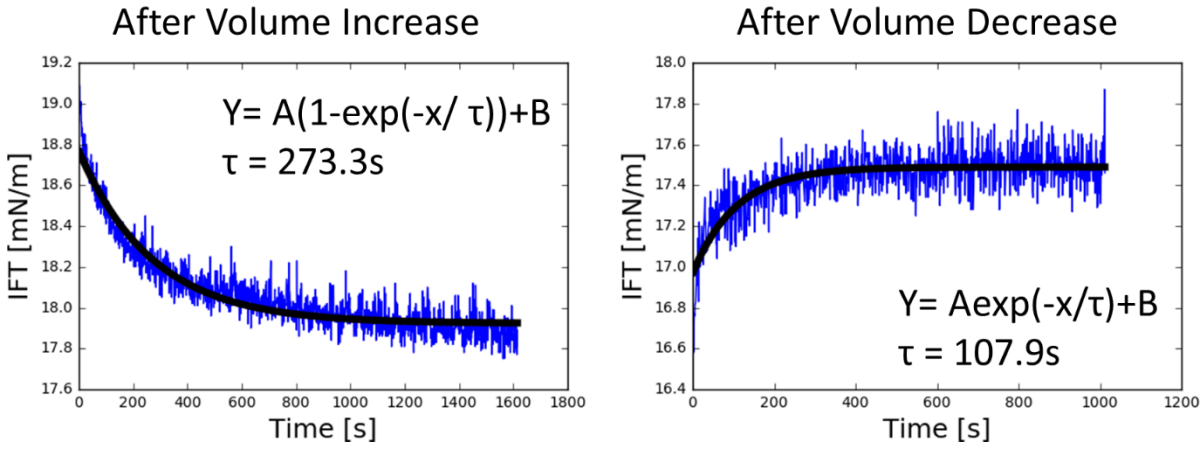

A.1.5 Fitting the relaxation of interfacial tension after the volume increase and decrease with a single exponential function

A.2 Supporting information for Chapter 3

A.2.1

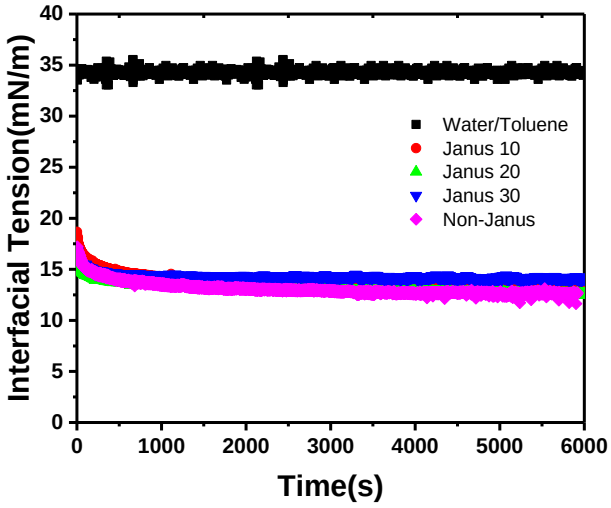

A.2.1 Time evolution of interfacial tension between water and JNPs and Non-JNPs toluene solutions (8mg/mL).

A.2.2

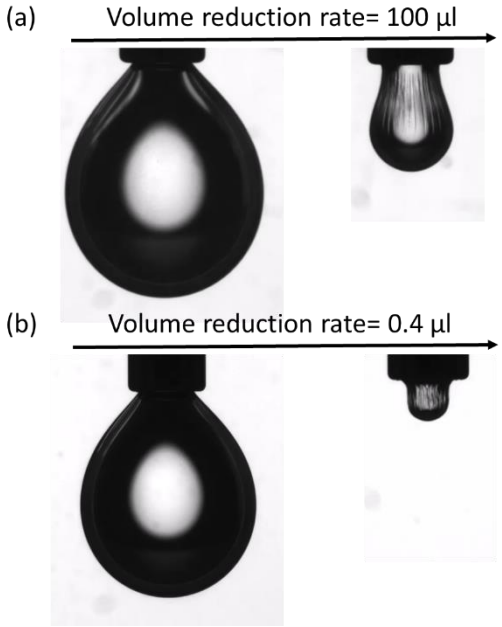

A.2.2 Volume reduction of water droplet immersed in 8 mg/ml Janus-30/toluene solution after aging for 6000 s at: (a) volume reduction rate of 100 µl/min, (b) volume reduction rate of 0.4 µl/min

A.2.3

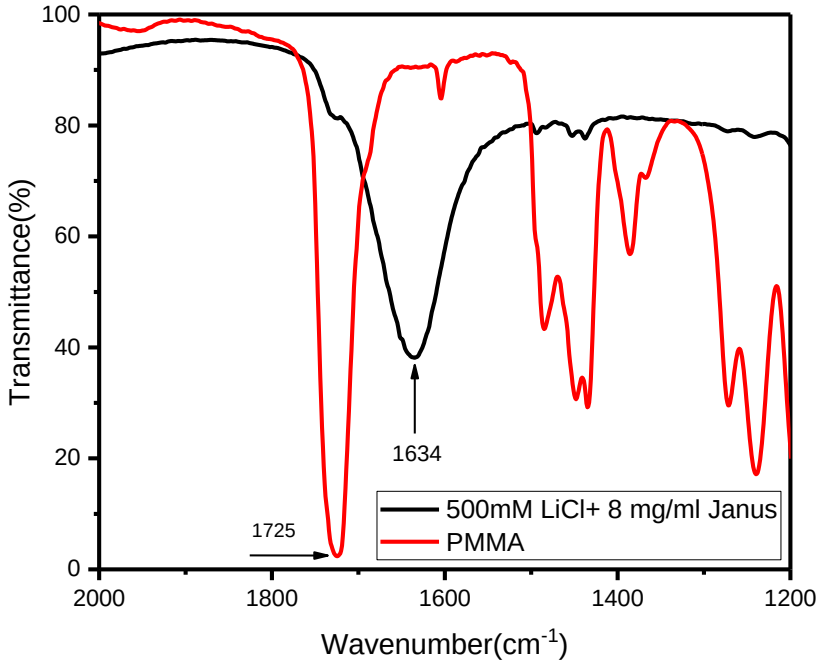

A.2.3 FT-IR spectra of pure PMMA (red) and JNPs (SBM30) after contact with lithium ion at water/toluene interface (black)

A.2.4

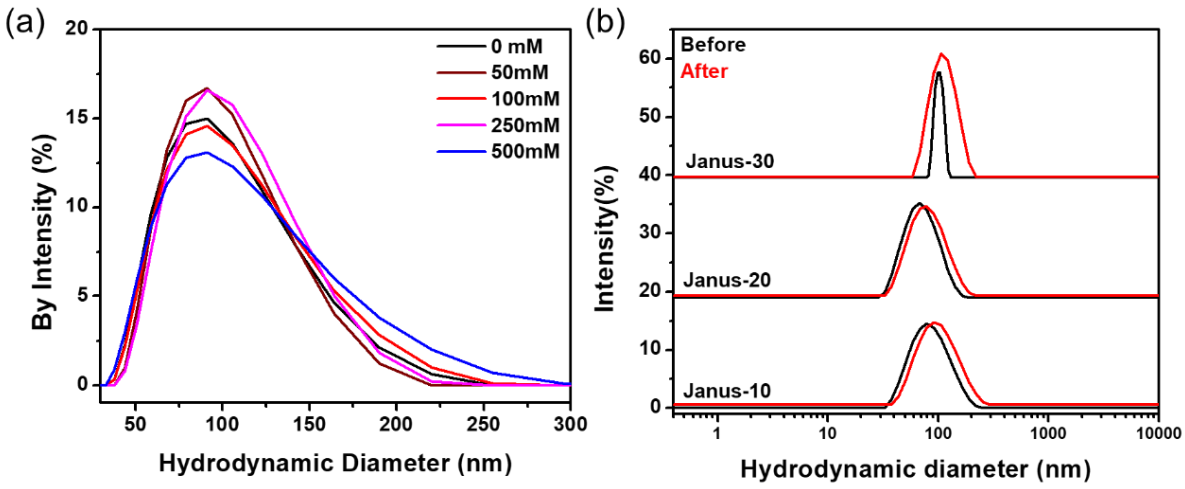

A.2.4 (a) Dynamic light scattering of JNP-10 in contact with an LiCl aqueous solution at different concentrations. (b) Dynamic light scattering measurement of JNPs (bottom: JNP-10, middle: JNP-20, Top: JNP-30) in toluene before (black) and after (red) contact with a 500mM LiCl aqueous solution.

A.3 Supporting information for Chapter 4

A.3.1

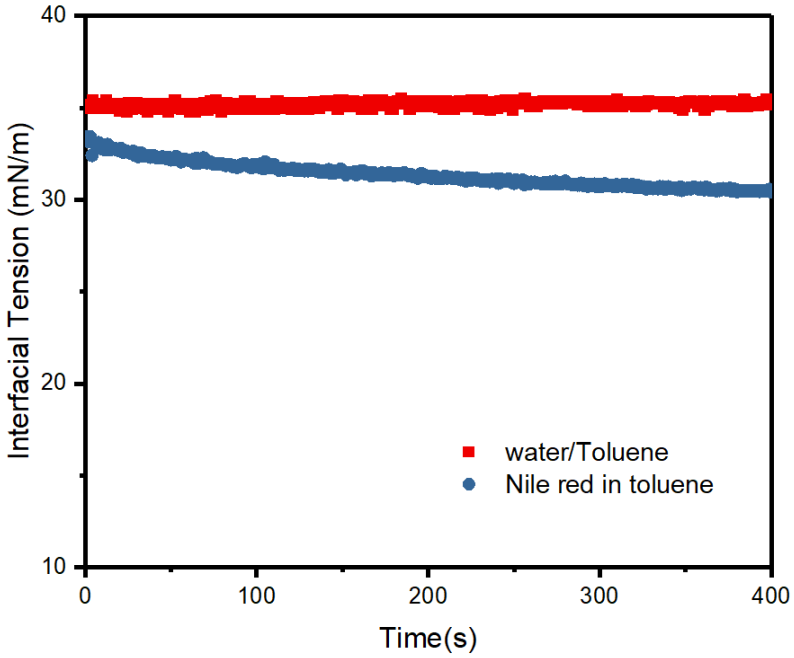

A.3.1 Interfacial tension between water toluene with or without 0.1% Nile Red solutions.

A.3.2

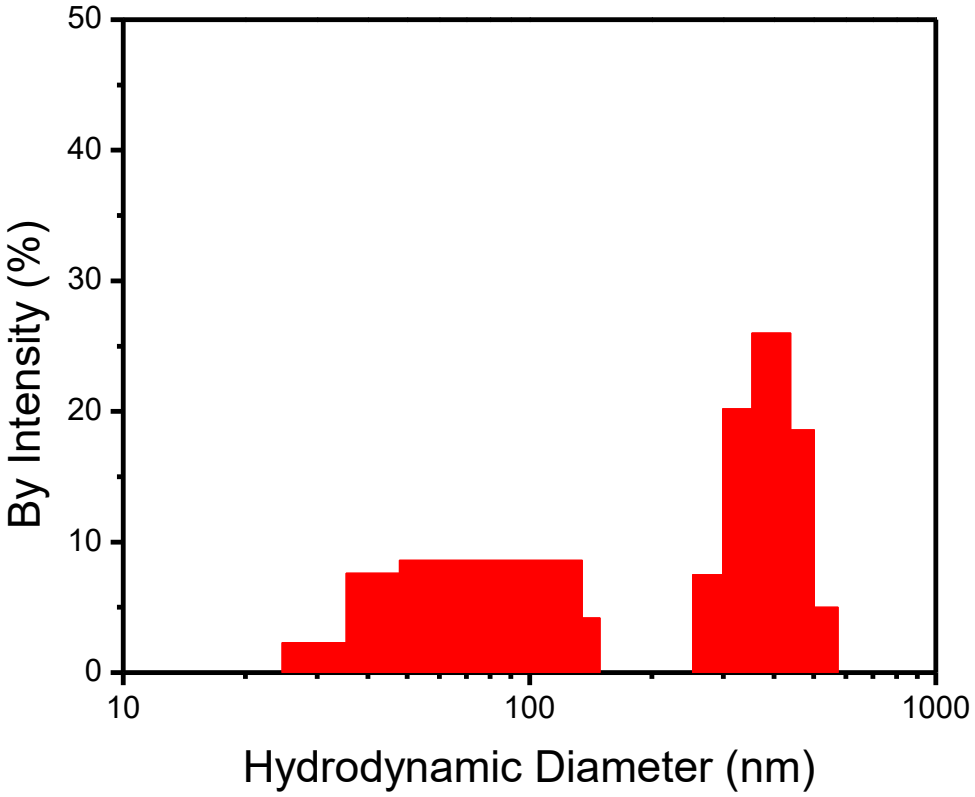

A.3.2 Size distribution of emulsion droplets stabilized with 1mL of 8mg/ml JNPs in toluene and 1mL 500 mM LiCl.